

AT&T
BELL LABORATORIES

March 1984
Vol. 63 No. 3

TECHNICAL JOURNAL

A JOURNAL OF THE AT&T COMPANIES

Signal Clipping

Click Modulation

Optical Fibers

Optical Directional Coupler

Speech Recognition

Signal Performance

EDITORIAL COMMITTEE

	A. A. PENZIAS, ¹ <i>Committee Chairman</i>	
M. M. BUCHNER, JR. ¹	D. HIRSCH ⁴	R. L. MARTIN ¹
R. P. CLAGETT ²	S. HORING ¹	J. S. NOWAK ¹
R. P. CREAM ²	R. A. KELLEY ¹	B. B. OLIVER ⁵
B. R. DARNALL ¹	R. W. LUCKY ¹	J. W. TIMKO ³
B. P. DONOHUE, III ³	J. F. MARTIN ²	

¹AT&T Bell Laboratories ²AT&T Technologies ³AT&T Information Systems

⁴AT&T Consumer Products ⁵AT&T Communications

EDITORIAL STAFF

B. G. KING, <i>Editor</i>	L. S. GOLLER, <i>Assistant Editor</i>
P. WHEELER, <i>Managing Editor</i>	A. M. SHARTS, <i>Assistant Editor</i>
B. G. GRUBER, <i>Circulation</i>	

AT&T BELL LABORATORIES TECHNICAL JOURNAL (ISSN0005-8580) is published by AT&T, 550 Madison Avenue, New York, NY 10022; C. L. Brown, Chairman and Chief Executive Officer; W. M. Ellinghaus, President; V. A. Dwyer, Vice President and Treasurer; T. O. Davis, Secretary.

The Journal is published ten times each year. The Computing Science and Systems section and the special issues are included as they become available. Subscriptions: United States—1 year \$35; 2 years \$63; 3 years \$84; foreign—1 year \$45; 2 years \$73; 3 years \$94. A subscription to the Computing Science and Systems section only is \$10 (\$12 foreign). Single copies of most issues of the Journal are available at \$5 (\$6 foreign). Payment for foreign subscriptions or single copies must be made in United States funds, or by check drawn on a United States bank and made payable to the Technical Journal and sent to AT&T Bell Laboratories, Circulation Dept., Room 1E335, 101 J. F. Kennedy Pky, Short Hills, NJ 07078.

Single copies of material from this issue of the Journal may be reproduced for personal, noncommercial use. Permission to make multiple copies must be obtained from the Editor.

Comments on the technical content of any article or brief are welcome. These and other editorial inquiries should be addressed to the Editor, AT&T Bell Laboratories Technical Journal, Room 1J319, 101 J. F. Kennedy Pky, Short Hills, NJ 07078. Comments and inquiries, whether or not published, shall not be regarded as confidential or otherwise restricted in use and will become the property of AT&T. Comments selected for publication may be edited for brevity, subject to author approval.

Printed in U.S.A. Second-class postage paid at Short Hills, NJ 07078 and additional mailing offices. Postmaster: Send address changes to the AT&T Bell Laboratories Technical Journal, Room 1E335, 101 J. F. Kennedy Pky, Short Hills, NJ 07078.

Copyright © 1984 AT&T.

AT&T Bell Laboratories

Technical Journal

VOL. 63

MARCH 1984

NO. 3

Copyright © 1984 AT&T. Printed in U.S.A.

Signals Designed for Recovery After Clipping—III: Generalizations	379
B. F. Logan, Jr.	
Click Modulation	401
B. F. Logan, Jr.	
Design Diagrams for Depressed Cladding Single-Mode Fibers	425
W. T. Anderson and P. F. Glodis	
Single GRIN-Lens Directional Couplers	431
F. H. Levinson and S. W. Granlund	
The DTWP: An LPC-Based Dynamic Time-Warping Processor for Isolated Word Recognition	441
M. K. Brown, R. Thorkildsen, Y. H. Oh, and S. S. Ali	
On the Application of Embedded Training to Connected Letter Recognition for Directory Listing Retrieval	459
L. R. Rabiner, J. G. Wilpon, and S. G. Terrace	
An Improved Word-Detection Algorithm for Telephone- Quality Speech Incorporating Both Syntactic and Semantic Constraints	479
J. G. Wilpon, L. R. Rabiner, and T. Martin	
Performance of Cross-Polarized M-ary QAM Signals Over Nondispersive Fading Channels	499
M. Kavehrad	
PAPERS BY AT&T BELL LABORATORIES AUTHORS	523
CONTENTS, APRIL ISSUE	529

Signals Designed for Recovery After Clipping— III: Generalizations

By B. F. LOGAN, JR.*

(Manuscript received March 26, 1982)

Let $S(b, c)$ be the class of all real-valued bounded functions $s(t)$ of the form

$$s(t) = g(t) + \cos ct, \quad (\text{i})$$

where g is bandlimited to $[-b, b]$ and $0 \leq b < c < \infty$ and such that

$$(-1)^k s(k\pi/c) > 0, \quad k = 0, \pm 1, \pm 2, \dots, \quad (\text{ii})$$

a condition that is always satisfied if $|g(t)| < 1$. In earlier papers we showed that such functions could be reconstructed from a knowledge of their zeros in the interval $(t - T, t + T)$ to within an accuracy $O(e^{-\lambda T})$, where $\lambda = c - b$. This paper generalizes these results to functions of the form (i) satisfying the condition that $s(t)$ have only real zeros, a condition which is weaker than (ii). The bounds on the accuracy of the reconstruction obtained are weaker. This paper also shows that every interval of length greater than $2\pi/\lambda$, where $\lambda = c - b > 0$, must contain at least one zero of $s(t)$, and that $s(t)$ satisfies

$$|s(t)| \leq 2^{p-1}, \quad -\infty < t < \infty,$$

where $p = 2c/\lambda$.

I. INTRODUCTION

References 1 and 2 present various practical means for recovery of signals $s(t)$ in a certain class $S(b, c)$ from their zeros. The class $S(b, c)$ consists of all real-valued bounded signals $s(t)$ of the form

$$s(t) = g(t) + \cos ct, \quad (\text{1a})$$

* AT&T Bell Laboratories.

Copyright © 1984 AT&T. Photo reproduction for noncommercial use is permitted without payment of royalty provided that each reproduction is done without alteration and that the Journal reference and copyright notice are included on the first page. The title and abstract, but no other portions, of this paper may be copied or distributed royalty free by computer-based and other information-service systems without further permission. Permission to reproduce or republish any other portion of this paper must be obtained from the Editor.

where g is bandlimited to $[-b, b]$, $0 \leq b < c < \infty$, and such that

$$(-1)^k s(k\pi/c) > 0, \quad k = 0, \pm 1, \pm 2, \dots, \quad (1b)$$

which is satisfied, for example, if $|g(t)| < 1$.

The alternation condition (1a) ensures that $s(t)$ has only real simple zeros $\{t_k\}$,

$$\frac{k\pi}{c} < t_k < (k+1)\frac{\pi}{c}, \quad k = 0, \pm 1, \pm 2, \dots, \quad (1c)$$

i.e., the zeros of $s(t)$ are interlaced with the zeros of $\sin ct$.

The recovery procedures involve operations on the so-called *fundamental function* associated with the zeros $\{t_k\}$ of s ,

$$h(t) = J(t) - ct, \quad (2)$$

where $J(t)$ is a jump function increasing by π at each zero t_k , $J(0) = 0$. The linearly decreasing term $-ct$ just offsets the growth of $J(t)$ so that

$$-\pi < h(t) < \pi, \quad -\infty < t < \infty. \quad (3)$$

The practicality of the recovery procedures owes to the fact, established in Ref. 1, that $h(t)$ is a high-pass function, having no spectrum in the (angular) frequency interval $(-\lambda, \lambda)$, where

$$\lambda = c - b \quad (4)$$

is the "gap frequency" associated with the class $S(b, c)$. The basic recovery formula given in Ref. 1 is

$$s(t) = \frac{1}{2} \{\text{sgn } s(t)\} \exp[\hat{h}(t)], \quad (5)$$

where \hat{h} is the Hilbert transform of h . Since $h(t)$ is a bounded high-pass function, a good estimate $\hat{h}_T(t)$ for $\hat{h}(t)$ can be made from the knowledge of h in a finite moving interval $(t - T, t + T)$; i.e., from the zeros t_k in the interval $(t - T, t + T)$, leading to an estimate $s_T(t)$,

$$s_T(t) = \frac{1}{2} \{\text{sgn } s(t)\} \exp[\hat{h}_T(t)] \quad (6)$$

such that

$$|s(t) - s_T(t)| \leq \frac{2e^{-\lambda T}}{(1 - e^{-\lambda T})^2} |s(t)|. \quad (7)$$

In Ref. 2, generalizations of the basic recovery formula were developed, showing how $s(t)$ could be recovered from bandlimited versions of $h(t)$ or, equivalently, from bandlimited versions of

$$h'(t) = \pi \sum_{-\infty}^{\infty} \delta(t - t_k) - c. \quad (8)$$

Here we wish to extend the validity of the previous results by removing the alternation condition (1b), simply requiring that $s(t)$ of the form (1) have only real zeros $\{t_k\}$. For practical purposes we would also require the zeros to be simple, but here we allow each zero t_k to have *multiplicity* m_k .

Several interesting questions now arise:

1. What is the longest possible zero-free interval for $s(t)$?
2. How many zeros, counted according to multiplicity, can $s(t)$ have in a closed interval of length T ?
3. How large can $|h(t)|$ be?
4. How large can $|s(t)|$ be?

The basic question here is the third question. A bound on $|h(t)|$ is needed to establish that $h(t)$ is a high-pass function with no spectrum in $(-\lambda, \lambda)$. In order for $|h(t)|$ to be bounded it is necessary, of course, for $s(t)$ to have a limited zero-free interval and a limited number of zeros in any interval of fixed length. The fourth question is one of corollary interest.

Once we establish that

$$-M \leq h(t) \leq M$$

we conclude that h is high-pass, so the results in Ref. 2 remain valid and the reconstruction algorithm in Ref. 1 remains valid, with (7) replaced by

$$|s(t) - s_T(t)| \leq \frac{1}{2} |s(t)| \left[\left(\frac{1 + e^{-\lambda T}}{1 - e^{-\lambda T}} \right)^{\frac{2M}{\pi}} - 1 \right].$$

In order to obtain a bound on $|h(t)|$ we consider

$$h'(t) = \pi \sum_{-\infty}^{\infty} m_k \delta(t - t_k) - c \quad (9)$$

and show that $h'(t)$ is a high-pass distribution with no spectrum in $(-\lambda, \lambda)$. To do this we must first show that the total mass of the distribution in any interval of fixed length T is uniformly bounded. A crude bound is obtained which, together with the exponential decay in the upper half plane $u > 0$ of

$$\frac{s'(t + iu)}{s(t + iu)} - ic,$$

establishes that $h'(t)$ has no spectrum in $(-\lambda, \lambda)$; that is,

$$\int_{-\infty}^{\infty} f_{\lambda}(t) h'(t) dt = 0$$

or

$$\frac{\pi}{c} \sum_{-\infty}^{\infty} m_k f_{\lambda}(t_k) = \int_{-\infty}^{\infty} f_{\lambda}(t) dt, \quad (10)$$

where $f_{\lambda}(t)$ is any bandlimited function of L_1 whose Fourier transform vanishes outside $(-\lambda, \lambda)$.

The “quadrature formula” (10), together with appropriately chosen f_{λ} , gives an upper bound for the longest possible zero-free interval of $s(t)$.

The fundamental function $h(t)$, under the less restrictive condition, is of the form

$$h(t) = J(t) - ct, \quad (11)$$

where now $J(t)$ is a jump function increasing by $m_k\pi$ at each zero t_k of multiplicity m_k . The levels of $J(t)$ are still multiples of π but we do not (necessarily) have $J(0) = 0$ as before. If, for example, $s(0) \neq 0$, then $J(0) = n\pi$, where n is determined by the condition that $h(t)$ have zero average value. To obtain an upper bound on $|h(t)|$ we write $h(t)$ as an “unbiased” integral of $h'(t)$. An unbiased integral of a high-pass function is a particular integral that is also high-pass; e.g., the unbiased integral of $\cos \lambda t$ is $\lambda^{-1}\sin \lambda t$. Owing to the spectral gap $(-\lambda, \lambda)$ the unbiased integral may be obtained by convolution with an integrating kernel (see Ref. 3) $I_{\lambda}(t)$ belonging to L_1 , satisfying

$$\int_{-\infty}^{\infty} I_{\lambda}(t)e^{-i\omega t}dt = \frac{1}{i\omega}, \quad |\omega| \geq \lambda. \quad (12)$$

There is, then, an equivalence class of kernels $\{I_{\lambda}(t)\}$. If we further require

$$\int_{-\infty}^{\infty} I_{\lambda}(t)dt = 0, \quad (13)$$

for example, by requiring $I_{\lambda}(t)$ to be an odd function, then

$$h(t) = \pi \sum_{-\infty}^{\infty} m_k I_{\lambda}(t - t_k). \quad (14)$$

We choose a particular integrating kernel $I_{\lambda}(t)$ and a particular $f_{\lambda}(t)$ [for which (10) is valid] such that

$$-f_{\lambda}(t) \leq I_{\lambda}(t) \leq f_{\lambda}(t), \quad -\infty < t < \infty, \quad (15)$$

and hence obtain

$$-c \int_{-\infty}^{\infty} f_{\lambda}(x)dx \leq h(t) \leq c \int_{-\infty}^{\infty} f_{\lambda}(x)dx, \quad -\infty < t < \infty. \quad (16)$$

The upper and lower bounds for $h(t)$ readily give an upper bound for the number of zeros of $s(t)$, counted according to multiplicity, in a closed interval of length T .

It is of interest to determine an upper bound for $|\hat{s}(t)|$, which amounts to determining an upper bound for $\hat{h}(t)$, the Hilbert transform of $h(t)$, in (5). Now $|\hat{h}(t)|$ is not bounded, since $\hat{h}(t)$ has logarithmic singularities at the discontinuities of $h(t)$, i.e., at the zeros of $s(t)$. However, $\hat{h}(t)$ is bounded above. The Hilbert transform is given by (see Ref. 4)

$$\hat{h}(t) = \int_{-\infty}^{\infty} h(x)K_{\lambda}(t-x)dx, \quad (17)$$

where K_{λ} is any function of the form

$$K_{\lambda}(t) = \frac{f_{\lambda}(t)}{\pi t} \quad (17a)$$

and

$$f_{\lambda}(t) \text{ is bandlimited to } [-\lambda, \lambda] \quad (17b)$$

$$f_{\lambda}(0) = 1 \quad (17c)$$

$$\int_{|t|>1} |f_{\lambda}(t)| \frac{dt}{|t|} < \infty. \quad (17d)$$

The integral in (17) is interpreted as a Cauchy principal value. With suitable further restrictions on f_{λ} we can write (17) as

$$\begin{aligned} \hat{h}(t) &= \frac{1}{\pi} \int_{-\infty}^{\infty} h'(x)L_{\lambda}(t-x)dx \\ &= \sum_{-\infty}^{\infty} m_k L_{\lambda}(t-t_k) - \frac{c}{\pi} \int_{-\infty}^{\infty} L_{\lambda}(x)dx, \end{aligned} \quad (18)$$

where

$$L_{\lambda}(t) = \int_{-\infty}^t \pi K_{\lambda}(x)dx, \quad t < 0, \quad (18a)$$

$$L_{\lambda}(t) = L_{\lambda}(-t). \quad (18b)$$

In accord with (17d) the integral in (18a) is absolutely convergent for $t < 0$ and we obtain (18b) by choosing f_{λ} even, and such that L_{λ} is integrable. For the problem here we further choose f_{λ} so that

$$L_{\lambda}(t) \leq 0, \quad -\infty < t < \infty, \quad (18c)$$

$$\begin{aligned}
\int_{-\infty}^{\infty} L_{\lambda}(x) dx &= 2 \int_{-\infty}^0 L_{\lambda}(x) dx \text{ (integrate by parts)} \\
&= \lim_{t \rightarrow 0} \left\{ t L_{\lambda}(t) - \pi \int_{-\infty}^t x K_{\lambda}(x) dx \right\} \\
&= -2 \int_{-\infty}^0 f_{\lambda}(x) dx = - \int_{-\infty}^{\infty} f_{\lambda}(x) dx. \quad (18d)
\end{aligned}$$

Then from (18), with (18c) and (18d), we have

$$\hat{h}(t) \leq \frac{c}{\pi} \int_{-\infty}^{\infty} f_{\lambda}(x) dx, \quad -\infty < t < \infty. \quad (19)$$

Here, we choose an appropriate f_{λ} , subject to (17b) through (17d) and (18c), so as to minimize the integral in (19).

The results stated below are sharp only for the case $2c/\lambda = m$, an integer. It is not at all clear how one would proceed to improve the results when $2c/\lambda$ is not an integer. Still, the results show that signals of the form (1) having only real zeros are very "nice" in that they behave, at worst, much like polynomials of order $[2c/\lambda]$ in $\cos \lambda t/2$.

II. RESULTS

Theorem 1: Let $s(t)$ be any function of the form

$$s(t) = \cos ct + g(t),$$

where $g(t)$ is a bounded real-valued function bandlimited to $[-b, b]$, $0 \leq b < c$, such that $s(t)$ has only real zeros $\{t_k\}$ with corresponding multiplicities $\{m_k\}$. Then the distribution

$$h'(t) = \pi \sum_{-\infty}^{\infty} m_k \delta(t - t_k) - c$$

has no spectrum in $(-\lambda, \lambda)$, where

$$\lambda = c - b.$$

That is, for every f_{λ} in L_1 of the form

$$f_{\lambda}(t) = \int_{-\lambda}^{\lambda} F(\omega) e^{i\omega t} d\omega$$

we have

$$\int_{-\infty}^{\infty} f_{\lambda}(t) h'(t) dt = 0$$

or

$$\frac{\pi}{c} \sum_{-\infty}^{\infty} m_k f_{\lambda}(t_k) = \int_{-\infty}^{\infty} f_{\lambda}(t) dt.$$

Theorem 2: Suppose

$$\sum_{-\infty}^{\infty} \mu_k f_{\lambda}(t_k) = \int_{-\infty}^{\infty} f_{\lambda}(t) dt,$$

where

$$\mu_k > 0, \quad t_{k+1} > t_k,$$

holds for every f_{λ} in L_1 of the form

$$f_{\lambda}(t) = \int_{-\lambda}^{\lambda} F(\omega) e^{i\omega t} d\omega.$$

Then

$$t_{k+1} - t_k \leq 2\pi/\lambda, \quad k = 0, \pm 1, \pm 2, \dots,$$

where equality holding for any k implies

$$t_k = \frac{2\pi}{\lambda} k + \theta, \quad k = 0, \pm 1, \pm 2, \dots$$

with

$$\mu_k = \frac{2\pi}{\lambda}, \quad k = 0, \pm 1, \pm 2, \dots$$

Corollary 2: Let $s(t)$ satisfy the hypotheses of Theorem 1. Then every interval of length $> 2\pi/\lambda$ contains at least one zero of $s(t)$. Furthermore, if $s(t)$ has a zero-free open interval of length $2\pi/\lambda$, then

$$\frac{2c}{\lambda} = m, \quad \text{an integer } (\geq 2),$$

and

$$s(t) = \frac{(-1)^n}{2} \left\{ 2 \cos\left(\frac{\lambda t}{2} + \frac{n\pi}{m}\right) \right\}^m,$$

where n is some integer.

Theorem 3: Under the hypotheses of Theorem 2, the distribution

$$\mu'(t) = \sum_{-\infty}^{\infty} \mu_k \delta(t - t_k) - 1$$

has an (unbiased) integral $\mu(t)$ satisfying

$$\frac{-\pi}{\lambda} \leq \mu(t) \leq \frac{\pi}{\lambda}, \quad -\infty < t < \infty,$$

where equality holding (on either side) for one value of t implies

$$t_k = \frac{2\pi}{\lambda} k + \theta, \quad k = 0, \pm 1, \pm 2, \dots$$

$$\mu_k = \frac{2\pi}{\lambda}, \quad k = 0, \pm 1, \pm 2, \dots$$

Corollary 3.1: Under the hypotheses of Theorem 1 there is a function of the form

$$h(t) = J(t) - ct,$$

where $J(t)$ is a jump function increasing by $m_k\pi$ at each zero t_k of multiplicity m_k , satisfying

$$\frac{-\pi c}{\lambda} \leq h(t) \leq \frac{\pi c}{\lambda}, \quad -\infty < t < \infty,$$

and

$$\int_{-\infty}^{\infty} h(t) f_{\lambda}(t) dt = 0$$

for every f_{λ} in L_1 whose Fourier transform vanishes outside $(-\lambda, \lambda)$,

$$\lambda = b - c > 0.$$

Furthermore, equality for one value of t in

$$|h(t)| \leq \frac{\pi c}{\lambda}$$

gives the same conclusion as Corollary 2.

Corollary 3.2: Let $s(t)$ satisfy the hypotheses of Theorem 1 and denote by $N_T(x)$, the number of zeros of $s(t)$, counted according to multiplicity, in the closed interval $[x, x + T]$. Then

$$N_T(x) \leq \frac{cT}{\pi} + \frac{2c}{\lambda}, \quad (-\infty < x < \infty)$$

with equality possible if, and only if,

$$\frac{2c}{\lambda} = m, \quad \text{an integer,}$$

and

$$s(t) = \frac{(-1)^n}{2} \left\{ 2 \cos\left(\frac{\lambda}{2} t + \frac{n\pi}{m}\right) \right\}^m, \quad n \text{ an integer,}$$

and x and $x + T$ are zeros of $s(t)$.

Theorem 4: Let $s(t)$ satisfy the hypotheses of Theorem 1. Then

$$|s(t)| \leq 2^{(2c/\lambda)-1}, \quad -\infty < t < \infty,$$

where equality for any t gives the conclusion of Corollary 2.

III. PROOF OF THEOREM 1

The basic definition of the class $\mathbf{H}(\lambda)$ of high-pass functions is as follows.

Definition: $\mathbf{H}(\lambda)$ consists of all functions $h(t)$ satisfying

$$1. \int_x^{x+T} |h(t)| dt \leq M(T), \quad -\infty < x < \infty$$

$$2. \int_{-\infty}^{\infty} h(t) f_\lambda(t) dt = 0, \quad \text{for all } f_\lambda \text{ in } L_1$$

whose Fourier transforms vanish outside $(-\lambda, \lambda)$.

The basic representation theorem for $\mathbf{H}(\lambda)$ established in Ref. 5 is as follows.

Representation Theorem: A real-valued function $h(t)$ belongs to $\mathbf{H}(\lambda)$, if, and only if,

$$h(t) = \lim_{u \rightarrow 0^+} h(t + iu) \text{ almost all } t,$$

where

$$h(t + iu) = \text{Re}\{H(t + iu)\}$$

and $H(\tau)$ is analytic in the upper-half plane $u > 0$,

$$|H(\tau)| = O(e^{-\lambda u}), \quad u \rightarrow \infty,$$

$$\int_x^{x+T} |h(t + iu)| dt \leq M(T), \quad -\infty < x < \infty, \quad u \geq 0.$$

Actually, $\mathbf{H}(\lambda)$ could have been defined to include distributions having limited mass in any interval of fixed length. As it stands, the closure of $\mathbf{H}(\lambda)$ includes such distributions.

We consider

$$H'(\tau) = i \frac{s'(\tau)}{s(\tau)} - c, \quad \tau = t + iu. \quad (20)$$

We have

$$\frac{s'(\tau)}{s(\tau)} = \frac{-c \sin c\tau + g'(\tau)}{\cos c\tau + g(\tau)}.$$

Since $g(t)$ and $g'(t)$ are bandlimited to $[-b, b]$, the growth of $g(\tau)$ and $g'(\tau)$ is no faster than that of $\cos b\tau$. Thus,

$$\begin{aligned} \frac{s'(t + iu)}{s(t + iu)} &= -c \tan c(t + iu) + O(e^{-\lambda u}), \quad u \rightarrow \infty, \\ &= -ic + O(e^{-\lambda u}), \quad u \rightarrow \infty (\lambda = c - b). \end{aligned} \quad (21)$$

We have

$$\frac{s'(\tau)}{s(\tau)} = \lim_{n \rightarrow \infty} \sum_{-n}^n \frac{m_k}{t - t_k}. \quad (22)$$

So

$$H'(t + iu) = \lim_{n \rightarrow \infty} i \sum_{-n}^n \frac{(t - t_k) - iu}{(t - t_k)^2 + u^2} m_k - c. \quad (23)$$

Setting

$$h'(t + iu) = \operatorname{Re}\{H'(t + iu)\} \quad (24)$$

we have

$$h'(t + iu) = \sum_{-\infty}^{\infty} \frac{m_k u}{(t - t_k)^2 + u^2} - c, \quad (25)$$

where the sum is absolutely convergent (p. 86, Ref. 6).

Now let $N_T(x)$ denote the number of zeros of $s(t)$, counted according to multiplicity, in the interval $[x - T, x + T]$. Then

$$\sum_{-\infty}^{\infty} \frac{m_k u}{(x - t_k)^2 + u^2} > N_T(x) \frac{u}{T^2 + u^2}.$$

Thus

$$N_T(x) \frac{u}{T^2 + u^2} < c + h'(x + iu).$$

Setting $u = T$ we have

$$N_T(x) < 2cT + 2Th'(x + iT). \quad (26)$$

Since $h'(x + iT) = O(e^{-\lambda T})$, $T \rightarrow \infty$, we have

$$N_T(x) < 2cT + \epsilon, \quad \text{for sufficiently large } T. \quad (27)$$

Now

$$\begin{aligned} \int_{x-T}^{x+T} |h'(t + iu)| dt &\leq 2cT + \int_{x-T}^{x+T} dt \left\{ \sum_{-\infty}^{\infty} \frac{m_k u}{(t - t_k)^2 + u^2} \right\} \\ &\leq 2cT + \int_{-\infty}^{\infty} \frac{u}{(t - x)^2 + u^2} N_T(t) dt \\ &\leq 2cT + \pi(2cT + \epsilon). \end{aligned} \quad (28)$$

It follows from (28) and (21) and the Representation Theorem that

$$\int_{-\infty}^{\infty} h'(t + iu)f_{\lambda}(t)dt = 0, \quad u > 0, \quad (29)$$

where f_{λ} is any function of L_1 given by a finite Fourier integral over $(-\lambda, \lambda)$. The integral in (29) is absolutely convergent.

$$\int_{-\infty}^{\infty} |h'(t + iu)| |f_{\lambda}(t)| dt \leq M(T) \sum \max_{kT \leq t \leq (k+1)T} |f_{\lambda}(t)| \quad (\text{see p. 101, Ref. 6})$$

with the bound independent of u .

Thus we may write

$$\int_{-\infty}^{\infty} h'(t + iu)f_{\lambda}(t)dt = \sum_k m_k \int_{-\infty}^{\infty} \frac{uf_{\lambda}(t)}{(t - t_k)^2 + u^2} dt - c \int_{-\infty}^{\infty} f_{\lambda}(t)dt$$

and let $u \rightarrow 0$ to obtain the quadrature formula

$$\frac{\pi}{c} \sum_{-\infty}^{\infty} m_k f_{\lambda}(t_k) = \int_{-\infty}^{\infty} f_{\lambda}(t)dt. \quad (30)$$

This completes the proof of Theorem 1.

IV. PROOF OF THEOREM 2

We are given for the stipulated f_{λ} ,

$$\sum_{-\infty}^{\infty} \mu_k f_{\lambda}(t_k) = \int_{-\infty}^{\infty} f_{\lambda}(t)dt$$

$$\mu_k > 0, \quad t_{k+1} > t_k, \quad (31)$$

and wish to prove that $t_{k+1} - t_k \leq 2\pi/\lambda$, all k . To do this we take

$$f_{\lambda}(t) = \frac{\left(\cos \frac{\lambda}{2} t\right)^2}{\frac{\pi^2}{\lambda^2} - t^2}, \quad (32)$$

which satisfies the stipulation and

$$f_{\lambda}(t) > 0, \quad \frac{-\pi}{\lambda} < t < \frac{\pi}{\lambda}, \quad (32a)$$

$$\leq 0, \quad |t| \geq \frac{\pi}{\lambda},$$

$$\int_{-\infty}^{\infty} f_{\lambda}(t) dt = 0. \quad (32b)$$

Now suppose in (31) that

$$t_{n+1} - t_n > \frac{2\pi}{\lambda}. \quad (33)$$

Setting $T_n = (t_{n+1} + t_n)/2$, we have for f_{λ} given by (32),

$$\sum_{-\infty}^{\infty} \mu_k f_{\lambda}(t_k - T_n) = 0, \quad (34)$$

where in accord with (33), $|t_k - T_n| > \pi/\lambda$, all k . Since

$$f_{\lambda}(t) \leq 0 \quad \text{for } |t| > \pi/\lambda$$

we conclude, since $\mu_k > 0$, that $t_k - T_n$ is a zero of $f_{\lambda}(t)$, greater in magnitude than the first; i.e., (33) implies

$$|t_k - T_n| = (2\nu_k + 1) \frac{\pi}{\lambda}, \quad \nu_k \text{ a positive integer (all } k). \quad (35)$$

But now if we apply the formula (31) to $g_{\lambda}(t - T_n)$, where

$$g_{\lambda}(t) = \frac{f_{\lambda}(t)}{\frac{\pi^2}{\lambda^2} - t^2} = \left\{ \frac{\cos \frac{\lambda}{2} t}{\frac{\pi^2}{\lambda^2} - t^2} \right\}^2 \geq 0 \quad (36)$$

we obtain, if (35) is true,

$$\int_{-\infty}^{\infty} g_{\lambda}(t - T_n) dt = \sum_{-\infty}^{\infty} \mu_k g_{\lambda}(t_k - T_n) = 0, \quad (37)$$

which is obviously false. Hence (33) is false, i.e., we must have

$$t_{k+1} - t_k \leq \frac{2\pi}{\lambda}, \quad \text{all } k. \quad (38)$$

Now suppose

$$t_{n+1} - t_n = \frac{2\pi}{\lambda}. \quad (39)$$

With the same f_{λ} as before, we conclude that (39) implies

$$t_k - T_n = (2\nu_k + 1)\pi/\lambda, \quad \nu_k \text{ an integer (all } k). \quad (40)$$

In other words, (39) implies that $(t_k - t_j)$ is an even multiple of π/λ , all k and j . We have established (38),

$$0 < t_{k+1} - t_k \leq \frac{2\pi}{\lambda} \quad \text{for all } k$$

Then (39) implies

$$t_k = \frac{2\pi}{\lambda} k + \theta, \quad k = 0, \pm 1, \pm 2, \dots \quad (41)$$

With t_k given by (41) we have for

$$s_\lambda(t) = \left\{ \frac{\sin \frac{\lambda}{2} t}{\frac{\lambda}{2} t} \right\}^2, \quad (42)$$

$$\begin{aligned} \int_{-\infty}^{\infty} s_\lambda(t - t_j) dt &= \sum_{-\infty}^{\infty} \mu_k s_\lambda(t_k - t_j) = \mu_j s_\lambda(0) \\ &= \mu_j = \frac{2\pi}{\lambda}, \quad \text{all } j, \end{aligned} \quad (43)$$

which completes the proof of Theorem 2.

V. PROOF OF COROLLARY 2

Under the hypotheses of Theorem 1 we have the quadrature formula,

$$\frac{\pi}{c} \sum_{-\infty}^{\infty} m_k f_\lambda(t_k) = \int_{-\infty}^{\infty} f_\lambda(t) dt,$$

where $\{t_k\}$ are the zeros of $s(t)$ having associated multiplicities $\{m_k\}$, $m_k \geq 1$, $t_{k+1} - t_k > 0$. It follows from Theorem 2 that $t_{k+1} - t_k \leq 2\pi/\lambda$, i.e., that every interval of length $> 2\pi/\lambda$ contains at least one zero of $s(t)$. Furthermore, if $t_{k+1} - t_k = 2\pi/\lambda$ for some k , then (Theorem 2)

$$t_k = \frac{(2k+1)\pi}{\lambda} + T, \quad \text{all } k,$$

$$\mu_k = \frac{\pi}{c} m_k = \frac{2\pi}{\lambda}, \quad \text{all } k,$$

i.e., the zeros have a common multiplicity

$$m_k = \frac{2c}{\lambda} = m \quad \text{an integer } (\geq 2).$$

Thus we can have $t_{k+1} - t_k = 2\pi/\lambda$ only if $2c/\lambda$ is an integer m (necessarily ≥ 2 , since $\lambda = c - b \leq c$) and then only if all zeros have multiplicity m on a lattice of spacing $2\pi/\lambda$; i.e., if

$$s(t) = A \left\{ 2 \cos \frac{\lambda}{2} (t - T) \right\}^m.$$

The possibilities for A and T are determined by the top frequency content;

$$s(t) = 2A \cos \frac{m\lambda}{2} (t - T) + g(t) = \cos \frac{m\lambda t}{2} + g(t),$$

i.e.,

$$\frac{m\lambda T}{2} = n\pi$$

$$2A = \cos n\pi.$$

VI. PROOF OF THEOREM 3

The high-pass distribution

$$\mu'(t) = \sum_{-\infty}^{\infty} \mu_k \delta(t - t_k) - 1, \quad \mu_k > 0, \quad (44)$$

has an unbiased integral given by

$$\mu(t) = \sum_{-\infty}^{\infty} \mu_k I_\lambda(t - t_k) - \int_{-\infty}^{\infty} I_\lambda(t) dt, \quad (45)$$

$$\int_{-\infty}^{\infty} |I_\lambda(t)| dt < \infty, \quad (45a)$$

$$\int_{-\infty}^{\infty} I_\lambda(t) e^{-i\omega t} dt = \frac{1}{i\omega}, \quad |\omega| \geq \lambda. \quad (45b)$$

It was shown in Ref. 3 that an equivalent description of an integrating kernel $I_\lambda(t)$ is

$$I_\lambda(t) = \frac{1}{2} \operatorname{sgn} t - g_\lambda(t), \quad (46)$$

where g_λ is any function bandlimited to $[-\lambda, \lambda]$ such that (45a) holds. A useful construction for g_λ is as follows.

Suppose $f_\lambda(t)$ is bandlimited to $[-\lambda, \lambda]$, even, and its analytic continuation $f(\tau)$ is positive on the imaginary axis. Then for each $\xi \geq 0$,

$$g_\lambda(t; \xi) = \frac{t \left\{ 1 - \frac{f_\lambda(t)}{f_\lambda(i\xi)} \right\}}{\pi(t^2 + \xi^2)} \quad (47)$$

is bandlimited to $[-\lambda, \lambda]$.

Now we define the bandlimited function g_λ as

$$g_\lambda(t) = \int_0^\infty g_\lambda(t; \xi) d\xi$$

$$\begin{aligned}
&= \frac{1}{\pi} \int_0^\infty \frac{t}{t^2 + \xi^2} d\xi - \frac{tf_\lambda(t)}{\pi} \int_0^\infty \frac{d\xi}{(t^2 + \xi^2)f_\lambda(i\xi)} \\
&= \frac{1}{2} \operatorname{sgn} t - \frac{tf_\lambda(t)}{\pi} \int_0^\infty \frac{d\xi}{(t^2 + \xi^2)f_\lambda(i\xi)}. \tag{48}
\end{aligned}$$

This gives the useful representation for integrating kernels

$$I_\lambda(t) = tf_\lambda(t) \int_0^\infty \frac{d\xi}{\pi(t^2 + \xi^2)f_\lambda(i\xi)}. \tag{49}$$

We have

$$\int_0^\infty \frac{d\xi}{\pi(t^2 + \xi^2)f_\lambda(i\xi)} < \frac{1}{t^2} \int_0^\infty \frac{d\xi}{f_\lambda(i\xi)}. \tag{50}$$

So I_λ will belong to L_1 if (and only if)

$$\int_{|t|>1} \frac{|f_\lambda(t)|}{|t|} dt < \infty. \tag{51}$$

Now if

$$f_\lambda(i\xi) > f_\lambda(0) \quad \text{for} \quad \xi > 0, \tag{52}$$

as is always the case for even f_λ having only real zeros,

$$f_\lambda(i\xi) = f_\lambda(0) \prod_k \left(1 + \frac{\xi^2}{t_k^2}\right),$$

then

$$\begin{aligned}
|t| \int_0^\infty \frac{d\xi}{\pi(t^2 + \xi^2)f_\lambda(i\xi)} &< \frac{1}{f_\lambda(0)} \frac{1}{\pi} \int_0^\infty \frac{|t| d\xi}{t^2 + \xi^2} \\
&= \frac{1}{2f_\lambda(0)}, \quad (t \neq 0). \tag{53}
\end{aligned}$$

Thus if (51) and (52) hold, we have

$$|I_\lambda(t)| \leq \frac{1}{2} \frac{|f_\lambda(t)|}{|f_\lambda(0)|}, \quad -\infty < t < \infty, \tag{54}$$

with equality for some nonzero t_k if and only if $f_\lambda(t_k) = 0$.

Now we choose

$$f_\lambda(t) = \frac{1}{2} \left\{ \frac{\sin \frac{\lambda}{2} t}{\frac{\lambda}{2} t} \right\}^2 \tag{55}$$

so that the corresponding integrating kernel (49) is odd and satisfies

$$-f_\lambda(t) \leq I_\lambda(t) \leq f_\lambda(t). \quad (56)$$

We then have for this I_λ

$$\mu(t) = \sum_{-\infty}^{\infty} \mu_k I_\lambda(t - t_k), \quad (57)$$

and since $\mu_k > 0$, we have

$$\mu(t) \geq - \sum_{-\infty}^{\infty} \mu_k f_\lambda(t - t_k) \quad (57a)$$

$$\leq \sum_{-\infty}^{\infty} \mu_k f_\lambda(t - t_k). \quad (57b)$$

But

$$\sum_{-\infty}^{\infty} \mu_k f_\lambda(t - t_k) = \int_{-\infty}^{\infty} f_\lambda(t - x) dx = \frac{\pi}{\lambda}.$$

Therefore,

$$\frac{-\pi}{\lambda} \leq \mu(t) \leq \frac{\pi}{\lambda}, \quad -\infty < t < \infty. \quad (58)$$

We have equality holding on either side in (56) only for $t = 2k\pi/\lambda$, $k \neq 0$, with

$$I_\lambda(0+) = f_\lambda(0) = 1/2$$

$$I_\lambda(0-) = -f_\lambda(0) = -1/2.$$

So equality can hold in (57a) as a limit from the left, and in (57b) as a limit from the right, if and only if

$$t_k = \frac{2k\pi}{\lambda} + \theta, \quad \text{all } k, \quad (59)$$

implying as before

$$\mu_k = \frac{2\pi}{k}, \quad \text{all } k. \quad (60)$$

VII. PROOF OF COROLLARY 3.1

We set $h'(t)/c = \mu'(t)$ and apply Theorem 3 to obtain

$$\frac{-\pi c}{\lambda} \leq h(t) \leq \frac{\pi c}{\lambda}. \quad (61)$$

If f_λ is any function of L_1 whose Fourier transform vanishes outside $(-\lambda, \lambda)$, then

$$\int_{-\infty}^{\infty} f_{\lambda}(t)h(t)dt = \int_{-\infty}^{\infty} g_{\lambda}(t)h'(t)dt,$$

where

$$g_{\lambda}(t) = \int_{-\infty}^{\infty} f_{\lambda}(x)I_{\lambda}(t-x)dx \quad (62a)$$

$$\int_{-\infty}^{\infty} |g_{\lambda}(t)|dt \leq \int_{-\infty}^{\infty} |f_{\lambda}(t)|dt \cdot \int_{-\infty}^{\infty} |I_{\lambda}(t)|dt. \quad (62b)$$

Thus g_{λ} belongs to L_1 and its Fourier transform

$$\tilde{g}_{\lambda}(\omega) = \tilde{f}_{\lambda}(\omega)\tilde{I}_{\lambda}(\omega)$$

vanishes outside $(-\lambda, \lambda)$. Hence

$$\int_{-\infty}^{\infty} f_{\lambda}(t)h(t)dt = \int_{-\infty}^{\infty} g_{\lambda}(t)h'(t)dt = 0. \quad (63)$$

We could also establish this result by using the Representation Theorem for high-pass functions in Section III, and identifying $h(t)$ as

$$h(t) = \lim_{u \rightarrow 0^+} \operatorname{Re}\{H(t + iu)\}, \quad (64)$$

where

$$H(\tau) = i \log G(\tau) \quad (64a)$$

and

$$G(\tau) = 2e^{icr}s(\tau) = 1 + 2e^{icr}g(\tau) + e^{2icr} \quad (65)$$

$$G(t + iu) = 1 + 0(e^{-\lambda u}), \quad u \rightarrow \infty. \quad (65a)$$

Here $H(\tau)$ is a particular integral of $H'(\tau)$ defined in (20), viz.,

$$H(\tau) = - \int_{\tau}^{i\infty} H'(z)dz. \quad (66)$$

However, bounds on $h(t)$ are not readily available from the representation (64) or (66), but more so from the unbiased integral of $h'(t)$.

The conditions for equality are argued as before in the proof of Corollary 2.

VIII. PROOF OF COROLLARY 3.2

We have

$$\mu'(t) = \frac{1}{c} h'(t) = \frac{\pi}{c} \sum_{-\infty}^{\infty} m_k \delta(t - t_k) - 1. \quad (67)$$

Then

$$\int_{x-0}^{x+T+0} \mu'(t)dt = \mu(x + T + 0) - \mu(x - 0). \quad (68)$$

Now the number of zeros of $s(t)$ in $[x, x + T]$ is

$$N_T(x) = \sum_{k:x \leq t_k \leq x+T} m_k. \quad (69)$$

Thus

$$\int_{x-0}^{x+T+0} \mu'(t)dt = \frac{\pi}{c} N_T(x) - T. \quad (70)$$

According to Theorem 3

$$\frac{-\pi}{\lambda} \leq \mu(t) \leq \frac{\pi}{\lambda}.$$

So

$$\frac{\pi}{c} N_T(x) - T \leq \frac{2\pi}{\lambda},$$

or

$$N_T(x) \leq \frac{2c}{\lambda} + \frac{c}{\pi} T. \quad (71)$$

The implications of equality are argued again as in Corollary 2.

IX. PROOF OF THEOREM 4

We have [cf. (64) and (65)]

$$h(t) + i\hat{h}(t) = \lim_{u \rightarrow 0^+} i \log\{e^{ic(t+iu)} 2s(t + iu)\}, \quad (72)$$

where \hat{h} is the Hilbert transform of h .

Then

$$|s(t)| = \frac{1}{2} e^{\hat{h}(t)}. \quad (73)$$

To obtain an upper bound on \hat{h} we use (18); i.e.,

$$\hat{h}(t) = \sum_{-\infty}^{\infty} m_k L_\lambda(t - t_k) - \frac{c}{\pi} \int_{-\infty}^{\infty} L_\lambda(x) dx, \quad (74)$$

where

$$L_\lambda(t) = \int_{-\infty}^t f_\lambda(x) dx, \quad t < 0, \quad (74a)$$

$$L_\lambda(t) = L_\lambda(-t) \quad (74b)$$

$$f_\lambda \text{ is bandlimited to } [-\lambda, \lambda] \quad (74c)$$

$$\text{with } f_\lambda(0) = 1,$$

$$f_\lambda(t) = f_\lambda(-t),$$

$$\text{and such that } \int_{-\infty}^{\infty} |L_\lambda(t)| dt < \infty.$$

We want an upper bound on $\hat{h}(t)$, say $\hat{h}(0)$. Since $\{m_k\}$ are positive (integers), we would like

$$L_\lambda(t) \leq 0, \quad -\infty < t < \infty, \quad (75)$$

so that

$$\hat{h}(t) \leq -\frac{c}{\pi} \int_{-\infty}^{\infty} L_\lambda(x) dx, \quad -\infty < t < \infty. \quad (76)$$

Then equality, e.g.,

$$\hat{h}(0) = -\frac{c}{\pi} \int_{-\infty}^{\infty} L_\lambda(x) dx,$$

would imply $L_\lambda(-t_k) = 0$, all k .

We expect the lattice distribution is extremal again, requiring $L_\lambda(t)$ to vanish with $(\cos \lambda t/2)^2$ in order to obtain the least upper bound for \hat{h} . We need an alternate construction for L_λ . To obtain this we write

$$\begin{aligned} L_\lambda(t) &= - \int_t^\infty \frac{f_\lambda(x)}{x} dx, \quad t > 0, \\ &= \log t + \int_t^1 \frac{1 - f_\lambda(x)}{x} dx - \int_1^\infty \frac{f_\lambda(x)}{x} dx. \end{aligned}$$

Then, since L_λ is even we have

$$L_\lambda(t) = \log |t| + F_\lambda(t), \quad (77)$$

where F_λ is an even entire function of exponential type λ such that $L_\lambda(t)$ is absolutely integrable,

$$F_\lambda(t) = \int_t^1 \frac{1 - f_\lambda(x)}{x} dx - \int_1^\infty \frac{f_\lambda(x)}{x} dx, \quad (77a)$$

$$F'_\lambda(t) = \frac{f_\lambda(t) - 1}{t}. \quad (77b)$$

Now we obtain an alternate construction for F_λ .

We suppose that g_λ is an even entire function of exponential type λ , positive on the imaginary axis and define for each $\xi \geq 0$

$$G_{\lambda}(t; \xi) = \frac{\xi \left(1 - \frac{g_{\lambda}(t)}{g_{\lambda}(i\xi)}\right)}{t^2 + \xi^2} - \frac{\xi}{1 + \xi^2}. \quad (78)$$

Then we set

$$\begin{aligned} F_{\lambda}(t) &= \int_0^{\infty} G_{\lambda}(t; \xi) d\xi \\ &= \int_0^{\infty} \left(\frac{\xi}{t^2 + \xi^2} - \frac{\xi}{1 + \xi^2} \right) d\xi - g_{\lambda}(t) \int_0^{\infty} \frac{\xi}{(t^2 + \xi^2)g_{\lambda}(i\xi)} d\xi \\ &= -\log|t| - g_{\lambda}(t) \int_0^{\infty} \frac{\xi d\xi}{(t^2 + \xi^2)g_{\lambda}(i\xi)} \end{aligned} \quad (79)$$

and then

$$L_{\lambda}(t) = \log|t| + F_{\lambda}(t) = -g_{\lambda}(t) \int_0^{\infty} \frac{\xi d\xi}{(t^2 + \xi^2)g_{\lambda}(i\xi)}. \quad (80)$$

We have

$$L_{\lambda}(t) \sim -\frac{g_{\lambda}(t)}{t^2} \int_0^{\infty} \frac{\xi d\xi}{g_{\lambda}(i\xi)}, \quad t \rightarrow \infty. \quad (81)$$

So L_{λ} will be absolutely integrable if (and only if)

$$\int_{|t|>1} |g_{\lambda}(t)| \frac{dt}{t^2} < \infty. \quad (82)$$

The particular L_{λ} we want is

$$L_{\lambda}(t) = -\cos^2 \frac{\lambda t}{2} \int_0^{\infty} \frac{\xi d\xi}{(t^2 + \xi^2) \cosh^2 \frac{\lambda \xi}{2}}. \quad (83)$$

We can evaluate the integral of L_{λ} indirectly by considering

$$\begin{aligned} \frac{2c}{\lambda} &= m, \\ s(t) &= \frac{1}{2} \left(2 \cos \frac{\lambda t}{2} \right)^m. \end{aligned}$$

Then

$$\log 2|s(t)| = \sum_{-\infty}^{\infty} m L_{\lambda}(t - t_k) - \frac{c}{\pi} \int_{-\infty}^{\infty} L_{\lambda}(x) dx,$$

where

$$t_k = (2k + 1) \frac{\pi}{\lambda},$$

$$\log 2 |s(0)| = -\frac{c}{\pi} \int_{-\infty}^{\infty} L_{\lambda}(x) dx,$$

$$m \log 2 = -\frac{m\lambda}{2\pi} \int_{-\infty}^{\infty} L_{\lambda}(x) dx,$$

i.e., for L_{λ} given by (83) we have

$$\int_{-\infty}^{\infty} L_{\lambda}(t) dt = -\frac{2\pi}{\lambda} \log 2. \quad (84)$$

Thus we have from (84) and (76)

$$\hat{h}(t) \leq \frac{2c}{\lambda} \log 2, \quad -\infty < t < \infty, \quad (85)$$

with equality attainable only for the lattice distribution, giving

$$|s(t)| \leq 2^{(2c/\lambda)-1}, \quad -\infty < t < \infty, \quad (86)$$

where equality for any t implies the conclusion of Corollary 2, by the same argument.

REFERENCES

1. B. F. Logan, Jr., "Signals Designed for Recovery after Clipping—I. Localization of Infinite Products," AT&T Bell Lab. Tech. J., 63, No. 2 (February 1984), pp. 261-85.
2. B. F. Logan, Jr., "Signals Designed for Recovery after Clipping—II. Fourier Transform Theory of Recovery," AT&T Bell Lab. Tech. J., 63, No. 2 (February 1984), pp. 287-306.
3. B. F. Logan, Jr., "Integrals of High-Pass Functions," SIAM J. Math. Anal., 15, No. 2 (March 1984), pp. 389-405.
4. B. F. Logan, Jr., "Optimal Truncation of the Hilbert Transform Kernel for Bounded High-Pass Functions," Proc. Fifth Annual Princeton Conference on Information Sciences and Systems, Dept. of Elec. Eng., Princeton Univ., Princeton, N.J., 1971, pp. 10-12.
5. B. F. Logan, Jr., "Properties of High-Pass Signals," doctoral thesis, Elec. Eng. Dept., Columbia Univ., New York, 1965.
6. R. P. Boas, Jr., *Entire Functions*, New York; Academic Press, 1974.

AUTHOR

Benjamin F. Logan, Jr., B.S. (Electrical Engineering), 1946, Texas Technological College; M.S., 1951, Massachusetts Institute of Technology; Eng.D.Sc. (Electrical Engineering), 1965, Columbia University; AT&T Bell Laboratories, 1956—. While at MIT, Mr. Logan was a research assistant in the Research Laboratory of Electronics, investigating characteristics of high-power electrical discharge lamps. Also at MIT he engaged in analog computer development at the Dynamic Analysis and Control Laboratory. From 1955 to 1956 he worked for Hycon-Eastern, Inc., where he was concerned with the design of airborne power supplies. He joined AT&T Bell Laboratories as a member of the Visual and Acoustics Research Department, where he was concerned with the processing of speech signals. Currently, he is a member of the Mathematical Research Department. Member, Sigma Xi, Tau Beta Pi.

Click Modulation

By B. F. LOGAN, JR.*

(Manuscript received March 26, 1982)

In this paper we show how one may determine a sequence of equal intensity impulses or clicks

$$\pi \sum_{-\infty}^{\infty} \delta(t - t_k)$$

such that a desired bandpass signal, $f'(t)$, may be obtained by filtering the clicks; i.e.,

$$f'(t) = \pi \sum_{-\infty}^{\infty} K(t - t_k),$$

where $K(t)$ is the impulse response of a suitable bandpass filter. The $\{t_k\}$ are found as the zeros of a bandlimited signal $s(t)$, where if $f(t)$, the bandpass signal whose derivative is $f'(t)$, is sufficiently small, we also have

$$f(t) = \int_{-\infty}^{\infty} q(x)K(t - x)dx,$$

where $q(x)$ is a square wave simply related to $s(t)$.

I. INTRODUCTION

Click modulation describes a sort of pulse-position modulation leading to a sequence of equal-intensity impulses or clicks,

$$\pi \sum_{-\infty}^{\infty} \delta(t - t_k) \tag{1}$$

* AT&T Bell Laboratories.

Copyright © 1984 AT&T. Photo reproduction for noncommercial use is permitted without payment of royalty provided that each reproduction is done without alteration and that the Journal reference and copyright notice are included on the first page. The title and abstract, but no other portions, of this paper may be copied or distributed royalty free by computer-based and other information-service systems without further permission. Permission to reproduce or republish any other portion of this paper must be obtained from the Editor.

such that a desired signal, say $f'(t)$, may be obtained by filtering the clicks; i.e.,

$$f'(t) = \pi \sum_{-\infty}^{\infty} K(t - t_k). \quad (2)$$

Here we suppose that $f'(t)$ is a bandpass signal with spectrum confined to $[\lambda, \mu]$ and $[-\mu, -\lambda]$, $0 < \lambda < \mu < \infty$, and $K(t)$ is any function satisfying

$$\int_{-\infty}^{\infty} |K(t)| dt < \infty \quad (3a)$$

$$\int_{-\infty}^{\infty} K(t) dt = 0 \quad (3b)$$

$$\begin{aligned} \tilde{K}(\omega) &= \int_{-\infty}^{\infty} K(t)e^{-i\omega t} dt = 1, \begin{cases} \lambda \leq \omega \leq \mu \\ -\mu \leq \omega \leq -\lambda \end{cases} \\ &= 0, |\omega| > \alpha. \end{aligned} \quad (3c)$$

The filter characterized by $K(t)$ is required to reproduce $f'(t)$, reject dc, and reject frequencies greater than α , where α is some specified frequency ($\alpha > \mu$). (See Fig. 1.) In other words, we are supposing some constant c , such that the "Fourier transforms" of $f'(t)$ and $h'(t)$ agree over $(-\alpha, \alpha)$, where

$$h'(t) = \pi \sum_{-\infty}^{\infty} \delta(t - t_k) - c. \quad (4)$$

The distribution $h'(t)$ then has no spectrum in $(-\lambda, \lambda)$ nor in the guard band (μ, α) and its reflection. In some applications a large guard band may be required to ease the filtering problem, while in others, e.g., audio, a small guard band may be tolerable.

II. THE SOLUTION OF THE PROBLEM OF CLICK MODULATION

The problem of click modulation is given $f'(t)$, λ , μ , and α , to find a set $\{t_k\}$ such that (2) holds. The basis for solving this problem is found in Refs. 1 through 4. The $\{t_k\}$ are assumed to be the zeros (real and simple) of a signal of the form

$$s(t) = \cos ct + g(t), \quad (5)$$

where g is bandlimited to $[-b, b]$ and

$$c - b = \lambda > 0 \quad (5a)$$

$$c > \alpha > \mu. \quad (5b)$$

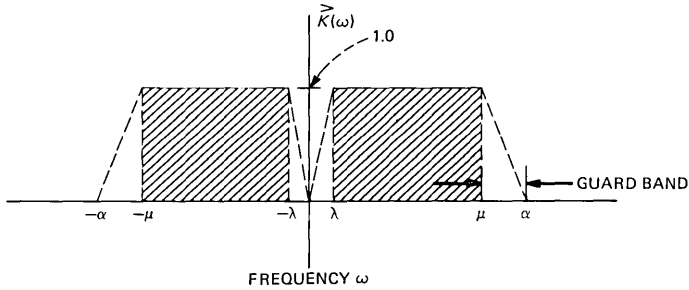


Fig. 1—Filter characteristic $K(\omega)$ for bandlimiting impulse train (clicks) to recover desired signal $f'(t)$ of spectral support $[-\mu, -\lambda] \cup [\lambda, \mu]$.

Then the function defined by

$$H(\tau) = i \log[2e^{ic\tau}s(\tau)] \quad (6)$$

is analytic in the upper half-plane of the complex variable $\tau = t + iu$, where the principal branch of log is taken;

$$\log(1 + z) = z + O(z^2), \quad z \rightarrow 0$$

giving

$$|H(t + iu)| = O(e^{-\lambda u}), \quad u \rightarrow \infty. \quad (7)$$

The function $h(t)$, defined by

$$h(t) = \lim_{u \rightarrow 0^+} \operatorname{Re}\{H(t + iu)\} \quad (8)$$

has the form

$$h(t) = J(t) - ct, \quad (9)$$

where $J(t)$ is a jump function increasing by π at each zero t_k of s , and h is high-pass with no spectrum in $(-\lambda, \lambda)$.

We then suppose that $f(t)$, with spectrum confined to $[\lambda, \mu]$ and $[-\lambda, -\mu]$, is given by

$$f(t) = \int_{-\infty}^{\infty} h(x)K(t - x)dx, \quad (10)$$

where K satisfies (3a), (3b), and (3c). Then differentiating, we obtain

$$\begin{aligned} f'(t) &= \int_{-\infty}^{\infty} h'(x)K(t - x)dx \\ &= \pi \sum_{-\infty}^{\infty} K(t - t_k). \end{aligned} \quad (11)$$

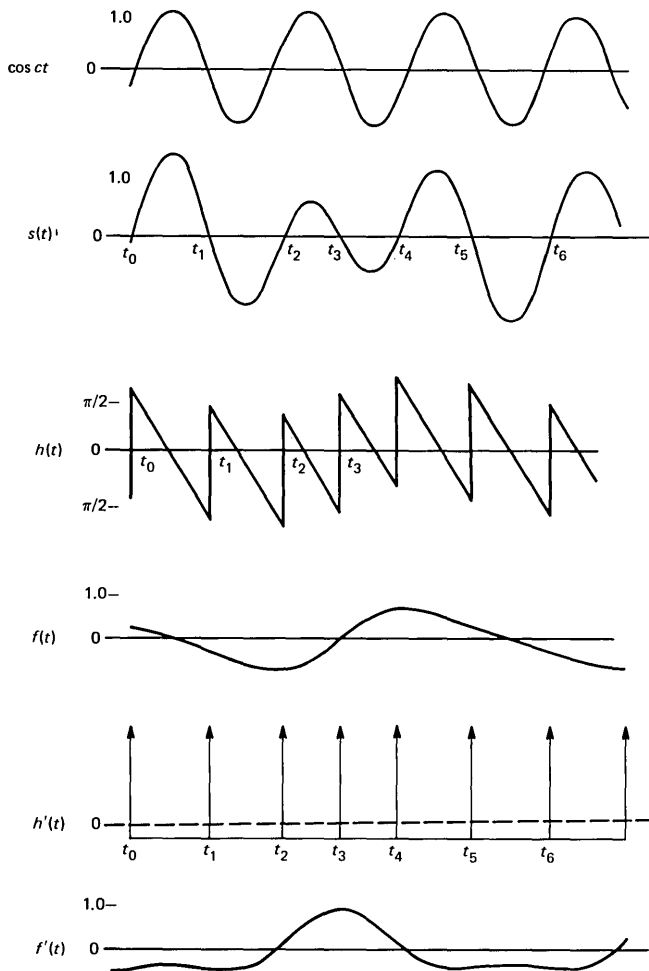


Fig. 2—Waveform relations in click modulation.

The relationships of $s(t)$, $h(t)$, $f(t)$, $h'(t)$, and $f'(t)$ are illustrated in Fig. 2.

Now we would like to find $s(t)$ and hence $h(t)$ so that (10) holds. To do this it is convenient to work with “analytic signals” having no negative frequency content, or in the terminology of Ref. 4, functions whose “Fourier transforms vanish over $(-\infty, 0)$ ”. (Refer to Fig. 3 in the course of the following development.) Thus we introduce

$$F(t) = f(t) + i\hat{f}(t), \quad (12)$$

where \hat{f} is the Hilbert transform of f . Then the Fourier transform of

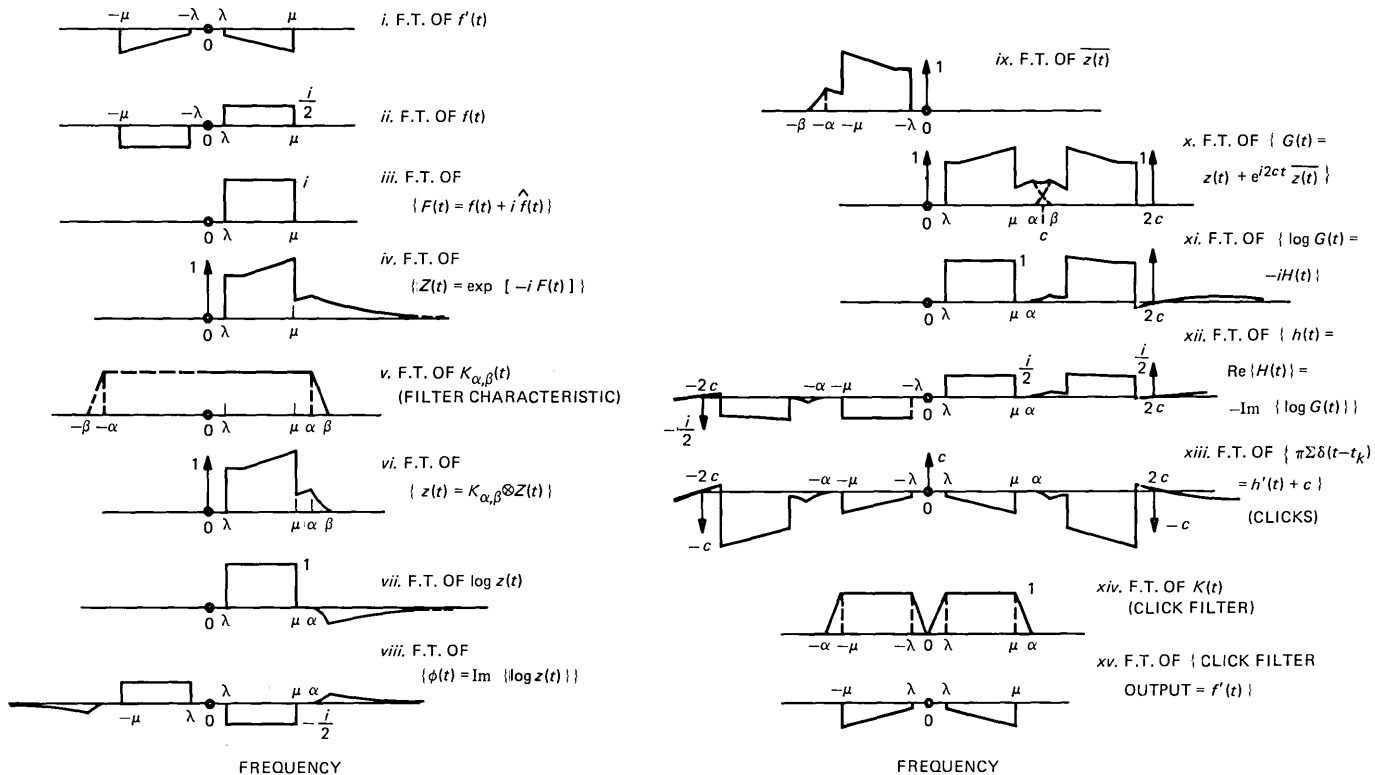


Fig. 3—Depiction of Fourier Transform (F.T.) relations in derivation of click modulation.

F vanishes outside the single interval $[\lambda, \mu]$. [It is important to note that a bounded bandpass signal f always has a bounded Hilbert transform \hat{f} .] Now we require that the Fourier transforms of $H(t)$ and $F(t)$ agree over $(-\infty, \alpha)$, i.e., in accord with (10),

$$F(t) = \int_{-\infty}^{\infty} H(x)K(t-x)dx. \quad (13)$$

We define

$$Z(t) = \exp[-iF(t)] \quad (14)$$

and then bandlimit Z to obtain

$$z(t) = \int_{-\infty}^{\infty} Z(x)K_{\alpha,\beta}(t-x)dx, \quad (15)$$

where the filter kernel $K_{\alpha,\beta}$ is absolutely integrable and

$$\begin{aligned} K_{\alpha,\beta}^>(\omega) &= \int_{-\infty}^{\infty} K_{\alpha,\beta}(t)e^{-i\omega t}dt \\ &= 1 \quad \text{for } 0 \leq \omega \leq \alpha \\ &= 0 \quad \text{for } \omega \geq \beta, \quad (\beta > \alpha). \end{aligned} \quad (15a)$$

Thus $z(t)$ is bandlimited to $[0, \beta]$, and the Fourier transforms of $z(t)$ and $Z(t)$ agree over $(-\infty, \alpha)$.

Now we set

$$\begin{aligned} G(t) = G(t; \theta, c) &= z(t) + e^{i2(ct+\theta)}\overline{z(t)} \\ &= e^{i(ct+\theta)}[z(t)e^{-i(ct+\theta)} + \overline{z(t)}e^{i(ct+\theta)}], \end{aligned} \quad (16)$$

where

$$2c - \beta \geq \alpha, \quad (16a)$$

$$\theta \text{ is any fixed angle,} \quad (16b)$$

and $\overline{z(t)}$ is the complex conjugate of $z(t)$. Now the Fourier transform of $\overline{z(t)}$ vanishes outside $[-\beta, 0]$. Thus the Fourier transform of

$$e^{i2(ct+\theta)}\overline{z(t)}$$

vanishes outside $[2c - \beta, 2c]$, and since $2c - \beta \geq \alpha$, the Fourier transforms of $Z(t)$, $z(t)$, and $G(t)$ agree over $(-\infty, \alpha)$. These relations are depicted in Fig. 3, parts (iv), (vi), and (x). Note that

$$Z(t) = \exp[-iF(t)] = 1 - iF(t) - \frac{F^2(t)}{2!} + \dots, \quad (17)$$

and since the Fourier transform of $\{F(t)\}^n$ vanishes outside $[n\lambda, n\mu]$, $Z(t)$ has a spectral gap $(0, \lambda)$.

We may write (16) as

$$G(t) = 2e^{i(ct+\theta)}s(t), \quad (18)$$

where

$$s(t) = \frac{1}{2} [z(t)e^{-i(ct+\theta)} + \bar{z}(t)e^{i(ct+\theta)}] \quad (19)$$

is real-valued and bandlimited to $[-c, c]$, and is of the form

$$s(t) = \cos(ct + \theta) + g(t), \quad (19a)$$

where g is bandlimited to $[-b, b]$, $b = c - \lambda$.

Now we suppose $s(\tau)$ has only real zeros. Then $\log G(\tau)$ is analytic in the upper half-plane. We compare it with

$$\log Z(\tau) = -iF(\tau),$$

which is certainly analytic in the upper half-plane. Since the Fourier transforms of $Z(t)$ and $G(t)$ agree over $(-\infty, \alpha)$ and both $\log Z(\tau)$ and $\log G(\tau)$ are analytic in the upper half-plane, it follows from the theory in Ref. 4 that the Fourier transforms of $\log G(t)$ and $\log Z(t)$ also agree over $(-\infty, \alpha)$; i.e., the Fourier transforms of

$$H(t) = i \log G(t)$$

and

$$F(t) = i \log Z(t)$$

agree over $(-\infty, \alpha)$ provided $s(\tau)$, the analytical continuation of $s(t)$ given by (19), has only real zeros $\{t_k\}$. We also require the zeros to be simple so that $h(t) = \text{Re}\{H(t)\}$ has the form (9). It was shown in Ref. 5 that a sufficient condition for s of the form (19), ($c > \beta/2$), to have only real simple zeros is that $z(\tau)$ be zero-free in the (closed) upper half-plane, $\text{Im } \tau \geq 0$.

Thus if $z(\tau)$, the analytic continuation of $z(t)$ obtained by bandlimiting $Z(t)$ where $Z(t) = \exp[-iF(t)]$, is zero-free in the upper half-plane $\text{Im } \tau \geq 0$, then $\log z(\tau)$ is analytic in the upper half-plane and then the Fourier transforms of

$$H(t) = i \log G(t),$$

$$F(t) = i \log Z(t),$$

and

$$i \log z(t)$$

agree over $(-\infty, \alpha)$, which means that the Fourier transforms of the real (imaginary) parts of these functions agree over $(-\alpha, \alpha)$.

Writing

$$z(t) = A(t)e^{i\phi(t)}, \quad (20)$$

where

$$A(t) = |z(t)|, \\ \phi(t) = \text{Im}\{\log z(t)\} = \text{phase } z(t),$$

we have the Fourier transforms of $h(t)$, $f(t)$, and $-\phi(t)$ agreeing over $(-\alpha, \alpha)$ whenever $z(\tau)$ is zero-free in the upper half-plane, $\text{Im } \tau \geq 0$.

Using (20), we may write

$$s(t) = A(t)\cos[ct + \theta - \phi(t)]. \quad (21)$$

Thus the zeros t_k of $s(t)$ are the zeros of the phase-modulated cosine,

$$\Phi(t) = \cos[ct + \theta - \phi(t)], \quad (22)$$

where $\phi(t)$ is the phase function of an analytic signal $z(t)$, with $z(t)$ bandlimited to $[0, \beta]$ and $z(t + iu)$ zero-free for $u \geq 0$, such that the Fourier transforms of $-\phi(t)$ and $f(t)$ agree over $(-\alpha, \alpha)$, $(\mu < \alpha < \beta)$, and

$$c \geq \frac{\alpha + \beta}{2}.$$

Now $\phi(t)$ is not bandlimited, but

$$-\phi(t) = f(t) + \epsilon(t), \quad (23)$$

where $\epsilon(t)$ is high-pass with no spectrum in $(-\alpha, \alpha)$ and $|\epsilon|$ may be small compared to $|f|$ if $|f|$ is small, or if α, β , and c are large compared to μ .

We have noted that the Fourier transforms of $-\phi(t)$, $f(t)$, and $h(t)$ agree over $(-\alpha, \alpha)$. It is interesting to observe that

$$h(t_k) = -\phi(t_k) \quad (24)$$

provided we take

$$h(t_k) = \frac{1}{2} [h(t_k+) + h(t_k-)], \quad (24a)$$

which, incidentally, follows by defining

$$h(t) = \lim_{u \rightarrow 0+} \text{Re}\{H(t + iu)\}.$$

To see (24) we consider

$$\begin{aligned} \log G(t) - \log z(\tau) &= \log \left\{ 1 + \frac{\overline{z(\tau)}}{z(\tau)} e^{i2(c\tau+\theta)} \right\} \\ &= \log[1 + U(\tau)], \end{aligned} \tag{25}$$

where

$$U(t) = e^{i2(ct+\theta-\phi(t))}$$

and

$$|U(t + iu)| \leq e^{-(2c-\beta)u}, \quad u \geq 0. \tag{25a}$$

We have shown elsewhere⁵ that

$$\phi'(t) \leq \beta/2$$

so that the total phase of $U(t)$ is an increasing function. With $|U(t)| = 1$, we have for the principal branch of the logarithm

$$-\pi/2 \leq \arg\{1 + U(t)\} \leq \pi/2. \tag{26}$$

We have $U(t_k) = -1$ and since the phase is increasing

$$\begin{aligned} \arg\{1 + U(t_{k-})\} &= \pi/2 \\ \arg\{1 + U(t_{k+})\} &= -\pi/2. \end{aligned}$$

Thus

$$\operatorname{Re}\{i \log G(t_{k-}) - i \log z(t_{k-})\} = h(t_{k-}) + \phi(t_k) = -\pi/2$$

$$\operatorname{Re}\{i \log G(t_{k+}) - i \log z(t_{k+})\} = h(t_{k+}) + \phi(t_k) = \pi/2$$

from which (24) follows. In fact, we have from (25) and (26)

$$-\pi/2 \leq h(t) + \phi(t) \leq \pi/2. \tag{27}$$

Then (24) follows from (27) and the fact that $\phi(t)$ is continuous with $h(t)$ increasing by π at t_k .

The condition that $z(\tau)$ be zero-free in the upper half-plane is difficult to quantify precisely in terms of all the parameters. Generally speaking, for fixed α and β , $z(\tau)$ will be zero-free in the upper half-plane if $\sup |F(t)|$ is sufficiently small. The problem is much the same as that of determining the bandwidth requirements for exponential single-sideband modulation.⁴ The problem will be treated in detail in a future paper. Suffice it here to say that a sufficient condition is

$$\operatorname{Re}\{z(t)\} > 0, \quad -\infty < t < \infty, \tag{28}$$

or

$$-\pi/2 < \phi(t) < \pi/2, \quad -\infty < t < \infty. \tag{29}$$

This condition is also of interest in obtaining a square wave representation of $f(t)$.

III. SQUARE WAVE REPRESENTATION OF $f(t)$

When $|\phi(t)| < \pi/2$, the zeros t_k of

$$s(t) = A(t)\cos[ct + \theta - \phi(t)] \quad (30)$$

interlace with the zeros of

$$\sin(ct + \theta).$$

For simplicity of discussion, we assume $\theta = 0$ (consider a translate). Then, as shown in Ref. 1, we have

$$h(k\pi/c) = 0 \quad k = 0, \pm 1, \pm 2, \dots \quad (31)$$

$$-\pi < h(t) < \pi. \quad (32)$$

Then if we subtract from $h(t)$ the periodic sawtooth function defined by

$$\begin{aligned} \sigma(t) &= \pi/2 - ct, & 0 < t < \pi/c, \\ \sigma(t) &= \sigma(t + \pi/c) \\ \sigma(0) &= 0, \end{aligned} \quad (33)$$

we obtain a square wave,

$$q(t) = h(t) - \sigma(t) = -\frac{\pi}{2} \{\text{sgn } s(t)\} \cdot \{\text{sgn } \sin ct\} \quad (34)$$

(see Fig. 4).

The Fourier series for $\sigma(t)$ is

$$\sigma(t) = \sum_1^{\infty} \frac{1}{n} \sin 2nct;$$

so the Fourier transforms of $q(t)$ and $h(t)$ agree over $(-2c, 2c)$, and since $c > \alpha$, the Fourier transforms of $q(t)$ and $f(t)$ agree over $(-\alpha, \alpha)$.

Thus we may filter the square wave to obtain $f(t)$:

$$f(t) = \int_{-\infty}^{\infty} q(x)K(t-x)dx, \quad (35)$$

where K is a reproducing kernel for f , which rejects all frequencies outside $(-\alpha, \alpha)$.

The square wave representation of $f(t)$ is of practical interest. First, one may regard the formulas (34) and (35) as a practical way of demodulating $s(t)$ after it is transmitted through a nonlinear medium.

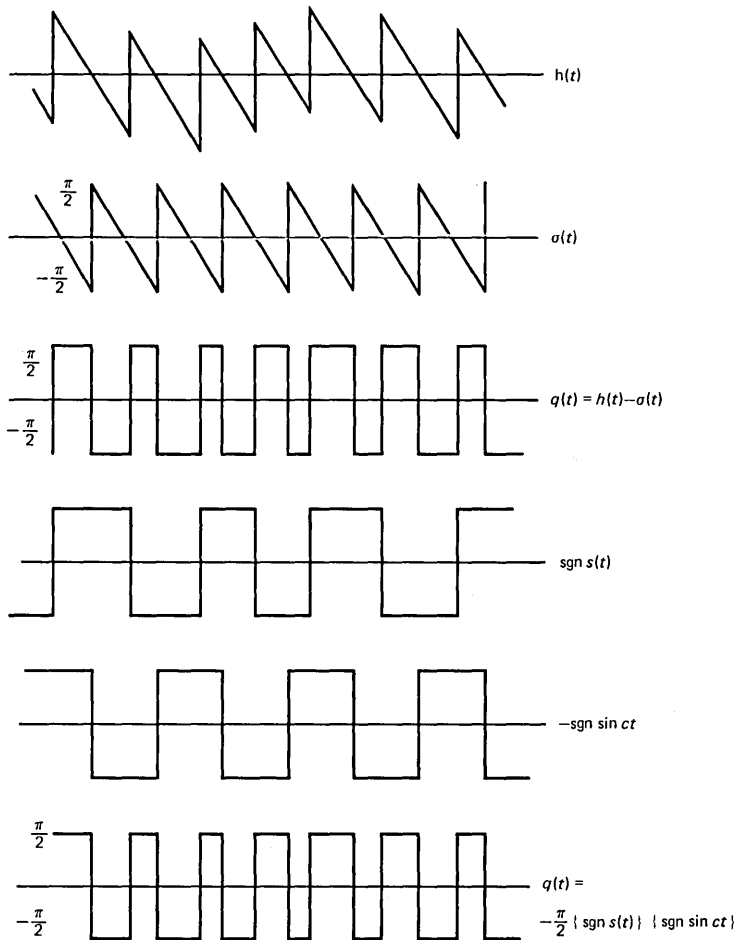


Fig. 4—Sum and product representation of square wave $q(t)$.

That is, $\text{sgn } s(t)$ is formed and then multiplied by $\text{sgn}\{\sin(ct + \Delta)\}$, where Δ is adjusted (to some multiple of π) by a phase-lock loop so that the average value of the product is zero. Then, filtering the resultant square wave gives a signal proportional to $f(t)$. In this application one may think of c large, with α and β not much larger than μ , the top frequency of f , so that $s(t)$ has the character of a single-sideband (lower-sideband) signal with spectrum confined to $[c, c - \beta]$ and $[-c, -(c - \beta)]$.

In another application, $f(t)$ may be thought of as an audio signal that is to be reproduced by driving a loudspeaker with a switching-type (class D) power amplifier having very good efficiency. The Sony

Corporation has marketed a switching-type amplifier using an approximate method of obtaining the square wave.⁶ Their approximation is equivalent to taking t_k to be the zeros of [cf. (22), (23)]

$$\cos[ct + \theta + f(t)],$$

where

$$\pi/2 < f(t) < -\pi/2,$$

which results in a good approximation for $c \gg \mu$ (in their case, $c = 2\pi \cdot 500$ kHz) but requiring an unnecessarily high switching frequency. [In the Sony system the square wave is generated by clipping the sum of the sawtooth $\sigma(t)$ and the signal $f(t)$; i.e.,

$$\frac{\pi}{2} \operatorname{sgn}\{\sigma(t) + f(t)\},$$

which is a conventional way of obtaining analog pulse-width modulation. This is to be compared with (34), which may be equivalently written

$$q(t) = -\frac{\pi}{2} \operatorname{sgn}\{\sigma(t) + \phi(t)\}.$$

IV. IMPLEMENTATION

Figure 5 is a block diagram of a click modulation system, including the optional square wave output. The input is the bandpass signal $f'(t + \Delta)$, which is fed to a Hilbert transform network, incurring a delay Δ , to obtain $\hat{f}'(t)$. The input is correspondingly delayed to obtain $f'(t)$. Then $f'(t)$ and $\hat{f}'(t)$ are fed to an Analytic Exponential Modulator (AEM), which furnishes the outputs

$$X(t) = e^{\hat{f}'(t)} \cos[f(t)] \quad (36)$$

$$Y(t) = -e^{\hat{f}'(t)} \sin[f(t)], \quad (37)$$

where

$$X(t) + iY(t) = Z(t) = \exp[-iF(t)] \quad (38)$$

and

$$F(t) = f(t) + i\hat{f}'(t). \quad (39)$$

These outputs are then bandlimited with identical low-pass filters having unity transmission over the band $(-\alpha, \alpha)$ and zero transmission outside the band $(-\beta, \beta)$ to obtain the signals $x(t)$ and $y(t)$, where

$$x(t) + iy(t) = z(t). \quad (40)$$

Then these signals are multiplied by $\cos(ct + \theta)$ and $\sin(ct + \theta)$ and

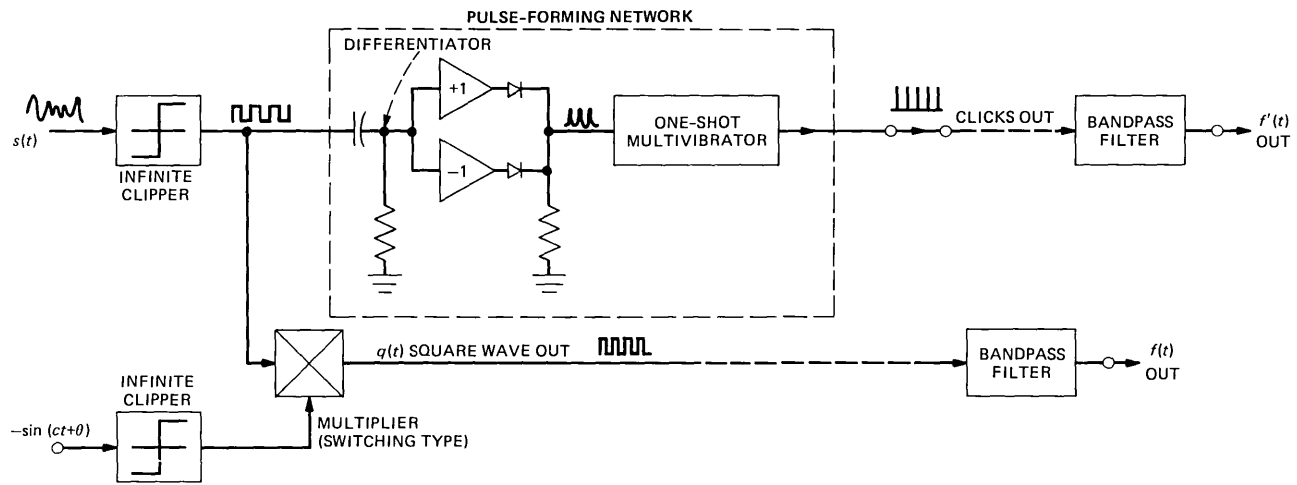
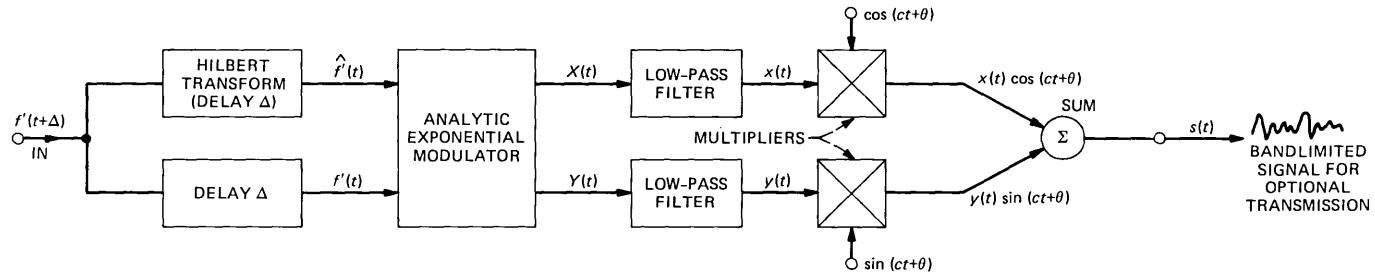


Fig. 5—A click modulation system.

then added to obtain the signal

$$s(t) = x(t)\cos(ct + \theta) + y(t)\sin(ct + \theta), \quad (41)$$

where the carrier frequency c must satisfy

$$c \geq \frac{\alpha + \beta}{2}.$$

The level of the input signal should be adjusted so that consecutive zeros of $s(t)$ never coalesce (in loud passages), or alternatively, to use the square wave output, the input level should be adjusted (made sufficiently small) so that $x(t)$ is always positive.

To obtain the click output, uniform pulses are formed at the zeros of $s(t)$. This may be accomplished as indicated by infinitely clipping $s(t)$, then differentiating, rectifying the resulting pulses, and using these to trigger a one-shot multivibrator. These pulses may be filtered to obtain $f'(t)$, the derivative of $f(t)$. To obtain the square wave output, the clipped signal $s(t)$, i.e., $\text{sgn } s(t)$, is multiplied by the clipped sine wave, $-\text{sgn}\{\sin(ct + \theta)\}$. When it is filtered, the resulting square wave, with suitable scaling (multiplied by $\pi/2$), will give $f(t)$, provided the input level is small enough so that $x(t)$ is always positive.

V. THE ANALYTIC EXPONENTIAL MODULATOR

The functions $X(t)$ and $Y(t)$, given by (36) and (37), may be generated using function generators and multipliers. However, they may be generated more simply in a feedback loop, which can be made stable, using the fact that $\{X(t) - 1\}$ and $Y(t)$ are high-pass signals containing no frequencies lower than λ , the lower frequency of $f(t)$.

Differentiating (38) we obtain

$$Z'(t) = iF'(t)Z(t)$$

or

$$X'(t) + iY'(t) = \{\hat{f}'(t) - if'(t)\}\{X(t) + iY(t)\}.$$

Then, equating real and imaginary parts we have

$$X'(t) = \hat{f}'(t)X(t) + f'(t)Y(t) \quad (42)$$

$$Y'(t) = \hat{f}'(t)Y(t) - f'(t)X(t). \quad (43)$$

Now integrators and multipliers can be connected so as to solve this pair of differential equations for $X(t)$ and $Y(t)$, given *arbitrary* functions $f(t)$ and $\hat{f}(t)$. However, drifts and offsets would soon cause trouble, resulting in exponential growth of the functions. This can be avoided when f and \hat{f} are high-pass Hilbert transform pairs.

In the theory we have treated all signals as dimensionless quantities.

Now, for clarity in implementing the analog circuitry, we attach the dimension of volts to all the signals and write

$$Z(t) = B \exp[-iF(t)/E] = X(t) + iY(t), \quad (44)$$

where B and E have the dimensions of volts. Then (42) and (43) become

$$\frac{dX}{dt} = \frac{d\hat{f}(t)}{dt} \frac{X(t)}{E} + \frac{df(t)}{dt} \frac{Y(t)}{E} \quad (45)$$

$$\frac{dY}{dt} = \frac{d\hat{f}(t)}{dt} \frac{Y(t)}{E} - \frac{df(t)}{dt} \frac{X(t)}{E}. \quad (46)$$

All the signals here are high-pass (lower frequency = λ), with the exception of $X(t)$, which we write as

$$X(t) = B + X_0(t), \quad (47)$$

where $X_0(t)$ is high-pass (lower frequency = λ). Then we rewrite eqs. (45) and (46) as

$$\frac{dX}{dt} = \frac{dX_0}{dt} = \frac{B}{E} \frac{d\hat{f}(t)}{dt} + \frac{d\hat{f}(t)}{dt} \frac{X_0(t)}{E} + \frac{df(t)}{dt} \frac{Y(t)}{E} \quad (48)$$

$$\frac{dY}{dt} = \frac{d\hat{f}(t)}{dt} \frac{Y(t)}{E} - \frac{B}{E} \frac{df(t)}{dt} - \frac{df(t)}{dt} \frac{X_0(t)}{E}. \quad (49)$$

We multiply all derivatives by some T , which has the dimensions of t (time), since analog circuitry for differentiating $f(t)$ will give $Tf'(t)$ in volts.

The analog implementation of the two differential eqs. (48) and (49) is shown in Fig. 6.

High-gain (negative) ac amplifiers are connected as ac integrators with feedback capacitors C and input resistors R , R , and $(M/B)R$ to give

$$RC \frac{dY}{dt} = \frac{T\hat{f}'(t)}{M} Y(t) - \frac{B}{M} Tf'(t) - \frac{T}{M} f'(t)X_0(t) \quad (50)$$

$$RC \frac{dX}{dt} = \frac{T\hat{f}'(t)}{M} X_0(t) + \frac{B}{M} T\hat{f}'(t) + \frac{T}{M} f'(t)Y(t). \quad (51)$$

Here M is the multiplier scale factor (volts); it is the output of the multiplier when both inputs are 1 volt. Comparing these equations with (48) and (49) we see that the "normalization factor" E introduced in (44) is

$$E = \frac{RCM}{T}. \quad (52)$$

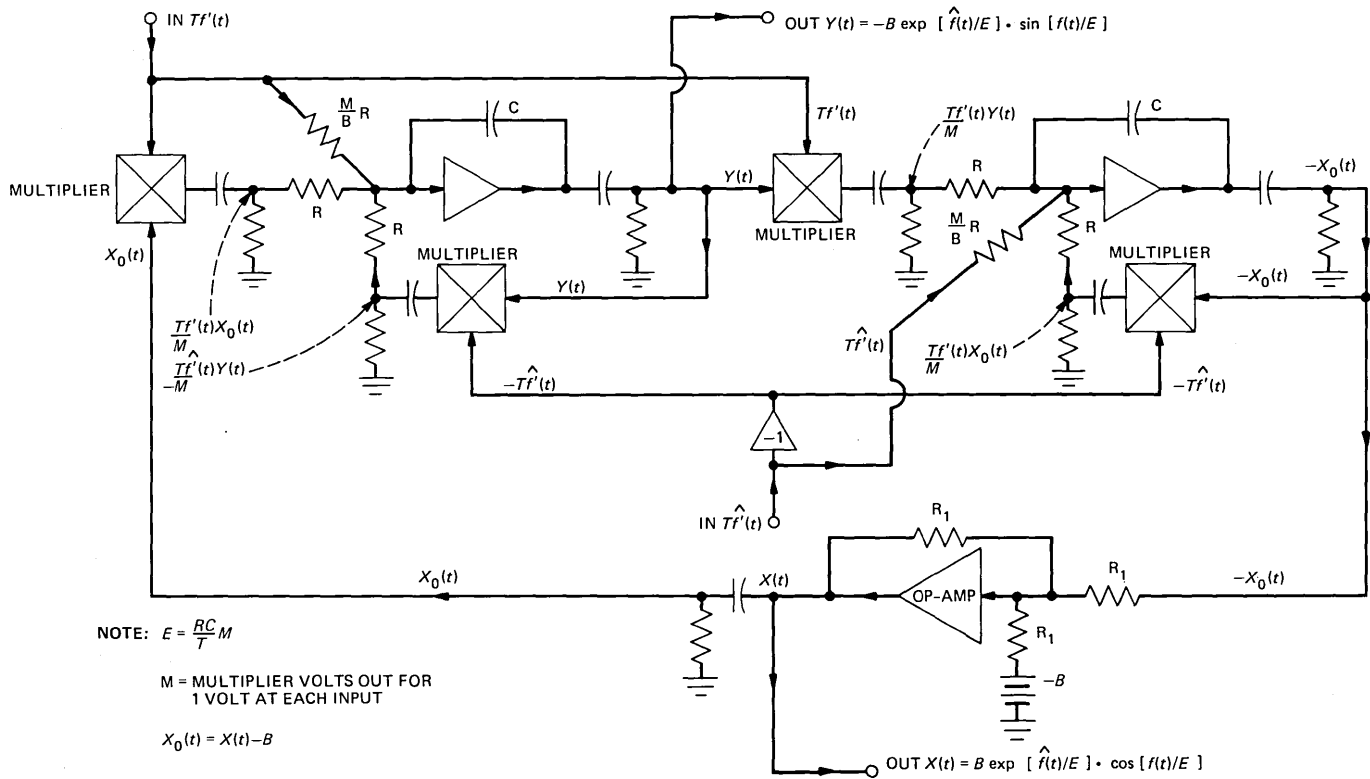


Fig. 6—Analytic exponential modulator.

Coupling networks employing dc blocking condensers are shown at the inputs and outputs of amplifiers and multipliers. The time constant of these networks should be large compared to the reciprocal of the lower frequency λ . Some of these networks may be incorporated in the ac amplifiers. The important point is that the inputs to the multipliers should not have dc components. Then when inputs $Tf'(t)$ and $T\hat{f}'(t)$ are zero (steady state), the circuit is in a quiescent condition with $X(t) = B$ and $Y(t) = 0$. If $f'(t)$ and $\hat{f}'(t)$ were not high-pass, and Hilbert transform pairs, then ac coupling could not be used, because the corresponding signals $X(t) - B$ and $Y(t)$ would not be high-pass.

A dc operational amplifier is shown in the feedback loop, connected to give a gain of -1 to the inputs $-X_0(t)$ and $-B$. This is not necessary, but provides a convenient way to add B to $X_0(t)$ and give a low impedance output for $X(t)$. The dc amplifier can be replaced by an ac amplifier (gain -1) and the summing of B with $X_0(t)$ incorporated elsewhere in the external circuitry.

Switching-type multipliers may be used in the AEM if $f'(t)$ and $\hat{f}'(t)$ are replaced by binary-valued switching signals, which, if integrated, give very close approximations to $f(t)$ and $\hat{f}(t)$. These switching signals may be obtained from a "delta mod", as shown in Fig. 7. The resulting error is mainly high frequency in $f(t)$ and $\hat{f}(t)$, which translates into high-frequency error in $X(t)$ and $Y(t)$. This error will subsequently be removed by bandlimiting $X(t)$ and $Y(t)$ to obtain $x(t)$ and $y(t)$.

VI. NUMERICAL EXAMPLE

To illustrate the theory we take a simple example:

$$\lambda = 1, \quad \mu = 2, \quad \alpha = 2.2, \quad \beta = 2.8, \quad c = 5/2,$$

$$f'(t) = -\frac{1}{2} \cos t + \frac{1}{4} \cos 2t,$$

$$f(t) = -\frac{1}{2} \sin t + \frac{1}{8} \sin 2t.$$

We have

$$\hat{f}(t) = \frac{1}{2} \cos t - \frac{1}{8} \cos 2t$$

so that

$$iF(t) = \hat{f}(t) - if(t) = \frac{1}{2} e^{it} - \frac{1}{8} e^{i2t}.$$

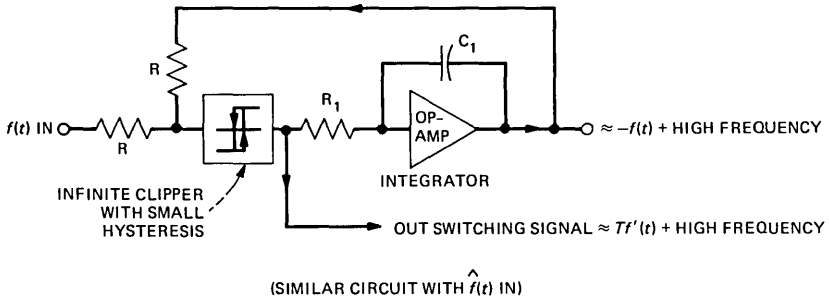


Fig. 7—Delta-mod circuit for deriving switching signals for multipliers in analytic exponential modulator.

Then

$$\begin{aligned}
 Z(t) &= \exp[-iF(t)] = 1 - iF(t) + \frac{(-iF(t))^2}{2!} \dots \\
 &= 1 + \frac{1}{2} e^{it} - \frac{1}{8} e^{i2t} + \frac{1}{2!} \left\{ \frac{1}{2} e^{it} - \frac{1}{8} e^{i2t} \right\}^2 \\
 &\quad + \frac{1}{3!} \left\{ \frac{1}{2} e^{it} - \frac{1}{8} e^{i2t} \right\}^3 + \dots \\
 &= 1 + \frac{1}{2} e^{it} - \frac{1}{8} e^{i2t} + \frac{1}{2!} \left(\frac{1}{4} e^{i2t} - \frac{1}{8} e^{i3t} + \frac{1}{64} e^{i4t} \right) \\
 &\quad + \frac{1}{6} \left(\frac{1}{8} e^{i3t} - \frac{3}{32} e^{i4t} \dots \right) + \frac{1}{24 \cdot 16} e^{i4t} + \dots \\
 &= 1 + \frac{1}{2} e^{it} + 0 - \frac{1}{24} e^{i3t} - \frac{1}{192} e^{i4t} + \dots
 \end{aligned}$$

Now we bandlimit $Z(t)$ by convolution with $K_{\alpha,\beta}(t)$ to preserve the spectrum in $[0, \alpha]$ and eliminate frequencies above β . (Here we assume $\alpha = 2.2$ and $\beta = 2.8$.) We thus obtain

$$z(t) = 1 + \frac{1}{2} e^{it}.$$

Clearly, $z(t + iu)$ is zero-free in the upper half-plane, $u \geq 0$. Then

$$\log z(t) = \frac{1}{2} e^{it} - \frac{1}{2} \left(\frac{1}{2} e^{it} \right)^2 + \frac{1}{3} \left(\frac{1}{2} e^{it} \right)^3 + \dots,$$

the first two terms agreeing with

$$\log Z(t) = -iF(t) = \frac{1}{2} e^{it} - \frac{1}{8} e^{i2t},$$

i.e., the Fourier transforms of $\log z(t)$ and $\log Z(t)$ agree over $(-\infty, \alpha)$.

Now we take $\theta = 0$, $c = 5/2$, and form

$$\begin{aligned} G(t; \theta, c) &= z(t) + e^{i2ct} \overline{z(t)} \\ &= 1 + \frac{1}{2} e^{it} + e^{i5t} \left(1 + \frac{1}{2} e^{-it}\right) \\ &= 1 + \frac{1}{2} e^{it} + \frac{1}{2} e^{i4t} + e^{i5t}. \end{aligned}$$

Then $G(\tau)$ has only real simple zeros, since $z(\tau)$ is zero-free in the (closed) upper half-plane. We have

$$G(t) = 2e^{i5t/2} s(t),$$

where

$$\begin{aligned} s(t) &= \frac{1}{2} \cos \frac{3t}{2} + \cos \frac{5t}{2} \\ &= 4 \left(-\frac{3}{4} + \cos \frac{t}{2} \right) \left(\frac{1}{2} + \cos \frac{t}{2} \right) \cos \frac{t}{2}. \end{aligned}$$

Writing $G(t)$ in factored form we have

$$G(t) = (1 + e^{it}) \prod_{k=1}^2 (1 - e^{i\theta_k} e^{it})(1 - e^{-i\theta_k} e^{it}),$$

where

$$\begin{aligned} \cos \theta_1 &= 3/4 \\ \cos \theta_2 &= -1/2. \end{aligned}$$

Since $G(\tau)$ and $z(\tau)$ are zero-free in the upper half-plane and the Fourier transforms of $G(t)$ and $z(t)$ agree over $(-\infty, \alpha)$, it follows that the Fourier transforms of $\log G(t)$ and $\log z(t)$ agree over $(-\infty, \alpha)$. We have

$$\log G(t) = \log(1 + e^{it}) + \sum_{k=1}^2 \log(1 - e^{i\theta_k} e^{it}) + \sum_{k=1}^2 \log(1 - e^{-i\theta_k} e^{it})$$

or

$$\begin{aligned}
 \log G(t) &= e^{it} - \frac{1}{2} e^{i2t} + \frac{1}{3} e^{i3t} - \frac{1}{4} e^{i4t} + \dots \\
 &\quad - 2(\cos \theta_1 + \cos \theta_2) e^{it} - 2(\cos 2\theta_1 + \cos 2\theta_2) \frac{e^{i2t}}{2} \\
 &\quad - 2(\cos 3\theta_1 + \cos 3\theta_2) \frac{e^{i3t}}{3} + \dots \\
 &= \frac{1}{2} e^{it} - \frac{1}{8} e^{i2t} + \frac{1}{24} e^{i3t} + \frac{31}{64} e^{i4t} + \frac{121}{160} e^{i5t} \\
 &\quad - \frac{145}{384} e^{i6t} + \frac{169}{7 \cdot 128} e^{i7t} - \frac{449}{8 \cdot 256} e^{i8t} - \frac{1511}{9 \cdot 512} e^{i9t} \\
 &\quad - \frac{1201}{10 \cdot 1024} e^{i10t} + \frac{4489}{11 \cdot 2048} e^{i11t} - \frac{6305}{12 \cdot 4096} e^{i12t} + \dots
 \end{aligned}$$

We have defined

$$H(t) = i \log G(t) = h(t) + i\hat{h}(t).$$

Then

$$\begin{aligned}
 h(t) = -\text{Im}\{\log G(t)\} &= -\frac{1}{2} \sin t + \frac{1}{8} \sin 2t \\
 &\quad - \frac{1}{24} \sin 3t - \frac{31}{64} \sin 4t + \dots
 \end{aligned}$$

This is the “meandering” sawtooth function, which increases by π at the zeros of $s(t)$. (The waveforms in Fig. 1 correspond to the example here.)

The phase $\phi(t)$ of the analytic bandlimited signal $z(t)$ is

$$\phi(t) = \text{Im}\{\log z(t)\} = \frac{1}{2} \sin t - \frac{1}{8} \sin 2t + \frac{1}{24} \sin 3t + \dots$$

We see that the Fourier transforms of $f(t)$, $h(t)$, and $-\phi(t)$ agree over $(-\alpha, \alpha)$. Then the Fourier transforms of $f'(t)$ and

$$\begin{aligned}
 h'(t) &= \pi \sum_{-\infty}^{\infty} \delta(t - t_k) - c \\
 &\sim -\frac{1}{2} \cos t + \frac{1}{4} \cos 2t - \frac{1}{8} \cos 3t - \frac{31}{16} \cos 4t + \dots
 \end{aligned}$$

agree over $(-\alpha, \alpha)$, where $\{t_k\}$ are the zeros of $s(t)$. [The Fourier series

of $h'(t)$ does not converge, of course.] Thus, if $K(t)$ is the kernel of a bandpass filter that reproduces frequencies between λ and μ , rejecting dc and frequencies greater than α , we have

$$\begin{aligned} f'(t) &= h'(t) \otimes K(t) = \pi \sum_{-\infty}^{\infty} K(t - t_k) \\ &= -\frac{1}{2} \cos t + \frac{1}{2} \cos 2t. \end{aligned}$$

Writing

$$z(t) = A(t)e^{i\phi(t)}$$

and

$$s(t) = \frac{1}{2} e^{-ict} G(t) = A(t) \cos\{ct - \phi(t)\}$$

we see that $\{t_k\}$ are the zeros of the phase-modulated signal

$$\cos[ct - \phi(t)].$$

Note that $\phi(t)$ is not bandlimited;

$$\phi(t) = \text{Im}\{\log[\mathbf{B}_{\alpha,\beta} e^{-i\{f(t)+i\hat{f}(t)\}}]\},$$

where $\mathbf{B}_{\alpha,\beta}$ is the bandlimiting operator defined by convolution with $K_{\alpha,\beta}(t)$, so that

$$-\phi(t) = f(t) + \epsilon(t),$$

where $\epsilon(t)$ is a high-pass function whose Fourier transform vanishes over $(-\alpha, \alpha)$. Had we taken α and β much larger, then $\epsilon(t)$ would have been extremely small, but this would have required a much larger c [$c \geq (\alpha + \beta/2)$] in forming $s(t)$, i.e., a much larger pulse rate in obtaining

$$f'(t) = \pi \sum_{-\infty}^{\infty} K(t - t_k).$$

In the example here we have

$$x(t) = \text{Re}\{z(t)\} = 1 + \frac{1}{2} \cos t \geq 0$$

and therefore

$$-\pi/2 < \phi(t) < \pi/2,$$

so that the zeros of $s(t)$ and $\sin ct$ interlace. Then [cf. (34)] with $c = 5/2$,

$$\begin{aligned} q(t) &= -\frac{\pi}{2} \{\operatorname{sgn} s(t)\} \cdot \{\operatorname{sgn} \sin ct\} = h(t) - \sigma(t) \\ &= -\frac{1}{2} \sin t + \frac{1}{8} \sin 2t - \frac{1}{24} \sin 3t - \frac{31}{64} \sin 4t - \frac{121}{160} \sin 5t \\ &\quad - \sin 5t + \dots \end{aligned}$$

is a square wave that may be bandlimited to obtain

$$f(t) = -\frac{1}{2} \sin t + \frac{1}{8} \sin 2t.$$

If we replace $f(t)$ by

$$f(t) = -a(\sin t - \frac{1}{4} \sin 2t)$$

we find that

$$z(t) = 1 + ae^{it} + \frac{a}{2} \left(a - \frac{1}{2} \right) e^{i2t}.$$

Then $z(\tau)$ will be zero-free in the upper half-plane for

$$\begin{aligned} -\frac{(\sqrt{33} - 1)}{4} < a < \frac{\sqrt{33} + 1}{4} \\ (-1.186141 < a < 1.68614). \end{aligned}$$

However, the real part of $z(t)$ will be positive, i.e., the square wave representation will be valid, only for the reduced range

$$-1.06 < a < 1.38.$$

REFERENCES

1. B. F. Logan, Jr., "Signals Designed for Recovery after Clipping—I. Localization of Infinite Products," AT&T Bell Lab. Tech. J., 63, No. 2, Part 1 (February 1984), pp. 261-85.
2. B. F. Logan, Jr., "Signals Designed for Recovery after Clipping—II. Fourier Transform Theory of Recovery," AT&T Bell Lab. Tech. J., 63, No. 2, Part 1 (February 1984), pp. 287-306.
3. B. F. Logan, Jr., "Signals Designed for Recovery after Clipping—III. Generalizations," AT&T Bell Lab. Tech. J., this issue.
4. B. F. Logan, Jr., "Theory of Analytic Modulation Systems," B.S.T.J., 57, No. 3 (March 1978), pp. 491-576.
5. B. F. Logan, Jr., "Information in the Zero-Crossing of Band-pass Signals," B.S.T.J., 56, No. 4 (April 1977), pp. 487-510 (see Theorem 12, p. 503).
6. Hirsch/Houk Laboratories, "Audio Test Reports; Sony Model TA-N88 Basic Power Amplifier," Popular Electronics (September 1978), pp. 32-6.

AUTHOR

Benjamin F. Logan, Jr., B.S. (Electrical Engineering), 1946, Texas Technological College; M.S., 1951, Massachusetts Institute of Technology; Eng.D.Sci. (Electrical Engineering), 1965, Columbia University; AT&T Bell Laboratories, 1956—. While at MIT, Mr. Logan was a research assistant in the Research Laboratory of Electronics, investigating characteristics of high-power electrical discharge lamps. Also at MIT he engaged in analog computer development at the Dynamic Analysis and Control Laboratory. From 1955 to 1956 he worked for Hycon-Eastern, Inc., where he was concerned with the design of airborne power supplies. He joined AT&T Bell Laboratories as a member of the Visual and Acoustics Research Department, where he was concerned with the processing of speech signals. Currently, he is a member of the Mathematical Research Department. Member, Sigma Xi, Tau Beta Pi.

Design Diagrams for Depressed Cladding Single-Mode Fibers

By W. T. ANDERSON* and P. F. GLODIS*

(Manuscript received June 24, 1983)

Dispersion, cutoff wavelength, and mode field radius requirements place conflicting demands on the design of single-mode fibers. Using empirical models that relate these requirements to the core parameters in the preform stage, we present a single-mode design diagram for a depressed cladding fiber design showing the regions of core diameter and index difference that satisfy the requirements. The requirements with the greatest impact on fiber yield are the maximum value of the zero dispersion wavelength, the maximum value of the cutoff wavelength, and the allowable variations in the mode field radius.

I. INTRODUCTION

The optical requirements on a single-mode fiber impose conflicting demands on the fiber design. To meet dispersion, cutoff wavelength, and mode field radius requirements, the fiber core diameter and index of refraction difference must be controlled to within small variations about a nominal value, and the tightness of these specifications will directly affect the yield when making the fiber. In this paper, we examine the effects of fiber requirements on yield and identify those requirements that have the greatest impact.

This study will deal with a depressed cladding fiber design, whose index profile is shown with its nominal parameters in Fig. 1. This fiber design has been thoroughly studied. Considerable measurement data are available for this type of fiber with wide variations in fiber

* AT&T Bell Laboratories.

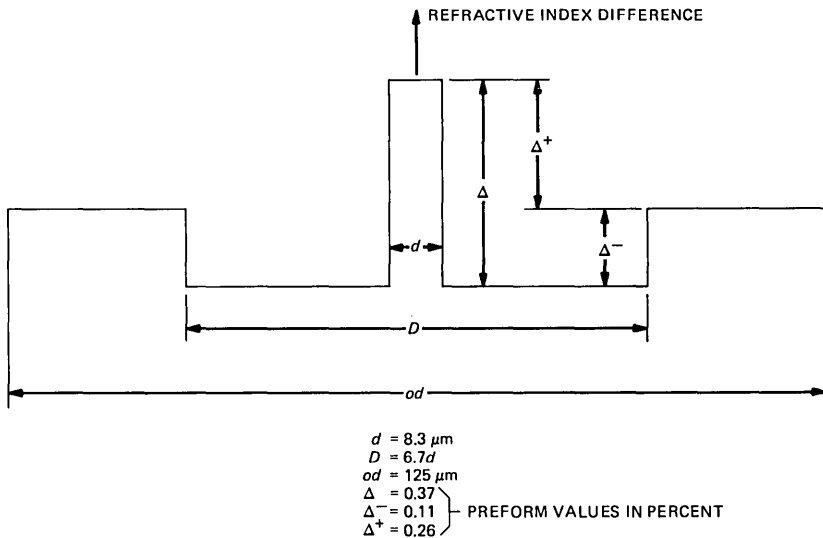


Fig. 1—Refractive index profile of a depressed cladding fiber. Nominal parameters are shown.

parameters about the nominal values except for the cladding index (Δ^-) and clad-to-core diameter ratio (D/d), which were well controlled at the nominal values shown in Fig. 1. These data have been used to develop simple empirical models that relate the core parameters (d and Δ) to the dispersion, cutoff wavelength, and mode field radius. Since the index-of-refraction profiles are more easily measured for preforms than for fibers, core dimensions scaled from their preform values were used. The index of refraction measured in the fiber will differ from that measured in the preform,¹ but as long as the preform values are used consistently, the validity of the empirical models should not be affected. Also, models based upon preform measurements are more useful for manufacturing.

In Section II we discuss the models in detail, and in Section III we present the single-mode design diagrams, which show the relationship between system requirements and fiber parameters.

II. EMPIRICAL MODELS

Chromatic dispersion, which limits the bit rate of a digital system operating on a single-mode fiber, passes through zero at a wavelength (λ_0) near $1.3 \mu\text{m}$. Since the shape of the chromatic dispersion curve as a function of wavelength for a nearly step-index fiber is not sensitive to the fiber design parameters, specifying λ_0 is sufficient to ensure that the fiber dispersion is adequately low over the range of wavelengths that may be used in the system. The dispersion in a single-

mode fiber may be predicted by numerical solutions of the field equations.² However, these solutions themselves give little insight into the dependence of λ_0 on core index parameters. Accordingly, a set of values encompassing the expected range of core diameters ($7 < d < 10 \mu\text{m}$) and index differences ($0.15\% < \Delta < 0.50\%$) were used in a program that solves the scalar wave equation numerically,² and the λ_0 for each combination was computed. The core parameters, d and Δ , and λ_0 were then used in a multiple linear regression program to find a simple, accurate relationship between λ_0 and d and Δ . After trying several different powers of d and Δ , the following model was selected:

$$\lambda_0 = C_0 + \frac{C_1}{d} + C_2\sqrt{\Delta}. \quad (1)$$

For example, after we compared the computed λ_0 's with eq. (1), we obtained a correlation coefficient (ρ^2) of 0.996 for a family of fibers with nearly step-index Ge-doped cores and pure SiO_2 claddings ($\Delta^- = 0$, or "matched"). λ_0 was calculated for a limited number of alternative profile shapes and dopants, and the same functional form with slightly different coefficients was an excellent fit to the computed values of λ_0 in every case. This model is also appropriate for depressed cladding fibers if the cladding diameter is large relative to the core diameter (i.e., $D/d > 5$), so that the dispersion behavior is similar to that of a matched cladding fiber. To use this model empirically, a set of coefficients that characterize measured, not computed, data was found. A linear regression analysis of measured values of λ_0 for a group of depressed-cladding fibers as a function of core diameter and delta gave the following best-fit coefficients:³

$$C_0 = 1.207$$

$$C_1 = 1.933$$

$$C_2 = -0.2149$$

with $\rho^2 = 0.94$. If we use these coefficients, eq. (1) gives λ_0 in micrometers if d is expressed in micrometers and Δ in percent. While core diameter and delta were varied, Δ^- and D/d were held at the nominal values, shown in Fig. 1.

Cutoff wavelength can also be modeled. For an ideal step-index fiber, the theoretical cutoff wavelength is

$$\lambda_{c_{th}} = \frac{\pi dn}{2.405} \sqrt{2\Delta}, \quad (2)$$

where n is the index of refraction of the cladding. The measured cutoff wavelength, λ_c , for the standard 5-meter sample length is well char-

acterized by the empirical relation

$$\left(\frac{\lambda_c}{d}\right)^2 = 0.861 \left(\frac{\lambda_{cth}}{d}\right)^2 + 0.0006 \quad (3)$$

with $\rho^2 = 0.92$. The λ 's and d 's are measured in micrometers. The measured cutoff wavelength is expected to be lower than the theoretical cutoff wavelength in depressed cladding designs since the higher-order mode becomes leaky and highly attenuated well below λ_{cth} . Defining the normalized frequency as

$$V = \frac{\pi d n}{\lambda} \sqrt{2\Delta}$$

then eq. (3) corresponds to a cutoff V value of approximately 2.61 instead of the theoretical value of 2.405 for an ideal step-index matched-cladding fiber.

The width of the field distribution in the core of the fiber (the mode field radius, or ω_0) is important in controlling splice loss and laser launching efficiency. Since the fields are nearly Gaussian,⁴ the width parameter of the Gaussian function that best fits the near field

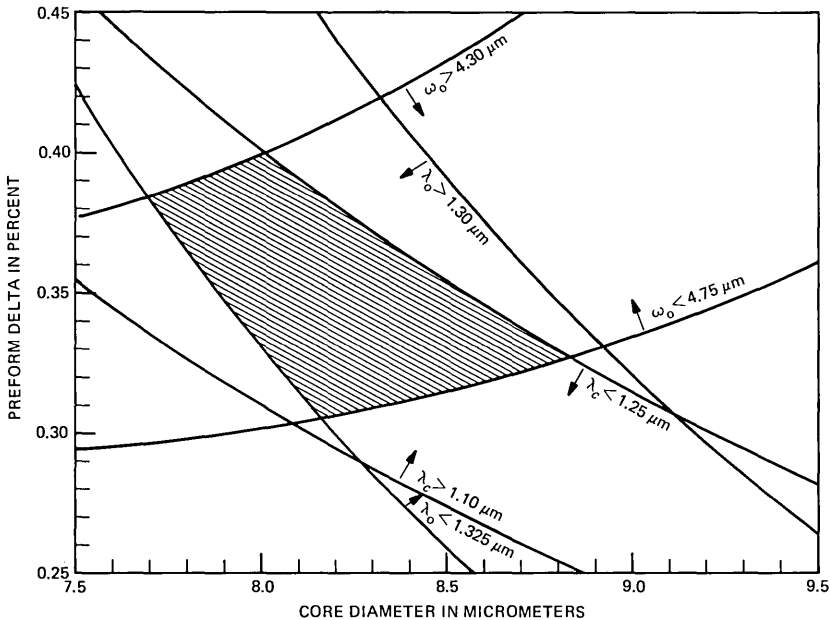


Fig. 2—Constraints imposed by tolerances on λ_0 , λ_c , and ω_0 . The trapezoidal region represents all combinations of d and Δ that meet the requirements placed upon λ_0 , λ_c , and ω_0 .

adequately characterizes the field distribution. Marcuse⁵ has found the following empirical relationship:

$$2 \frac{\omega_0}{d} = 0.65 + \frac{1.619}{V^{3/2}} + \frac{2.879}{V^6}. \quad (4)$$

This empirical formula has been found to agree well with measured values.

III. SINGLE-MODE FIBER DESIGN DIAGRAMS

Consider the following system requirements as an example:

$$1.300 \leq \lambda_0 \leq 1.325 \mu\text{m}$$

$$1.10 \leq \lambda_c \leq 1.25 \mu\text{m}$$

$$4.30 \leq \omega_0 \leq 4.75 \mu\text{m}.$$

Using the empirical models developed in the previous section, curves of constant λ_0 , λ_c , and ω_0 corresponding to these limits are plotted as a function of d and Δ in Fig. 2. (A somewhat similar diagram for matched-cladding fibers has been published by Ainslie et al.⁶) The area inside the nearly trapezoidal shaded region represents the allow-

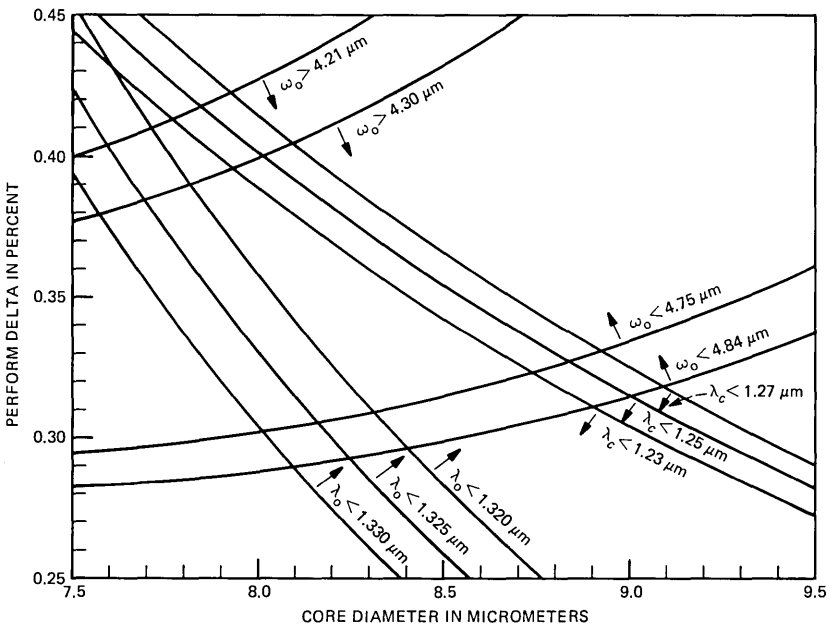


Fig. 3—Sensitivity to parameter tolerances. Changing the maximum λ_0 , λ_c , or ω_0 can severely alter the size of the allowable region.

able combinations of d and Δ required to meet dispersion, cutoff, and mode field radius requirements. Several conclusions may immediately be drawn. First, only the upper limit on λ_0 will affect yield. The lower limit will not be approached if the cutoff wavelength and mode field radius requirements are met. Second, $\lambda_c > 1.10 \mu\text{m}$ if all other requirements are met, so the minimum λ_c requirement also appears to be unnecessary. Finally, the tolerance on ω_0 (± 5 percent) does significantly reduce the size of the allowable region. The effect of the various parameter values on the size of the allowable region is shown in Fig. 3.

These diagrams also provide immediate feedback before fibers are drawn from the preforms. If a preform profile indicates that the fibers drawn from the preform will not have the desired properties, then the preform may be scrapped to avoid drawing and measuring fibers that will not be acceptable.

REFERENCES

1. M. J. Saunders, "A Comparison of Single-Mode Refractive Index Profiles in Preforms and Fibers," 8th ECOC, Cannes, September 21-24, 1982, Paper C17.
2. W. L. Mammel and L. G. Cohen, "Prediction of Fiber Transmission Characteristics from Arbitrary Refractive-Index Profiles," *Applied Optics*, 21, No. 4 (February 15, 1982), pp. 699-703.
3. P. F. Glodis, W. T. Anderson, and J. S. Nobles, "Control of Zero Chromatic Dispersion Wavelength in Fluorine Doped Single-Mode Optical Fibers," *Technical Digest, OFC '83*, New Orleans, February 28-March 2, 1983, Paper MF6.
4. D. Marcuse, "Gaussian Approximation of the Fundamental Modes of Graded-Index Fibers," *J. Opt. Soc. Am.*, 68, No. 1 (January 1978), pp. 103-9.
5. D. Marcuse, "Loss Analysis of Single-Mode Fiber Splices," *B.S.T.J.*, 56, No. 5 (May-June 1977), pp. 703-18.
6. B. J. Ainslie, K. J. Beales, C. R. Day, and J. D. Rush, "The Design and Fabrication of Monomode Optical Fiber," *IEEE Trans. MTT*, MTT-30, No. 4 (April 1982), pp. 360-9.

AUTHORS

William T. Anderson, B.S.E.E., 1970, Georgia Institute of Technology; M.S. (Electrical Engineering), 1971, Stanford University; Ph.D. (Electrical Engineering), 1979, Georgia Institute of Technology; AT&T Bell Laboratories, 1970—. Since joining AT&T Bell Laboratories, Mr. Anderson has analyzed the transmission and crosstalk performance of telephone cables. Since 1979, he has developed measurement techniques and designs for single-mode optical fibers.

Paul F. Glodis, B.S. (Physics), 1966, Worcester Polytechnic Institute; Ph.D. (Physics), 1972, Yale University; Research Associate/Adjunct Assistant Professor, Department of Physics, University of California at Los Angeles, 1972-1980; AT&T Bell Laboratories, 1980—. At AT&T Bell Laboratories, Mr. Glodis is involved in work on single-mode fiber design and fabrication techniques.

Single GRIN-Lens Directional Couplers

By F. H. LEVINSON* and S. W. GRANLUND†

(Manuscript received June 10, 1983)

Two types of small, rugged, gradient-index (GRIN) rod-lens directional couplers have been made. One is a three-port directional coupler and the other is an asymmetric four-port coupler. Each coupler can have various splitting ratios from 1:1 to 20:1. Excess insertion loss is less than 1.0 dB, and directivity is greater than 30 dB for the three-port couplers, while these same figures are 1.2 dB and 40 dB for the asymmetric four-port couplers. The couplers are stable between -40 and $+80^{\circ}\text{C}$.

I. INTRODUCTION

Several designs for directional couplers that use gradient index (GRIN) rod lenses have been published; many of these are discussed in the review by Uchida and Kobayashi.¹ We report the results of two multimode fiber coupler designs. The first is a three-port directional coupler similar to that of Nishimoto et al.,² described in Ref. 1. Our design, however, incorporates a single GRIN lens and a unique angled mirror for performing the power division. The other coupler is an asymmetric four-port that is useful in fiber networking applications. Waveguide and notched fiber manifestations of this coupler exist.^{3,4} This GRIN-lens design is more flexible and useful for a wide range of fibers and applications. The three-port coupler is described first since its fabrication, performance, and stability are similar to that of the asymmetric four-port. Following this, details specific to the four-port coupler are presented.

* AT&T Bell Laboratories; present affiliation Bell Communications Research, Inc. † AT&T Bell Laboratories.

Copyright © 1984 AT&T. Photo reproduction for noncommercial use is permitted without payment of royalty provided that each reproduction is done without alteration and that the Journal reference and copyright notice are included on the first page. The title and abstract, but no other portions, of this paper may be copied or distributed royalty free by computer-based and other information-service systems without further permission. Permission to reproduce or republish any other portion of this paper must be obtained from the Editor.

II. THREE-PORT DIRECTIONAL COUPLER

2.1 Design

The upper portion of Fig. 1 presents the design of the three-port directional coupler with a 1:1 or 3 dB splitting ratio. Light from fiber 1 passes through the quarter-pitch lens and is collimated at the end face. Collimated light from a GRIN lens is not normally parallel to the lens axis, but is usually at an angle related to the distance of fiber 1 from the lens axis. Any change in the direction of this beam, other than 180 degrees, after reflection from the lens end-face mirror results in a positional change when the beam is refocused back to the original plane of incidence. In this way, the part of the light from fiber 1 that strikes the portion of end face covered by the fixed mirror (evaporated Au deposited directly on the lens) is reflected symmetrically about the lens axis and refocused into fiber 2. The remaining light is reflected off the tilted mirror and can be refocused into fiber 3 by precise angular adjustment of that mirror.

2.2 Fabrication

The assembly of the three-port device is accomplished in two independent steps. First, an array of three fibers is brought near the lens and permanently set with its position adjusted for optimum light

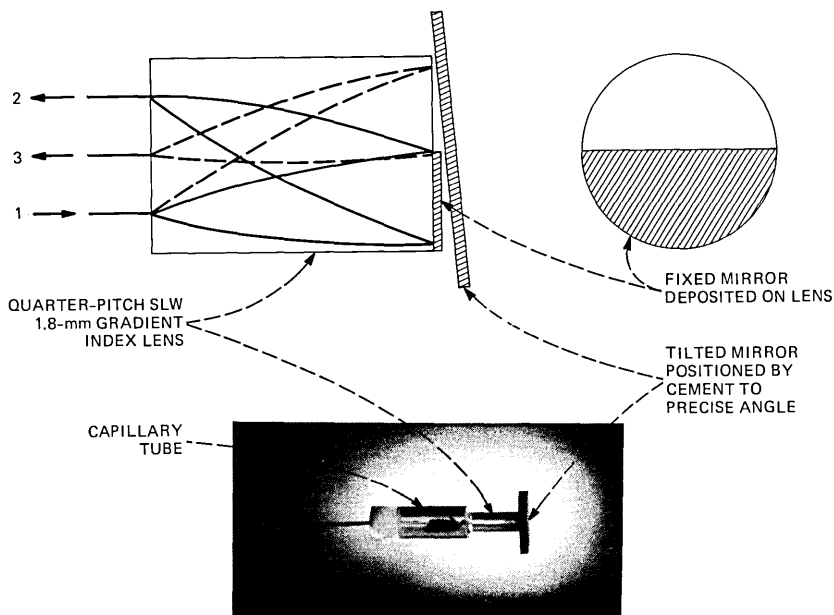


Fig. 1—Schematic diagram of GRIN-lens three-port directional coupler and photograph of a finished device.

coupling between the input fiber and either of the two output fibers. Next, a mirror is brought near the lens end face. After the lens-mirror joint is filled with an optical cement, which has an index similar to that of the fiber and GRIN lens, the mirror is angularly adjusted and permanently set for optimum coupling between the input fiber and the remaining output fiber. An angle of $\sim 1.3^\circ$ is typical for a SLW 1.8-mm *Selfoc** lens and fibers with outer diameters (ODs) of 125 μm . An important aspect of this two-step assembly process is the independent alignment of the fibers, which results in optimum coupling. The lower portion of Fig. 1 contains a photograph of a completed miniature three-port directional coupler. The overall length of this device is 1.5 cm; however, couplers as short as 1 cm were fabricated.

An additional step can be taken to compensate for the cement's shrinkage during curing by increasing the tilted mirror's angle and the fibers' distance from the lens before curing by an amount proportional to the shrinkage. However, cement shrinkage during curing is small, and when a device is made (using 50/125- μm fiber) without compensating for cement shrinkage during cure, a degradation of at most 0.1–0.2 dB results.

2.3 Performance characteristics

A flexibility inherent in both the three-port and four-port coupler designs is the change in the splitting ratio that results from varying the area of the end-face mirrors. As Nishimoto et al. reported,² we have found a fan-shaped mirror to be the best approach in order to minimize modal sensitivity of the coupler. Couplers have been fabricated with splitting ratios of 1:1, 5:1, 10:1, and 20:1.

The coupler loss and crosstalk measurements were made using either a $\lambda = 0.87\text{-}\mu\text{m}$ or $\lambda = 1.3\text{-}\mu\text{m}$ Light Emitting Diode (LED) light source and a calibrated optical power meter. Light from the LED was coupled to a length of fiber that includes a mandrel wrap to provide a steady-state mode excitation. This fiber was then spliced to the device fiber pigtail and the signal level (after a mandrel wrap) on the output fibers (P_{out}) were recorded. Following the necessary optical power measurements, the input fiber was broken to obtain the input-power zero point (P_{in}). The insertion loss of a particular channel is defined to be 10 log ($P_{\text{out}}/P_{\text{in}}$). The excess insertion loss is defined to be that portion of the insertion loss that is not attributable to the power division. For example, if a three-port coupler is designed to split the input power equally between the two outputs, then, ideally, each output port would have a 3-dB insertion loss. If each port shows a 3.8-dB insertion loss, then the coupler has a 0.8-dB excess insertion loss.

The excess insertion loss of the experimental coupler models was

* Registered trademark of Nippon Sheet Glass.

between 0.6 and 1.0 dB (see Table I). As a result, although couplers with splitting ratios higher than 20:1 are possible, there is little performance improvement in excess insertion loss to be realized on the high reflection channel over that of a 20:1 coupler. Minimum excess insertion loss in the coupler appears to be attributable to the following sources: 0.2 dB from lens aberration,⁵ 0.1-dB Au mirror loss,⁶ and 0.3-dB misalignment and cement curing losses.

The directivity of the three-port coupler was measured by determining the coupler's insertion loss between fibers 2 and 3 (see Fig. 1), while the end of fiber 1 was immersed in index matching fluid. An average of 32 dB was found for a 1:1 splitting-ratio coupler, and the directivity increases with increasing splitting ratio. The dominant source of this crosstalk is the light from fiber 2 or 3 that is reflected by the fiber 1-cement interface and refocused back into fibers 3 or 2, respectively. A reflection also occurs at the lens-cement interface, but this is not properly focused and as such does not significantly contribute to the crosstalk. Using the simple fresnel formula with a fiber index, n_f , of ~ 1.46 and a cement index, n_c , of ~ 1.56 ,

$$R = (n_f - n_c)/(n_f + n_c)^2 = 0.11\% \text{ or } 29.6 \text{ dB.}$$

Practical directivity values are better than this because we are making two passes through a 50-percent transmission mirror (3-dB coupler case), and hence, this provides an additional 6 dB of directivity. Some of our best 3-dB couplers have approached this theoretical limit of 35 dB.

Table I—Insertion losses for three-port directional couplers

SPLITTING RATIO	MIRROR SHAPE	INSERTION LOSS IN DECIBELS*		EXCESS
		THEORETICAL	ACTUAL*	
1:1		3.0/3.0	3.8/3.8	0.8
5:1		7.8/0.8	8.8/1.7	0.9
10:1		10.4/0.4	10.0/1.4	0.8
20:1		13.02/0.2	13.0/1.0	0.8

*ACTUAL LOSSES OF MORE THAN 20 DEVICES SHOW APPROXIMATELY 0.3-dB VARIATION ABOUT THESE MEANS.

The couplers can also be constructed with relatively good spectral independence. Longer wavelengths increase the GRIN-lens focal length, but this sensitivity can be reduced by optimizing for an average of the system wavelengths. For example, using 50- μm core multimode fiber in a dual wavelength system at $\lambda = 0.87 \mu\text{m}$ and $1.3 \mu\text{m}$, a focus set for $\lambda = 1.05\text{-}\mu\text{m}$ degrades the performance of the coupler by less than 0.2 dB.

2.4 Temperature stability

Temperature stability of the coupler was investigated, and variations in performance of <0.2 dB were observed over the range -40 to $+80$ $^{\circ}\text{C}$. Devices were subjected to 100 hours of cycling, 1 hour at each extreme. Figure 2 shows the stability of the coupler for the $1 \rightarrow 2$ and $1 \rightarrow 3$ channels. The plotted data are from 100 cycles of a device between -40 and $+80$ $^{\circ}\text{C}$. The hatch-shaded region is the performance of the fixed-mirror channel, while the dot-shaded region is the performance of the tilted-mirror channel. The ± 0.1 -dB variation of the fixed-mirror reflection is attributed to lateral cure strains in the fiber-lens joint. The ± 0.2 -dB insertion loss variation in the light reflected from the tilted mirror is the sum of two separable small shifts, the ± 0.1 -dB variation of the fiber-lens joint is still present, and an additional ± 0.1 dB is attributable to the thermal expansion and contraction of the cement wedge at the mirror. For a mirror bonded at a 1.3 -degree angle

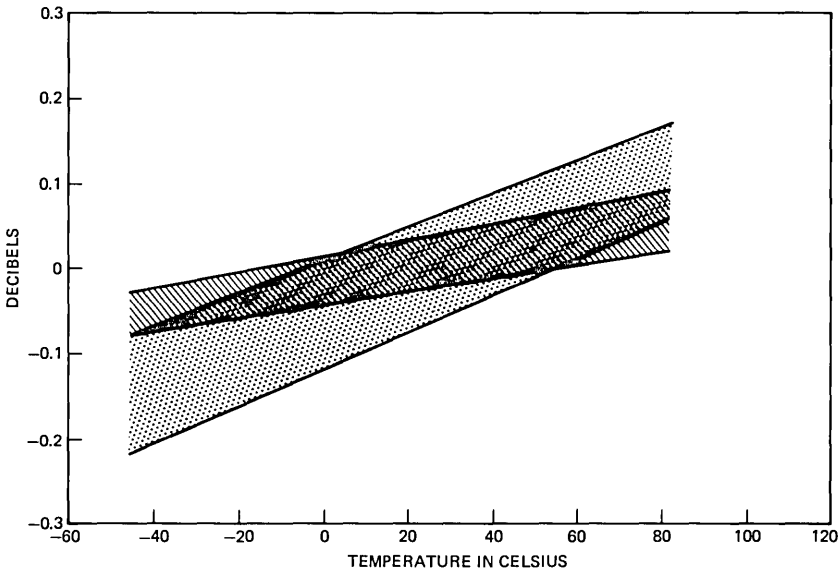


Fig. 2—Plot of coupler excess loss variation versus temperature. The hatch-shaded region is the coupler performance for the fixed mirror channel; the dot-shaded region is for the tilted mirror.

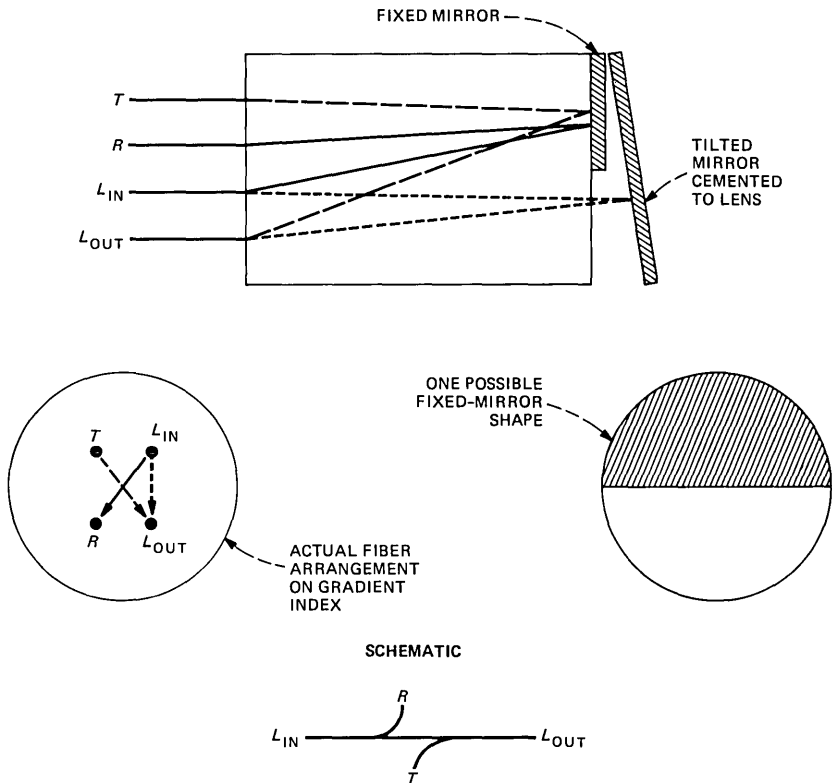


Fig. 3—Schematic diagram of GRIN-lens asymmetric four-port coupler.

to a 1.8-mm diameter lens, there is a thickness variation of $41\ \mu\text{m}$. If the cement has an average thermal expansion coefficient of $100 \times 10^{-6}\ \text{mm/mm}/^\circ\text{C}$, the angle can vary by ± 0.6 percent, which translates to a $\sim \pm 1\text{-}\mu\text{m}$ shift of the focal point in the focal plane or a $\pm 0.1\text{-dB}$ variation with temperature. As for the improved performance at higher temperature, we believe it can be attributed to thermal relaxation of the curing stresses and cement contraction that disturbed the original alignments.

III. FOUR-PORT DESIGN

Figure 3 gives the design of an asymmetric four-port coupler. This component couples light passively on a throughput [line in (L_{in}) \rightarrow line out (L_{out})] channel; a portion of the signal is also tapped. The same modes of the input fiber, L_{in} , which are diverted to the R (receiver) fiber, are available to be refilled with modes from the T (transmitter) fiber. This data-bus transceiver coupler allows for the

Table II—Insertion losses for four-port directional couplers

Device	Channel	Insertion Loss (dB)	
		Theoretical	Actual
1	$L_{in} \rightarrow R$	7.8	8.8
	$T \rightarrow L_{out}$	7.8	10.3
	$L_{in} \rightarrow L_{out}$	0.8	1.7
	$T \rightarrow R$		46.5
	excess		1.2
2	$L_{in} \rightarrow R$	3.0	3.8
	$T \rightarrow L_{out}$	3.0	4.2
	$L_{in} \rightarrow L_{out}$	3.0	4.0
	$T \rightarrow R$		43.5
	excess		1.0
3	$L_{in} \rightarrow R$	0.8	1.6
	$T \rightarrow L_{out}$	0.8	1.8
	$L_{in} \rightarrow L_{out}$	7.8	7.0
	$T \rightarrow R$		42.0
	excess		0.6

“listen while talking” function important to the *Ethernet** or Carrier-Sense Multiple-Access with Collision Detection (CSMA/CD) local-area network protocol since the T and R fibers are optically isolated by more than 40 dB. In addition to being useful in CSMA/CD-based fiber networks, these couplers are also important in fiber-optic fail-safe nodes.⁷

The one difference in fabrication lies in the arrangement of the fibers on the GRIN-lens face. In the three-port coupler the fibers are held in a close-packed triangular array; in the asymmetric four-port coupler they must be held on the corners of a square (actually, a rhombus will do). This is because the $L_{in} \rightarrow R$ and $T \rightarrow L_{out}$ couplings are achieved simultaneously by reflections from the fixed mirror when the four fibers are arranged symmetrically about the GRIN-lens axis (see Fig. 3). The $L_{in} \rightarrow L_{out}$ coupling is made using a tilted mirror similar to that described in the three-port coupler. High isolation between the T and R ports results because the remaining portion of the beam from fiber T is directed (by the tilted mirror) far from fiber R .

Since the coupler is so very similar to the three-port coupler previously described, it is not surprising that its performance is the same as far as its temperature stability and wavelength insensitivity. Excess insertion losses less than 1.0 dB are obtained for this coupler as well. Table II summarizes the performance for three different splitting ratios of this coupler.

Consistent asymmetric four-port coupler performance is (at present)

* Registered trademark of Xerox Corporation.

somewhat more difficult to achieve because of the simultaneous $L_{in} \rightarrow R$ and $T \rightarrow L_{out}$ alignment condition required by the device. This condition is easier to meet if a larger core fiber is used at the receiver port. Such large core fibers are common in receiver designs to promote better coupling. For the asymmetric four-port, such a fiber choice allows for the four fibers to be on the corners of the square with a lower precision and still not affect the overall excess insertion loss of the device.

This occurs in the following way. Alignment of the square fiber array is made by optimizing light from $T \rightarrow L_{out}$. Then the light from $L_{in} \rightarrow R$ is checked. When port R is a large fiber, all that is required for excellent coupling is that the image of L_{in} falls somewhere inside the R fiber core area. If a 50/125- μm fiber is used at the input and an 80/125- μm fiber is at port R , then this fiber pair can have a $\pm 15\text{-}\mu\text{m}$ error with respect to the T/L_{out} pair and the corners of the square. The losses in Table II are for the case where all four ports are 50/125- μm fiber. An average of 0.2-dB improvement is seen for the case of a large core 80/125- μm fiber at the R port.

IV. CONCLUSION

Small, $\sim 1\text{-cm}$, three- and four-port directional couplers have been designed for independent alignment of the fibers, for freedom in splitting-ratio variation, and for a certain degree of spectral independence. These couplers have also been tested for stable operation between -40 and $+80$ $^{\circ}\text{C}$.

These GRIN-lens couplers typically exhibit 0.8-dB excess insertion loss. The splitting ratio of the coupler can be varied by changing the area of a deposited Au mirror on the lens end face. Fiber-optic local-area network transceivers can be constructed using the asymmetric four-port coupler.

REFERENCES

1. T. Uchida and K. Kobayashi, "Micro-Optic Circuitry for Fiber Communications," in "Japan Annual Reviews in Electronics, Computer and Telecommunications, Optical Devices and Fibers, 1982," Y. Suematsu, ed.
2. H. Nishimoto et al. (title and paper in Japanese), Proceedings of the National Conference on Optical and Radio-Wave Electronics, IECE Japan, 1980, p. 301.
3. E. Weidel and J. Guttman, "Asymmetric T-Couplers for Fiber-Optic Data Buses," *Electron. Lett.*, *16*, No. 17 (August 1980), p. 673.
4. A. D. De Oliveira and M. G. F. Wilson, "Stripe Waveguide Y-Intersection as Efficient Coupler for Multimode Optical Communications Systems," *Electron. Lett.*, *17*, No. 2 (January 1981), p. 100.
5. T. W. Cline and R. B. Jander, "Wave-Front Aberration Measurements on GRIN Rod Lenses," *Appl. Opt.*, *21*, No. 6 (March 1982), pp. 1035-41.
6. *American Institute of Physics Handbook*, 3rd ed., D. E. Gray, ed., New York: McGraw Hill, 1972, pp. 6-157.
7. A. Albanese, "Fail-Safe Nodes for Lightwave Digital Networks," *B.S.T.J.*, *61*, No. 2 (February 1982), p. 247.

AUTHORS

Stephen W. Granlund, B.S. (Physics), 1980, Moravian College, Bethlehem, PA; AT&T Bell Laboratories, 1980—. At AT&T Bell Laboratories, Mr. Granlund is currently working on the development and reliability of various fiber-optic components.

Frank Levinson, B.S. (Mathematics and Physics), 1975, Butler University, Indianapolis, IN; M.S., 1978 and Ph.D. 1980 (Astronomy), University of Virginia; AT&T Bell Laboratories, 1980–1983. Now a member of the Central Services Organization of the Regional Bell Operating Companies. Mr. Levinson has done research and development on fiber-optic couplers, hybrid optical transceivers, and other fiber components suitable for fiber-optic local-area networks. In September of 1983 he joined the CSO as a member of the Communications Sciences Department, where he is involved in fiber-optic local- and metropolitan-area network hardware and systems research. Member, Optical Society of America and IEEE.

The DTWP: An LPC-Based Dynamic Time-Warping Processor for Isolated Word Recognition

By M. K. BROWN,* R. THORKILDSEN,* Y. H. OH,* and
S. S. ALI*

(Manuscript received August 1, 1983)

Special-purpose hardware for calculating dynamic time-warp distances has been designed and tested utilizing technology. The Dynamic Time-Warp Processor (DTWP) performs all of the necessary arithmetic and decision-making operations for selecting a word from a given vocabulary based on log likelihood distance measurements. The speed limitation in previously designed hardware was due to programmed decision making (often referred to as combinatorics). The combinatorics have been implemented in hardware in such a way that the decisions are made in the time of several gate delays rather than the time of several program cycles. Thus, a dynamic time warp (DTW) is performed on typical 40-frame templates in less than one millisecond. The DTWP serves as a slave to a 16-bit microcomputer. It performs all of the computation and control necessary for pattern classification, and is now operating on the board level. The processor is now being implemented for very large-scale integration. All logic has been designed in 2.5 μm , Complementary Metal-Oxide Semiconductor polycells and has been simulated on the Metal-Oxide Semiconductor Timing Simulator (MOTIS). The timing simulations indicate that the DTW time of 1 ms implemented at the board level can also be met on the integrated circuit.

I. INTRODUCTION

The typical isolated speech recognition system attempts to recognize

* AT&T Bell Laboratories.

Copyright © 1984 AT&T. Photo reproduction for noncommercial use is permitted without payment of royalty provided that each reproduction is done without alteration and that the Journal reference and copyright notice are included on the first page. The title and abstract, but no other portions, of this paper may be copied or distributed royalty free by computer-based and other information-service systems without further permission. Permission to reproduce or republish any other portion of this paper must be obtained from the Editor.

an unknown utterance by comparing the unknown with each of a number of previously stored reference templates. The recognition accuracy of speech is substantially increased when variations in the rate of speech production are taken into consideration. This is accomplished by dynamically warping the time axis of the reference utterance to the unknown utterance so that the minimum difference is found. In this way the majority of temporal variation in the speech is removed while the underlying spectral sequential structure is preserved. We have used the normalize-and-warp procedure of Myers, Rabiner, and Rosenberg,¹ with the global constraints proposed by Sakoe and Chiba.² The well-known Itakura algorithm has been implemented in a manner similar to that described by Ackenhusen and Rabiner.³ The identification of the unknown is based on the minimum dynamic time-warp (DTW) distance obtained over the set of reference templates.

Let us assume that we are given a characterization of the isolated word, which consists of a set of N vectors of Linear Predictive Coding (LPC) coefficients. The test pattern, \mathbf{T} , is represented as:

$$\mathbf{T} = \{T(1), T(2) \dots T(N)\}, \quad (1)$$

where the vector $T(i)$ is a spectral (LPC) representation of the i th frame of the test word. In our system a set of nine autocorrelations constitutes the vector from which an eighth-order LPC model is derived. The duration of the test utterance is N frames, where each frame represents 45 mS of speech, and adjacent frames are spaced 15 mS apart.

For a given vocabulary of V words, the reference vector, \mathbf{R}_v , is represented as:

$$\mathbf{R}_v = \{R(1), R(2) \dots, R(M_v)\} \quad (2)$$

where each vector, $R(j)$, is again a spectral representation of the corresponding j th frame within the reference utterance, and M_v is the number of frames in the v th reference.

To optimally align the time scale of the reference pattern (the dependent m index) to the test pattern (the independent n index), we must solve for a warping path function of the form:

$$m = w(n) \quad (3)$$

and thereby seek to minimize the total distance

$$D = \sum_{n=1}^N d[T(n), R(w(n))] \quad (4)$$

over all possible paths, $w(n)$, within the constraints, where $d(T(n), R(m))$ is the local distance between test frame n and reference frame $m = w(n)$. This operation must be performed for each reference vector,

$R(j)$, in the vocabulary. The test pattern is classified as belonging to the class for which the smallest accumulated DTW distance, D , is obtained. In addition to the standard DTW algorithm, we have employed linear time normalization of the normalize-and-warp procedure described by Myers et al.,¹ thus allowing the widest range of time alignment paths to be considered. This procedure linearly normalizes the test and reference utterances to a fixed length (in this case 40 frames) before the DTW is performed. This prenormalization greatly simplifies the processor design since the control logic can be fixed rather than have to respond to variables associated with warps of varying length.

Dynamic time warping has been implemented based on the Itakura⁴ constraints as follows:

$$\omega(1) = 1 \quad (5)$$

$$\omega(40) = 40 \quad (6)$$

$$g(n, m) = \begin{cases} 1, & \text{if } \omega(n) \neq \omega(n-1) \\ \infty, & \text{if } \omega(n) = \omega(n-1), \end{cases} \quad (7)$$

where accumulated distance is given by

$$\begin{aligned} D(n, m) = & d(T(n), R(m)) + \\ & \min[D(n-1, m) g(n-1, m), \\ & D(n-1, m-1), \\ & D(n-1, m-2)] \end{aligned} \quad (8)$$

and

$$D(1, 1) = d(T(1), R(1)). \quad (9)$$

Constraints (5) and (6) require the endpoints of the test and reference to match. Time alignment is performed between the endpoints constrained locally by (7). Basically, constraint (7) and eq. (8) allow the reference utterance to be time compressed by skipping one frame for each test frame. Time stretching is accomplished by duplicating a reference frame. This constraint limits the number of times a reference frame may be repeated to one, as shown in Fig. 1a. The path marked "x" is not allowed.

The terminal endpoint conditions must be satisfied by applying global constraints, as illustrated in Fig. 1b. The parallelogram constraint shown forms the basic constraint requirement such that local constraint (7) is satisfied from either endpoint. Sakoe and Chiba² have found that a further global constraint limiting the deviation of the solution path from the diagonal to $\pm R$ substantially reduces the

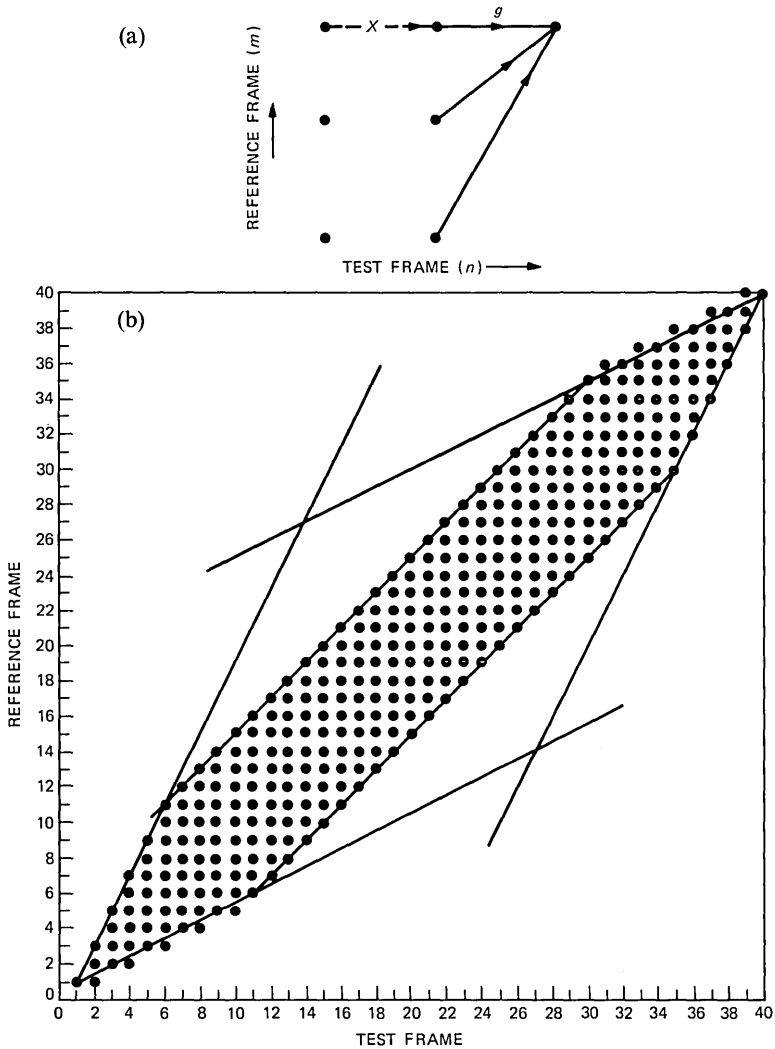


Fig. 1—Dynamic time warp for (a) local constraints, and (b) global constraints.

number of distance calculations necessary without suffering a significant loss in accuracy. In this implementation R is five.

Comparison of a test frame to a reference frame requires a measure of closeness in some sense. Several distance measures have been investigated and used for utterance comparison purposes. A method developed by Itakura⁴ has been found to yield high recognition accuracy and costs relatively little in computation. This distance function, often referred to as the log likelihood ratio (LLR), yields numerical values that are indicative of the spectral energy difference between

the two frames of speech. The form of the function is

$$d(x, y) = \ln[(a_r \mathbf{V}_t a'_r)/(a_t \mathbf{V}_t a'_t)], \quad (10)$$

where t refers to a test frame and r refers to a reference frame, a is a $(1 \times p + 1)$ vector consisting of a 1 followed by p LPC coefficients of a p th-order LPC model of the speech and \mathbf{V} is the $(p + 1 \times p + 1)$ autocorrelation matrix of the test frame. By appropriately computing a set of reference coefficients and test coefficients, $d(x, y)$ can be obtained as the result of a $(p + 1)$ -point dot product as described by Itakura.⁴

The DTW algorithm, which has traditionally been performed by a general-purpose processor or microprocessor, requires 360 distance calculations, 630 two-way comparisons, and 359 additions for eighth-order LPC. We have developed a finite-state machine specifically for DTW calculations which performs these calculations in 902.5 microseconds. The processor currently operates with a 4-MHz clock, but it is estimated from design analysis that the clock rate could be increased to 6 MHz for the board-level implementation.

In the following section we will discuss the architecture of the DTWP and explain its operation. Modules of particular interest are the combinatoric logic and the logarithm calculation logic, which will be described in Sections III and IV. Some preliminary specifications on the VLSI implementation will be discussed in Section V. Options of system integration are covered in Section VI with an example of a multiprocessor system implementation.

II. PROCESSOR ARCHITECTURE

The DTWP architecture is specifically designed to implement a particular DTW algorithm used in the speech recognizer described by Ackenhusen and Rabiner.³ Both the test utterance and reference template contain 40 frames each of LPC features. The Itakura constraints are applied so that expansion and compression ratios of the reference time axis with respect to the test time axis are limited to two to one or one half to one, respectively. Furthermore, the additional constraints described by Sakoe and Chiba² are applied (with $R = 5$) so that the number of distance calculations per column is limited to 11. In part, the high effective processing speed obtained with the DTWP is due to this specialization of the design. Changes in the number of frames to be warped, the constraints, and the Sakoe constraint (R) will require redesign of the DTWP.

The DTWP is interfaced to the control microprocessor via the data and address buses and four control lines from an I/O port. The microprocessor can load LPC values into both the test memory and reference memory. The test and reference templates are stored as 12-

bit values, 9 values per frame. Thus, each template requires 4320 bits of memory. The number of warps to be performed by the DTWP depends on the number of reference patterns stored in reference memory. An 8-bit register is provided in the DTWP for telling the processor the number of patterns to warp. After this value is loaded, the DTWGO signal is asserted by the microprocessor and the DTWP takes over control of its memories. These memories are removed from the microprocessor bus and split so that test and reference memories are individually accessible. In this way, data are obtained from the two memories in parallel at the rate of 24 bits per clock cycle or 96 million bits per second.

Warps are performed every 902.5 microseconds. The DTWP may be interrupted between warps so that the microprocessor can obtain the accumulated warp distances for each reference. The DTWP keeps track of the best distance and the corresponding reference index, which can be read back by the microprocessor between warps. If the DTWP is not interrupted between warps, it can perform 256 warps in 231 milliseconds.

An LPC distance is computed by multiplying the nine values of a test frame with the nine values of a reference frame, accumulating the sum of the products, and taking the logarithm (in this case a base two logarithm). These operations are performed by a 12×12 Wallace tree multiplier with a 24-bit accumulator in a pipelined fashion. Referring to Fig. 2, which shows a block diagram of the distance calculator, the sequence of operation is:

1. Apply addresses to the test and reference memories
2. Clock data into the multiplier input registers
3. Clock the product into the accumulator
4. Repeat steps 1, 2, and 3 eight times
5. Clock the logarithm result into the combinatoric logic.

Thus, it takes 13 clock cycles to obtain the first distance, and 10 clock cycles for each succeeding distance. The first three operations require nine clock cycles to compute the nine-point dot product. Operation (5) is performed on the tenth clock cycle.

A diagram of a DTW calculation is shown in Fig. 1. Each point on the diagram indicates a distance calculation consisting of a 9-point dot product and its logarithm, which is the LPC distance between one test frame and one reference frame. After the distance is computed, all calculations in the processor are performed in 16-bit unsigned arithmetic. An accumulated distance is calculated at each point, which consists of the local distance (or dot product) and the minimum of three possible predecessor distances, as shown in Fig. 1a. Thus, if each point is calculated sequentially (from bottom to top and from left to right on the diagram), only the previous column of points needs to be

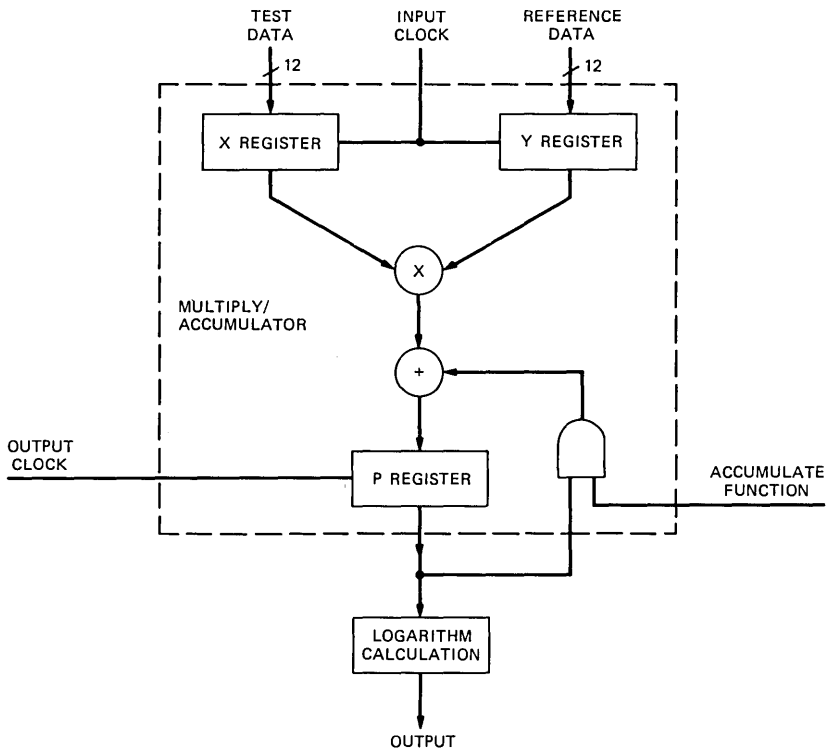


Fig. 2—Distance calculator.

available at any one time.

This is accomplished in the DTWP by a 14-stage shift register, as shown in the block diagram of Fig. 3. The boundary conditions of the warp are established by inserting large values, which we will call infinities, into the shift register at the top and bottom of each column of distances. These infinities will never be chosen as a minimum by the minimum selector for the accumulated distance calculation. Thus, when columns of 11 distances are processed (the middle portion of the warping function), two infinities must be inserted into the shift register after each column to separate one column from another. The number of stages in the shift register (14) comes from an analysis of the central portion of the warp. The 11 distances and two infinities occupy 13 stages. The 14th stage is necessary to position the accumulated distances of the previous column at the correct inputs of the three-way minimum selector. In this way, accumulated distances of the preceding column and the local distances currently being calculated are properly associated.

The number of distances in a column is fewer than 11 and increases

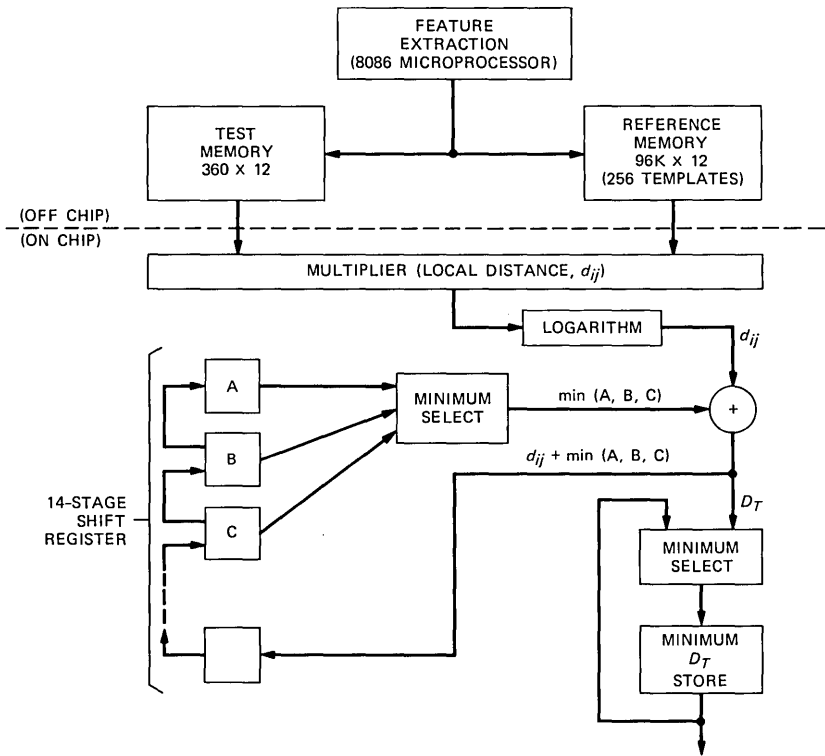


Fig. 3—Architecture of the dynamic time-warping processor.

at the beginning of the warp and decreases at the end of the warp. To properly align the columns of distances an appropriate number of infinities must be inserted into the shift register after each column. The number of distances and the number of infinities needed for each column are stored in Read-Only Memory (ROM). The sequence used in the DTWP is shown in Table I.

These values are critical to proper operation of the circuitry and cannot be usefully modified without corresponding changes in the surrounding hardware. Since one processor clock cycle is required to insert each infinity into the shift register, distance calculations are performed in parallel with the shifting operation. Normally, the number of infinities to be inserted is fewer than 10, so the shifting is normally completed before the next distance calculation is finished. There are four columns of distances, however, that require 10 or more infinity shifts. In these cases the distance calculator enters a wait state after the 10th clock cycle until the shifts are completed. During a warp, six wait-state clock cycles are used.

The last three stages of the 14-stage shift register deliver 16-bit

Table 1—Sequence of distances and infinities for DTWP

Test Frame	Distances	Infinities	Test Frame	Distances	Infinities
1	1	11	21	11	2
2	3	10	22	11	2
3	4	8	23	11	2
4	6	7	24	11	2
5	7	5	25	11	2
6	9	4	26	11	2
7	9	3	27	11	2
8	10	3	28	11	2
9	10	2	29	11	2
10	11	2	30	11	2
11	11	2	31	11	2
12	11	2	32	10	3
13	11	2	33	10	3
14	11	2	34	9	4
15	11	2	35	9	5
16	11	2	36	7	7
17	11	2	37	6	8
18	11	2	38	4	10
19	11	2	39	3	11
20	11	2	40	1	0

values to the three inputs of a three-way comparator shown in the block diagram of Fig. 3. The first of these three comparator inputs corresponds to a horizontal path segment, as shown in Fig. 1a. This comparator input can be disabled by a control bit stored in an auxiliary shift register, which indicates if a horizontal path was taken when the previous column of distances was calculated. This auxiliary shift register is 12 stages long and is clocked at the same time as the 14-stage shift register. If the horizontal path input is not disabled, and it is found that this input gives the lowest accumulated distance, then the path disable bit is set in the first stage of the auxiliary shift register in preparation for the following column of distances. Further details on the three-way comparator are given in the next section.

The output of the three-way minimum selector is added to the local distance from the distance calculator and the result is inserted into the first stage of the shift register between columns, until all 360 distances have been calculated. At this point a 4-clock cycle sequence is entered, which compares the current warp distance with the best previously stored warp distance and updates the stored value if necessary. Also, during this 4-cycle sequence, internal registers are cleared, the reference index is updated, and the control logic is initialized for the next warp. Thus, a warp is performed in 3600 clock cycles for distance calculations, plus 6 clock cycles for wait states, and 4 clock cycles for classification and reinitialization for a total of 3610 clock cycles.

III. COMBINATORIC LOGIC

The three-way minimum selector performs the equivalent of three memory reads, two comparisons, and two memory writes in slightly more than 50 ns in Transistor-Transistor Logic (TTL). MOTIS simulation indicates that the three-way comparison can be done in about 75 ns in Complementary Metal-Oxide Semiconductor (CMOS) logic. This very fast selection logic, coupled with the shift register architecture, allows the combinatorics of the DTW to be performed as fast as distances can be calculated. A hardware adder combines the minimum values selected with the LPC distance from the distance calculator and delivers the result to the first stage of the shift register. This combinatoric procedure occurs within one 250-ns clock cycle.

An expanded block diagram of the three-way minimum selector is shown in Fig. 4. The three-way selector is implemented as a pair of two-way selectors. The first selector determines the minimum of inputs A and B, and the second selector chooses between the A or B output of the first selector and input C. If input A is selected, the path disable bit is set in the auxiliary shift register. This bit is used to disable input C of the three-way minimum selector so that a horizontal path (in the sense of Fig. 1) can be inhibited.

The three-way selector is designed so that it will favor input A or B in the event that all three inputs are presented with equal values. This characteristic is considered to be the best since it assumes no expansion or compression of the test utterance with respect to the reference template and does not constrain the horizontal path unnecessarily.

The adder is a standard logic circuit. It performs a 16-bit unsigned addition in about 35 ns. The output of this adder is made available to the shift register at the next processor clock time.

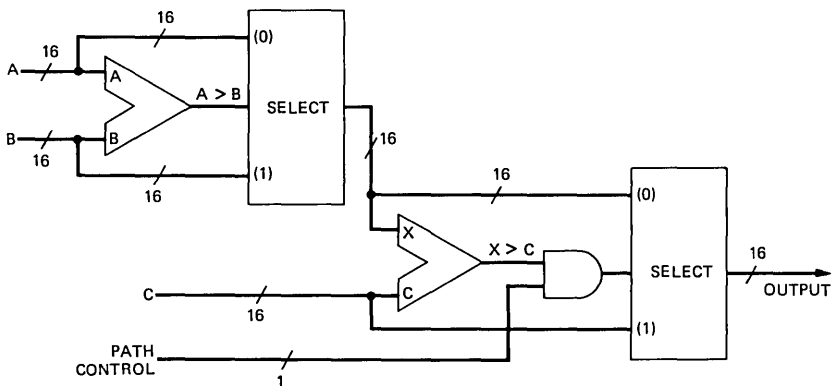


Fig. 4—Minimum selector.

IV. LOGARITHM FUNCTION LOGIC

It is well known that the logarithm of a number can be estimated from a geometric series. Since we are applying the logarithm as a multiplicative function (and performing a relative comparison of the results), the base of the log is unimportant. The logarithm function circuitry makes use of a first-order approximation of the log base two in the range of one to two as follows:

$$\log(x) = x - 1 \quad \text{for } 1 < x < 2. \quad (11)$$

The maximum amount of error between the straight line approximation and the base two logarithm function is less than 0.09 in magnitude. Relative error approaches about 30 percent near $x = 0$; however, this has little impact on the relative comparison of accumulated distances. A plot of logarithm calculation error versus x is shown in Fig. 5a.

The logarithm for values of x greater than two can be approximated by dividing x by the largest value of 2^n that results in a quotient that is greater than or equal to one. Thus, the logarithm base two may be approximated with a piecewise linear function as:

$$\log(x) = n + (x/2^n) - 1 \quad \begin{array}{l} \text{for } x \geq 1 \\ \text{and} \\ 1 \leq (x/2^n) \leq 2. \end{array} \quad (12)$$

This function is implemented with a priority encoder and multiplexor as shown in Fig. 5b. The priority encoder determines the value of n and the multiplexor performs the division by 2^n . This logic functions accurately only for values of x greater than or equal to 1.0. The TTL design requires four dip packages and yields a propagation delay of about 25 ns. The implementation of Very Large-Scale Integration (VLSI) has been simulated with MOTIS and requires 35 ns for the equivalent operation using 2.5- μm CMOS. This is a substantial improvement over an earlier design that used an Erasable Programmable Read-Only Memory (EPROM) with an access time of about 350 ns. For VLSI design, this approach is much more desirable since it only requires about 200 gates as compared to about 25,000 bits of ROM.

V. CHIP DESCRIPTION

The DTWP chip will be packaged in a 68-pin chip carrier. The allocation of pins is given in Table II. The 68-pin chip carrier is a standard of AT&T Technologies, Inc. The six additional pins will be used for testing purposes.

The data pins will be multiplexed so that the DTWP can access the reference and test memories while it is calculating a warp path, and

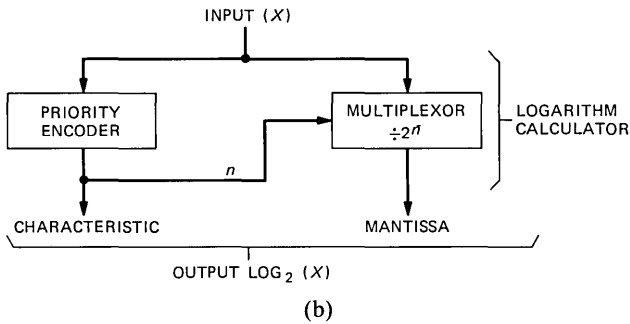
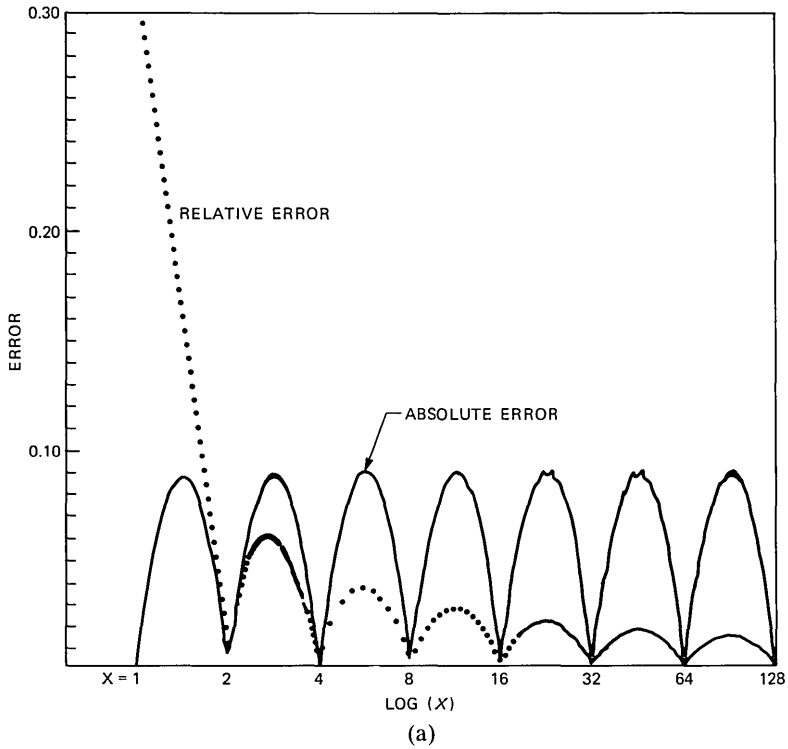


Fig. 5—(a) Logarithm calculation error. (b) Logarithm calculator.

the microprocessor can access internal DTWP registers while the DTWP is idle. Access to the internal DTWP registers is controlled by three Read/Write Control lines. The Interrupt Enable and Interrupt Flag will allow the microprocessor to halt the DTWP temporarily while the internal registers are being read. DTWP Busy is provided to aid in interfacing the test and reference memories, which must appear to be dual-port memories to the DTWP. The Hard Reset allows the micro-

Table II—DTWP chip pin allocation

Reference addressing	17
Reference data and DTWP low byte for distance, index, number of warps	12
Test addressing	9
Test data and DTWP high byte	12
Read/write control:	
*Load register	1
†DTWP go	1
*Read distance	1
*Read best distance	1
*Read index	1
†Interrupt enable	1
†Interrupt flag	1
†DTWP busy	1
*Hard reset	1
Clock	1
Power	1
Ground	2
Total pins currently (others used for testing)	63

* Address decoded.

† I/O control.

processor to reset internal registers and clear all pending DTWP operations.

As shown in Table II, several registers are available to the microprocessor. The Distance Register will allow the microprocessor to read the accumulated warp distance of each warp, if desired, under control of the Interrupt function. This is accomplished by enabling the DTWP interrupt via Interrupt Enable and waiting for the Interrupt Flag to be asserted. At this time the DTWP is idle and the microprocessor can read the internal distance register, the best distance found so far, and the index of the best reference template. When the read is complete, the Interrupt Enable is lowered by the microprocessor, the DTWP then clears the Interrupt Flag and proceeds with the next warp. If the distance for the next warp is required by the microprocessor, then it must enable the interrupt within 900 microseconds in order to catch the next interrupt.

The multiplier consists of three stages. The first latches the multiplicand and multiplier and generates six partial products in parallel using a two bit at a time algorithm.⁵ The partial products are added together in the last two stages, which are a bit slice adder and a full-carry look-ahead adder. Since the output of the multiplier is latched and then gated back to the top of the bit slice adder, accumulation of products is done along with partial product addition when required. This operation is selected or inhibited by the gate.

As we mentioned previously, the multiplier accumulator performs a 12×12 -bit multiply and 24-bit accumulate in less than one clock cycle (250 ns). Thus, each clock pulse latches new data into the first

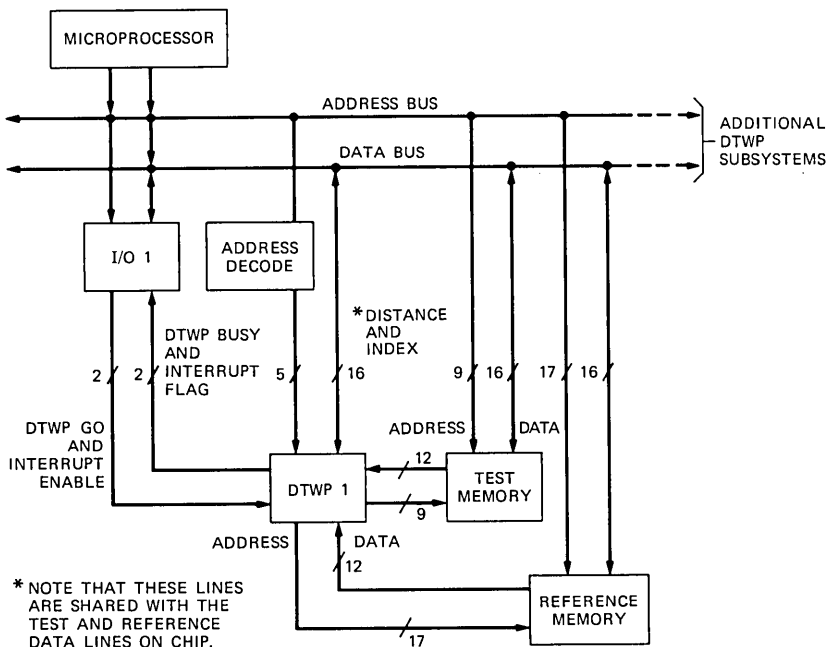


Fig. 6—DTWP interfacing.

stage and simultaneously latches the previous result at the multiplier output in a pipeline manner.

Current estimates indicate that the chip will contain about 6,600 gates, or 40,000 transistors. Of these, approximately 11,000 transistors comprise the multiplier-accumulator. This should result in a chip size of about 9 mm by 9 mm when implemented by polycell design techniques in 2.5- μ m CMOS technology.

VI. SYSTEM IMPLEMENTATION

A block diagram of a typical DTWP configuration is shown in Fig. 6. Both DTWP test and reference template memories are accessible to the microprocessor via the bus by appropriate addressing. The number of DTWP's that can be handled by the microprocessor depends on the amount of memory address space for reference memory since each reference memory requires 192K bytes of address space. The 8086 microprocessor, for example, can handle only about four DTWPs. If the reference memory is stored in ROM, then this addressing limitation is removed.

It should be noted that the test and reference memories here appear to be dual port. This is accomplished by use of tri-state buffers that are controlled by the DTWP Busy signal. When this signal indicates a

warp is in progress the memories are floated off the microprocessor address/data/control buses and connected to the DTWP address/data bus. This allows the microprocessor to have access to the system bus so that it may execute another program during DTWs.

Each DTWP is controlled by the microprocessor through either I/O control signals or memory address lines. The memory address must be decoded by outside logic to provide the desired reset, load, or read command. The Interrupt Flag and DTWP Busy can be handled by the microprocessor through polling or as a true interrupt.

The DTWP Reset should be triggered on power up and should also be able to be triggered by software. This clears all DTWP registers and resets internal control logic to standby. In this mode the test and reference memories are available to the microprocessor.

The reference memories are loaded by the microprocessor in the training mode with the appropriate number of reference templates (up to 512 templates in this case). At this point the recognition mode is entered. The two test memories are loaded by the microprocessor with an unknown test utterance. Each DTWP must have its own copy of the test word. The Load Register line is enabled and a microprocessor write cycle is performed to enter into each DTWP the number of reference templates to compare. This can be performed simultaneously for all DTWPs if the same number is to be written to each DTWP.

When the DTWP Go is triggered for each DTWP, the DTWP Busy flag for each processor will be asserted. Each DTWP will then sequentially compare the test word against each reference in its reference memory until the designated number of references have been checked. Optionally, within 900 μ s after the DTWP Go, the user may assert the Interrupt Enable and thus cause the DTWP to enter an idle state after completing the first warp. At this point the microprocessor may read the distance score for the first comparison. Clearing the Interrupt Enable causes the DTWP to resume operation. If the Interrupt Enable is asserted again within 900 μ s, the DTWP will stop after the next warp. In this way the distances for each comparison may be obtained by the user. When the specified number of warps is complete, the DTWP Busy flag will be cleared and the DTWP enters the idle state. The microprocessor can read the Best Distance and Index by sending the appropriate Read Enable signal to the DTWP and performing a read cycle. Each DTWP must be handled separately by the microprocessor during a read cycle so that data from the two DTWPs are not mixed together. In this configuration, 512 warps can be performed in about 231 ms if intermediate distance readings are not taken.

VII. SUMMARY

The dynamic time-warping processor described here is a key element

in the single-board isolated word recognizer. The DTWP chip will perform dynamic time warps at about 50 times the speed of the currently used microprocessor-based hardware. A single DTW requires $902.5 \mu\text{s}$ (3610 clock cycles at 4 MHz). The number of warps performed is controllable by the microprocessor and may currently be set for up to 256 warps. The DTWP also performs a single nearest neighbor rule classification. The index of the best reference candidate, warp distance to the best reference checked, and warp distance to the current reference are available to the control microprocessor after each warp by raising an Interrupt Enable Input to the DTWP. This will cause the DTWP to interrupt its processing at the end of the current warp and wait for the control microprocessor to read data from the DTWP registers. If the DTWP is not interrupted between warps, it can perform 256 warps in 231 ms (a rate of about 1108 warps per second).

The architecture and logic design have been tested with a TTL board-level implementation. A VLSI multiplier chip is the most complicated device used. Except for ROM memories, all of the other logic is of Medium-Scale Integration (MSI) complexity requiring about 100 packages. A 96K by 12-bit reference memory and a 1K by 12-bit test memory are used for template storage. The processor consumes about 1.8 *INTERPAC** 13-inch wirewrap boards, including reference memories. The DTWP chip, which will replace these 100 packages, is currently projected to contain about 6600 gates or 40,000 transistors.

REFERENCES

1. C. S. Myers, L. R. Rabiner, and A. E. Rosenberg, "Performance Trade-offs in Dynamic Time Warping Algorithms for Isolated Word Recognition," *IEEE Trans. on Acoustics, Speech, and Signal Processing, ASSP-28*, No. 6 (December 1980), pp. 622-33.
2. H. Sakoe and S. Chiba, "Dynamic Programming Algorithm Optimization for Spoken Word Recognition," *IEEE Trans. on Acoustics, Speech, and Signal Processing, ASSP-26*, No. 1 (February 1978), pp. 43-9.
3. J. G. Ackenhusen and L. R. Rabiner, "Microprocessor Implementation of an LPC-Based Isolated Word Recognizer," *IEEE Conf. Acoustics, Speech, and Signal Processing* (March 1980), pp. 746-9.
4. F. Itakura, "Minimum Prediction Residual Principle Applied to Speech Recognition," *IEEE Trans. Acoustics, Speech, and Signal Processing, ASSP-23*, No. 1 (February 1975), pp. 67-72.
5. R. M. M. Oberman, *Digital Circuits for Binary Arithmetic*, New York: John Wiley and Sons, 1979, pp. 151-62.

AUTHORS

Syed S. Ali, M.S. (Physics), 1973, University of Punjab, Pakistan; AT&T Bell Laboratories, 1980—. Since joining AT&T Bell Laboratories Mr. Ali has been involved in the development of software and hardware for speech recognition subsystems.

* Trademark of AT&T Technologies, Inc.

Michael K. Brown, B.S.E.E., 1973, M.S., 1977, and Ph.D., 1981 (Electrical Engineering), all from the University of Michigan, Ann Arbor; Burrough's Corporation, 1973-1980; AT&T Bell Laboratories, 1980—. From 1973 to 1976 Mr. Brown was employed with the Burrough's Corporation and was involved in the development of ink jet printer systems. From 1976 to 1980 he continued his work with Burrough's Corporation as a consultant while pursuing his Ph.D. Degree at the University of Michigan. His thesis was in the area of image processing and pattern recognition. In 1980 he joined the Speech Processing Group at AT&T Bell Laboratories, Murray Hill, New Jersey, where he was involved in research in speech recognition and synthesis techniques. Since 1983, he has been with the Robotics Principles Research Department.

Young Hwan Oh, B.S., 1971, M.S., 1974, Ph.D., 1978 (Electrical Engineering), University of New Mexico; M.B.A. Program, 1971-1972; GTE Automatic Electric Laboratories, 1978-1981; AT&T Bell Laboratories, 1981—. While at GTE Automatic Electric Laboratories, he was involved in hardware design, debugging, and testing for an I/O module for GTD5-EAX, Class 5 Digital End Office (DEO) Switching System. Also, he was a responsible engineer for converting the analog DTMF receiver to the digital DTMF receiver for No. 5 application. At AT&T Bell Laboratories, Murray Hill, he has been with the Speech Processing Group, where he has been involved in speech synthesis and recognition projects. His dissertation was in the area of digital filtering and performance analysis. Member, IEEE, Tau Beta Pi.

Reed Thorkildsen, B.S. (Physics), 1976, East Tennessee State University; Ph.D. (Physics), 1981, University of Virginia; AT&T Bell Laboratories, 1981—. Mr. Thorkildsen is engaged in development of voice recognition integrated circuits and subsystems. Member, Phi Kappa Phi, Sigma Xi.

On the Application of Embedded Training to Connected Letter Recognition for Directory Listing Retrieval

By L. R. RABINER,* J. G. WILPON,* and S. G. TERRACE*

(Manuscript received August 26, 1983)

Automatic speech recognition has advanced to the stage where it is now possible to recognize connected strings of words (e.g., digits, letters, city names, airline terms) from a word reference set of isolated tokens of each of the words in the vocabulary. Recently, an improved training technique called embedded word training was proposed, in which reference word patterns were extracted from within connected word sequences themselves. In this investigation we extend the embedded word training procedure to handle letters of the alphabet for use in a directory listing retrieval task. By performing connected letter recognition of spoken names based on letter classes (rather than specific letters themselves), we show how reliable name recognition results can be achieved using a fairly straightforward system on 200 randomly chosen names (chosen from an 18,210-name directory) spoken at a normal rate by four talkers (three male, one female) in a speaker-trained mode. We have found that an 8-percent improvement in name recognition accuracy is obtained when using embedded letter training patterns over that obtained from isolated letter patterns alone. The overall name recognition accuracy was close to 95 percent.

I. INTRODUCTION

Research in the area of isolated word recognition has progressed to the state where a wide variety of practical recognition systems exist both in the laboratory and in the commercial world.¹⁻⁷ These systems

* AT&T Bell Laboratories.

Copyright © 1984 AT&T. Photo reproduction for noncommercial use is permitted without payment of royalty provided that each reproduction is done without alteration and that the Journal reference and copyright notice are included on the first page. The title and abstract, but no other portions, of this paper may be copied or distributed royalty free by computer-based and other information-service systems without further permission. Permission to reproduce or republish any other portion of this paper must be obtained from the Editor.

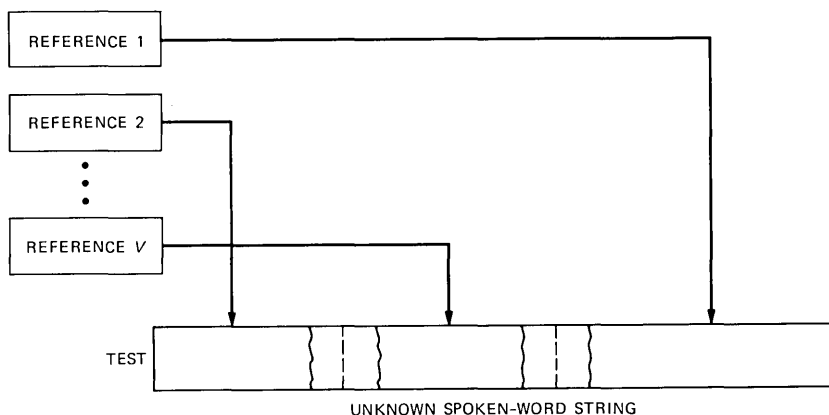


Fig. 1—Illustration of connected word recognition by concatenation of individual reference patterns.

are often capable of handling medium- to large-size (100- to 1000-word) vocabularies; they can work in both speaker-trained and speaker-independent modes; they can work over dialed-up (local) telephone lines; and they can take advantage of task syntax to improve overall system accuracy. The major shortcoming of these recognition systems is the isolated word format itself, since it is highly unnatural for use in a wide variety of tasks (e.g., digit dialing, word spelling, etc.).

The area of connected word recognition has made great strides forward in the last few years, and it has reached the point where there are several laboratory and commercial systems that attain some limited degrees of success.⁸⁻¹¹ Figure 1 summarizes the basic idea in a pattern-based approach to connected word recognition. Assume we are given a test pattern, \mathbf{T} , which represents an unknown spoken-word string, and we are given a set of V reference patterns, $\{R_1, R_2, \dots, R_v\}$, each representing some word of the vocabulary. The connected word recognition problem consists of finding the "super" reference pattern \mathbf{R}^s ,

$$\mathbf{R}^s = R_{q(1)} \oplus R_{q(2)} \oplus \dots \oplus R_{q(L)}. \quad (1)$$

This is the concatenation of L reference patterns, $R_{q(1)}, R_{q(2)}, \dots, R_{q(L)}$, which best matches the test string, \mathbf{T} , in the sense that the overall distance between \mathbf{T} and \mathbf{R}^s is minimum over all possible choices of $L, q(1), q(2), \dots, q(L)$, where the distance is an appropriately chosen distance measure.

There are several problems associated with solving the above connected word recognition problem. First, we don't know L , the number

of words in the word string. Hence, our proposed solution must provide the best matches for all reasonable values of L , e.g., $L = 1, 2, \dots, L_{\text{MAX}}$. Second, we don't know, nor can we reliably find, word boundaries, even when we have postulated L , the number of words in the string. The implication of this observation is that our word recognition algorithm must work without direct knowledge of word boundaries; in fact, the estimated word boundaries will be shown to be a byproduct of the matching procedure. The third problem with a template matching approach is that the word matches are generally much poorer at the boundaries than at frames within the word. In general, this is a weakness of word-matching schemes, which can be somewhat alleviated by the matching procedures that can apply lesser weight to the match at template boundaries than at frames within the word. A fourth problem is that word durations in the string are often grossly different (shorter) from the durations of the corresponding reference patterns. To alleviate this problem, one can use some time prenormalization procedure¹² to warp the word durations accordingly, or rely on reference patterns extracted from embedded word strings, as will be described later in this paper. Finally, the last problem associated with matching word strings is that the combinatorics of matching strings exhaustively (i.e., by trying all combinations of reference patterns in a sequential manner) is prohibitive.

A number of different ways of solving the connected word recognition problem, which avoid the plague of combinatorics mentioned above, have been proposed. Among these algorithms are the two-level Dynamic Programming (DP) approach of Sakoe,⁸ the level-building approach of Myers and Rabiner,⁹ the parallel single-stage approach of Bridle et al.,¹⁰ and the nonuniform sampling approach of Gauvain and Mariani.¹¹ Although each of these approaches differs greatly in implementation, all of them are similar in that the basic procedure for finding \mathbf{R}^s is to solve a time-alignment problem between \mathbf{T} and \mathbf{R}^s using Dynamic Time Warping (DTW) methods.

Figure 2 illustrates the level-building DTW-based approach to connected word recognition. Shown in this figure are the warping paths for all possible length matches to the test pattern, along with the implicit word boundary markers ($e_1, e_2, \dots, e_{L-1}, e_L$) for the dynamic path of the L -word match. The level-building algorithm builds up all possible L -word matches one level (word in the string) at a time. For each string match found, a segmentation of the test string into appropriate matching regions for each reference word in \mathbf{R}^s is obtained. In addition, for every string length L , the best β matches (i.e., the β lowest-distance L -word strings) can be found. The details of the actual level-building algorithm are available elsewhere,⁹ and will not be discussed here. Instead, we will rely on the properties of the algorithm,

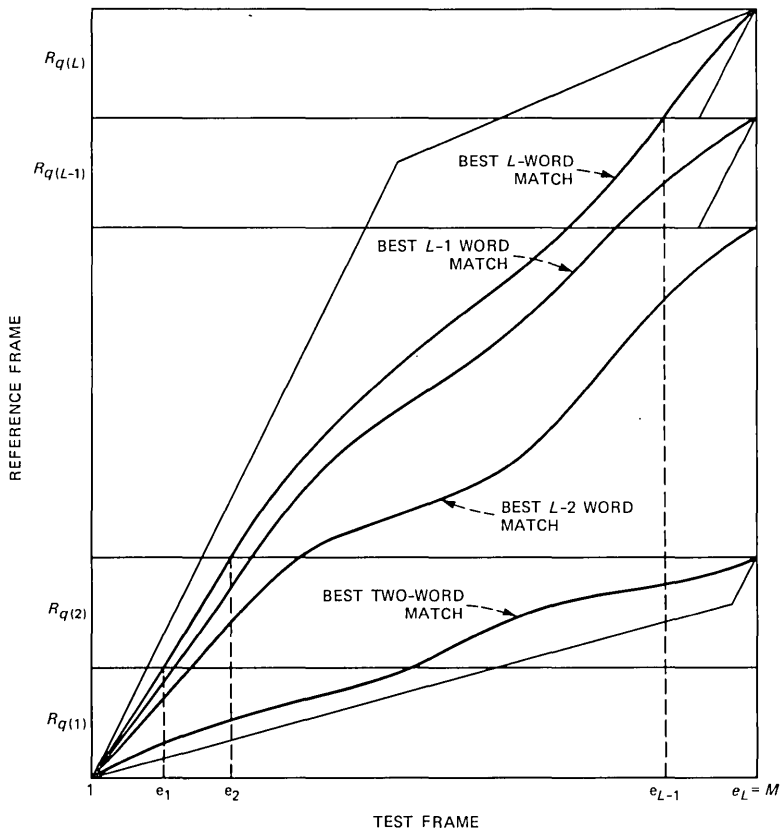


Fig. 2—Sequence of level-building DTW warps to provide best word sequences of several different lengths.

mentioned above, to show how we can use them to obtain improved speaker-independent word reference patterns.

Generally, the single word reference patterns used in the matching procedure of Figs. 1 and 2 are chosen as isolated occurrences of each vocabulary word (often obtained by some form of robust training procedure¹³). This form of training is adequate as long as the rate of articulation of the spoken connected word strings is not too high (e.g., typically fewer than 150 words per minute). However, for high rates of articulation, problems occur in the matching due to the gross differences between isolated words and those in fluent strings.

One solution to the problem of high rate of articulation is to use reference tokens extracted from connected word strings to supplement the isolated word reference tokens.¹⁴ Such embedded training tokens are extracted from known training strings and can be used in a

modified form of the robust training procedure to give robust embedded training tokens for each word of the vocabulary. Such techniques have been applied to the problem of connected digit recognition in both the speaker-trained mode,¹⁴ and in the speaker-independent mode,¹⁵ with very good success. The connected digits case was a natural first application since the number of environments in which each digit occurs is strictly limited (i.e., there are at most 10 predecessor digits and 10 following digits; furthermore, there is great similarity in many of these combinations).

Another natural application of connected word recognition is the case of recognition of connected letters for retrieving a name from a fixed directory of names.^{16,17} Early experimentation with this system indicated that the task was a viable one (if the rate of articulation was not too high), based on isolated reference patterns for each letter.¹⁸ In this paper we extend the embedded training procedure to handle the case of connected letters, and show how the resulting embedded letter templates can be used to improve recognition performance in a name retrieval task. The systems we used are speaker-trained ones; however, previous studies indicate that our results can readily be extended to the speaker-independent case.¹⁵

The organization of this paper is as follows. In Section II we review the structure of the overall connected letter recognition system and show how it can be used to retrieve the "best" matching name in a fixed directory of names. In Section III we discuss an evaluation of the overall connected letter, directory listing retrieval system, running in a speaker-dependent mode. In Section IV we discuss the results and give an analysis of the errors. Finally, in Section V we summarize our results and our main conclusions.

II. THE CONNECTED LETTER RECOGNITION SYSTEM

Figure 3 is a block diagram of the connected letter recognition system, as it used in the directory listing retrieval application. The system operates as follows. A user spells the last name of the person for whom directory information is desired as a connected sequence of spoken letters, followed by a brief pause, followed by the initials (again as a connected sequence). A conventional endpoint detector¹⁹ finds the beginning and ending of each of the two spoken strings. An example of such endpoint detection is given in Fig. 4, where the dashed lines indicate the speech endpoints. An 8-pole Linear Predictive Coefficient (LPC) analysis is performed on each frame of both the spoken last name and the initials, where the analysis frame size is 45 ms and consecutive frames are spaced 15 ms apart. For both the spoken last name and the initials, a level-building Dynamic Time Warping (DTW) fit to a set of letter classes is made (based on letter reference patterns)

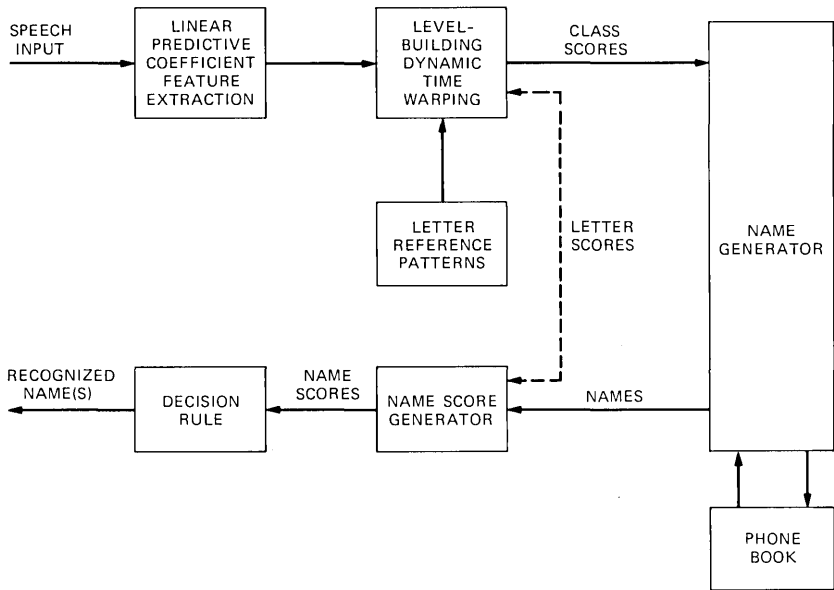


Fig. 3—Automatic directory listing retrieval system based on connected letter spelling of names.

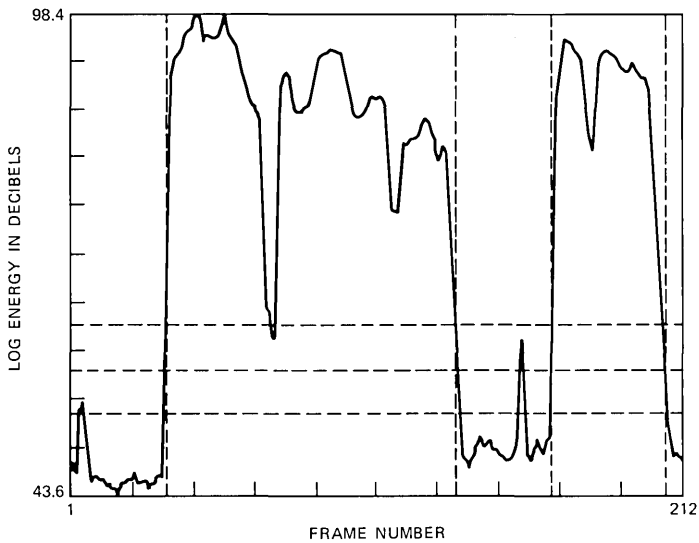


Fig. 4—Intensity contour for spelled name. The first set of vertical dashed lines delimits the beginning and end of the spoken last name; the second set of vertical dashed lines delimits the initials. The horizontal dashed lines indicate energy thresholds from which the beginning and ending frames are found.

and both the individual letter scores and the classes scores are saved. Last name class scores for all possible last name classes are generated and sorted by distance. A name generator sequentially goes through the sorted class list and generates all valid names within the class (i.e., those stored in the phone book). A name score generator uses the letter scores to give a total name score for each name within each class. Name scores are sorted in a list according to total name distance. Classes are searched until the best possible name score exceeds a specified threshold (related to the best name distance achieved so far). A list of the best name scores is then returned and the name recognized is the one at the top of the list.

In the remainder of this section we briefly describe the individual steps used to recognize the name. First we describe some characteristics of the letter classes and the phone book and then discuss the way in which we extract the embedded letter reference patterns for each talker. Next we review the level-building DTW algorithm and follow with a discussion of the name generation, name scoring, and decision rules.

2.1 Classification of letters into letter classes

The concept of blocking letters into letter classes, for purposes of speech recognition, was introduced by Aldefeld et al.²⁰ for the connected letter recognition application. The basic idea is that highly accurate recognition of spelled letters (over dialed-up telephone lines) cannot be achieved. Hence it is preferable to combine highly confusable letters into letter classes, perform recognition on letter classes, and decode the letter classes into actual directory names by searching a directory sorted by letter class combinations. Name scores are generated on the basis of individual letter scores (which are also generated in the recognition phase).

In particular, the 26 letters of the alphabet were assigned to 3 letter classes as shown in Table I. (A fourth class, class 0, contains the space

Table I—Assignment of letters into letter classes

Letter Class			
0	1	2	3
<i>b</i>	B	A	F
	C	H	L
	D	I	M
	E	J	N
	G	K	Q
	P	O	R
	T	W	S
	V	Y	U
	Z		X

character, \emptyset). Class 1 contains the /EE/ letters, whereas classes 2 and 3 are a partitioning of the remaining 17 letters into two disjoint sets with minimal interclass confusion.²¹ We denote the total number of classes as C .

For each name in the directory a set of I indices for the last name are defined. These indices define the letter class of each letter of the last name. Hence the names Rabiner and Wilpon would be represented by the indices:

NAME: RABINER WILPON
 CLASS: 3 2 1 2 3 1 3, 2 2 3 1 2 3.

If we restrict ourselves to using $I = 6$ indices for the last name, and we adopt the convention that we use the character \emptyset to pad out last names of fewer than six letters, then we have a total of

$3^6 =$	729	Classes with 6 letters
$3^5 =$	243	Classes with 5 letters
$3^4 =$	81	Classes with 4 letters
$3^3 =$	27	Classes with 3 letters
$3^2 =$	9	Classes with 2 letters
$3^1 =$	3	Classes with 1 letter
		1092 Total Classes.

After sorting an AT&T Bell Laboratories directory of 18,210 names according to the letter class assignment, a total of 1053 of the 1092 classes actually had one or more names assigned to it. Hence, coding of the last name to six indices is an efficient representation in terms of usage of possible letter classes.

2.2 Extraction of embedded letter patterns

The set of letter reference patterns for each talker consisted of three robust tokens of each letter, obtained as follows. An isolated robust token was obtained in the conventional manner, i.e., the talker spoke the letter repeatedly until two tokens were sufficiently similar (at a small enough distance) that they could be averaged.¹³ Two embedded robust tokens of each letter were obtained by having the talker speak specified three-letter strings, extracting the middle letter via DTW alignment, and then using the standard robust training procedure on the embedded letters.¹⁴ One of the embedded robust tokens was extracted from three-letter strings with minimal coarticulation between letters at the boundary. The other embedded robust token was extracted from three-letter strings with strong coarticulation between letters at the boundary.

Table II—Training sequences used for extraction of robust embedded letters for A, E, S, and W

Letter			
A	E	S	W
Noncoarticulated Sequences			
FAC	FEK	FSR	SWP
HAP	SEQ	XSW	XWT
XAT	XEK	HSL	FWK
SAQ	HEK	XSN	HWQ
FAP	FEQ	FSR	FWC
HAQ	XEQ	HSW	SWK
XAC	HEK	XSR	HWQ
Coarticulated Sequences			
RAL	WEL	WSC	WWR
MAN	NES	NSK	LWY
PAY	MEL	LSP	MWW
RAW	YEN	RSQ	LWR
ZAL	WER	LST	MWN
JAR	MEN	MSP	NWF
DAN	DEY	YSK	TWN

By way of example, Table II shows the three-letter training sequences used to obtain the robust tokens for the letters A, E, S, and W. The first seven sequences for each letter represent noncoarticulated strings; the next seven sequences for each letter represent coarticulated strings. The talker was only required to speak as many strings as required for obtaining a robust token of the letter. In theory as few as two strings could be adequate for this purpose; in practice it usually took four or five strings to give a pair of consistent embedded tokens. This is due to the high degree of variability of spoken letters in spelled strings.

An important point should be made about the training sequences. In theory the three-letter sequences were obtained by randomly selecting an initial and a final letter from a set of candidates based on the manner of production of the middle letter (the one being extracted) at the beginning and end of the word. In fact we found that the conventional vowels, namely A, E, I, O, and U, could not be used in either initial or final position in the training strings. Such combinations almost always led to extremely poor alignment paths for determining the embedded letter boundaries. As such, these letters were eliminated from consideration for use in the embedded training procedure.

The results of the training (which typically required about 30 minutes per talker) were a set of three reference patterns for each letter or a total of 78 reference patterns for the 26 letters.

Table III—Example of use of LB DTW algorithm in recognizing a spoken name

(a) Level-Building Distance Scores for Last Name and Initial Classes		
<u>Name:</u>	ZBOYAN	AM
<u>Class:</u>	1 1 2 2 2 3	2 3
<u>Last Name Class Scores:</u>		
$l = 1, 2, 3, 4, 5$	No matches found	
$l = 6$	<u>Class</u>	<u>Distance</u>
	112213	0.214
	112223	0.224
	212213	0.246
<u>Initial Class Scores:</u>		
$l = 1$	<u>Class</u>	<u>Distance</u>
	2	0.449
$l = 2$		
	23	0.232
	13	0.267
(b) Overall Name Distance Scores		
<u>Class</u>	<u>Name</u>	<u>Overall Distance</u>
112223	ZBOYAN AM	0.226
112223	ZBOYAN DL	0.235

2.3 Level-building recognition procedure

The recognition procedure is based on using the Level-Building (LB) DTW algorithm on strings of letter classes by using all 26 letters at each level but considering them only as different class templates. That is, different letters in the same letter class are considered as different templates for their common letter class. In the LB implementation we keep track of the C best (class) candidates at each level and use the standard LB traceback algorithm⁹ to generate a name class score for each of the 1053 possible last name classes.

By way of example, Table III illustrates the application of the LB DTW algorithm on the spoken name ZBOYAN AM. We use the $C = 3$ letter classes shown in Table I. The first step is to generate last name class scores for each of the 1053 last name classes and to order these scores by distance. The results are shown in Table IIIa for the top three classes. Since a six-letter last name was spelled, the top three last name class distance scores are for three-letter last names. The last name class corresponding to the spoken name is not the best class, but instead has the second best distance score.

The next step is to generate initial scores for all possible sets of one or two initials. For both the last name and the initials, the LB

algorithm keeps track of the best individual letter scores at each level. This requires a reasonable amount of storage but leads to a very efficient procedure for generating name scores. To generate a name score, one merely backtracks the individual letter scores (for both last name and initials) from the appropriate memory stacks, and a total name score is generated as

$$D_{\text{NAME}} = \frac{D_{LN} \cdot L_{LN} + D_I \cdot L_I}{L_{LN} + L_I}, \quad (1)$$

where D_{LN} and D_I are the normalized distances for the last name and initials, and L_{LN} and L_I are the number of letters in the last name and initials.

2.4 Stopping criteria

As we discussed above, the process of recognizing a name from spoken spelled letters consists of:

1. Running the LB on the last name and initials.
2. Generating all possible last name class scores.
3. Sorting the list of last name class scores.
4. Examining the sorted last name class score list sequentially and generating names and name scores for all names in each class that is examined. Name scores are sorted directly into a name score list.
5. Continuing this procedure until a stopping criterion is satisfied. The stopping criterion is that the best possible name score for a given class exceeds the best actual name score (based on previously checked names) by a given threshold. The best possible name score for a given class is given by

$$\hat{D}_C = \frac{D_{LNC} \cdot L_{LNC} + \tilde{D}_I \cdot \tilde{L}_I}{L_{LNC} + \tilde{L}_I}, \quad (2)$$

where D_{LNC} is the last name class score for the class being examined, L_{LNC} is the number of letters in the last name class score, \tilde{D}_I is the best possible initials score (as determined by the LB output on the initials), and \tilde{L}_I is the number of initials corresponding to the best initials score. The threshold used (in our simulation) for the stopping criterion was the value 0.06.

6. Once the stopping criterion was satisfied, the system returned the sorted list of names scores, and the recognized name was chosen as the one with the smallest distance.

Table IIIb shows the results of running steps 4 and 5 on the sequence of last name and initial scores used to generate the data of Table IIIa. Only two names had distance scores within the threshold, the best score corresponded to the actual spoken name in this case.

III. EXPERIMENTAL EVALUATION

To evaluate the performance of the directory listing retrieval system described in Section II, four talkers (three male, one female) each trained the recognizer using the robust training procedure to give the isolated and embedded templates for each letter. The four talkers were all experienced users of speech recognition systems. These same talkers each provided a test set of 50 randomly chosen names from the 18,210-name directory (the set of 50 names was different for each talker). Each name in the test set was spoken as a sequence of connected letters for the last name, followed by a pause, followed by a sequence of connected letters for the initials. The talkers spoke each name at a normal rate. All recordings were made over local dialed-up telephone lines. The average talking rates for the four talkers are shown in Table IV. The average rates for the last name vary from 189 words per minute (wpm) to 218 wpm; for the initials the rates vary from 140 to 167 wpm. Thus, the names were spoken at very fast rates of articulation.

IV. RECOGNITION RESULTS—SPEAKER-TRAINED CASE

The directory listing retrieval system of Section II was run on the 200 names by the four talkers in a speaker-dependent mode. The LB parameters (see Ref. 9 for a complete description of these parameters) were set to:

1. ϵ = width of DTW search region = 99
2. M_T = multiplier for interlevel scores = 2.2
3. δ_{END} = search region at end of string = 4
4. δ_{R1} = number of frames that can be skipped at beginning of reference template = variable
5. δ_{R2} = number of frames that can be skipped at end of reference template = variable
6. Inserted silence at beginning or end of reference template = variable.

The values for δ_{R1} and δ_{R2} were made variable with the templates—i.e., different values were used for the isolated pattern than for each

Table IV—Talking rates (wpm)
for the four talkers

Talker	Last Name Rate (wpm)	Initials Rate (wpm)
1	189	140
2	210	142
3	210	159
4	218	167

of the embedded patterns. In particular we considered three sets of δ_{R1} and δ_{R2} values, namely:

1. $\delta_{R1} = (0, 0, 0)$, $\delta_{R2} = (4, 0, 0)$
2. $\delta_{R1} = (4, 0, 0)$, $\delta_{R2} = (6, 0, 0)$
3. $\delta_{R1} = (4, 2, 0)$, $\delta_{R2} = (6, 3, 0)$,

where the first value is for the isolated pattern, the second value is for the noncoarticulated pattern, and the third value is for the coarticulated pattern. The first set of values was the optimal one for speaker-independent patterns for digits;¹⁵ the second set of values was optimal for speaker-dependent patterns for digits;¹⁴ the third set of values is a compromise that provides some template shortening for the noncoarticulated reference patterns.

The inserted silence parameter is the number of frames of silence put at either the beginning or end of templates to reflect the presence of initial or final stops in the word. The letters of the alphabet for which initial silence was used were b, d, g; and p, t, k, and q. None of the letters used final silence insertion. Based on some preliminary experimentation, three sets of silence values were used, namely:

1. 0 for {b, d, g}, 0 for {p, t, k, q}
2. 2 for {b, d, g}, 3 for {p, t, k, q}
3. 4 for {b, d, g}, 6 for {p, t, k, q},

where the parameter values are in terms of frames; hence, four frames corresponds to 60 ms of silence insertion.

A series of recognition tests were performed in which δ_{R1} and δ_{R2} were varied along with the silence insertion variable. For each of these tests, name recognition accuracy was measured for three sets of speaker-dependent reference templates,* namely:

1. IS = Isolated templates alone
2. IS \oplus NC = Isolated plus noncoarticulated embedded templates
3. IS \oplus NC \oplus CO = Isolated plus both types of embedded templates.

Results for each of the nine sets of variables and for the three template sets are given in Table V. The results given in this table show the following:

1. For the IS template set, values of (0, 0, 0) and (4, 0, 0) for δ_{R1} and δ_{R2} lead to extremely poor performance. For all other choices of parameter values, the system performance is essentially identical at 86 percent \pm 1 percent. These results point out the necessity of being able to skip some reference frames at the beginning of each template.

2. For the IS \oplus NC template set, there is only a small variation in performance (from a low of 91 percent to a high of 94 percent) as the

* Runs were also made with other combinations of reference patterns (e.g., NC templates alone), but the three sets discussed below provided the most interesting and informative results.

Table V—Recognition accuracy as a function of silence parameters

Template Set	δ_{R1} and δ_{R2} Values		
	(0, 0, 0)	(4, 0, 0)	(4, 2, 0)
	(4, 0, 0)	(6, 0, 0)	(6, 3, 0)
(a) Values of 0 for {b, d, g} and 0 for {p, t, k, q}			
IS	53.5	86	86
IS \oplus NC	92	93	94
IS \oplus NS \oplus CO	93	94	91.5
(b) Values of 2 for {b, d, g}, and 3 for {p, t, k, q}			
IS	50.5	87	87
IS \oplus NC	92.5	92.5	91
IS \oplus NC \oplus CO	94	93.5	95
(c) Values of 4 for {b, d, g} and 6 for {p, t, k, q}			
IS	45.5	85	85
IS \oplus NC	91	93	92
IS \oplus NC \oplus CO	91.5	94	94

δ_{R1} , δ_{R2} , and silence parameters are varied. When we compare the performance to that obtained from the IS template set, we can see that the inclusion of the embedded NC templates leads to improved performance, as well as to insensitivity to the exact parameter values of the variable system parameters.

3. For the IS \oplus NC \oplus CO template set, only very slight improvements in performance are obtained over that of the IS \oplus NC template set, and these improvements do not occur for all values of the variables. The highest accuracy obtained is 95 percent; however, four different sets of parameter values yield 94-percent name accuracy.

A further analysis of the results for the best parameter set is given in Table VI. Included in this table are the individual recognition accuracies as a function of candidate position (top β candidates, $\beta = 1, 2, 3, 4, 5$) for each talker (along with the average), as well as two measures of the amount of searching performed to find the best name. The search measures are \bar{C}_s , the average number of last name classes searched, and \bar{N}_s , the average number of names whose distance score was evaluated. The results in Table VI show that two of the talkers performed well using IS templates, but the other two talkers performed very poorly. For these other two talkers the inclusion of embedded templates led to improvements in performance. It can also be seen that a 2- to 3-percent improvement in accuracy can be obtained by considering the second candidate position scores—i.e., about 2 to 3 percent of the time the correct name is in second position. Such cases are typically names with slight (within letter class) errors in the initials.

By examining the search statistics we see that the average search

Table VI—Percentage of individual recognition accuracies as a function of candidate position and search statistics for each talker for three template sets using $\delta_{R1} = (4, 2, 0)$ and $\delta_{R2} = (6, 3, 0)$, and silence for $\{b, d, g\} = 2$ and $\{p, t, k, q\} = 3$

Talker	Candidate Position					\bar{C}_s	\bar{N}_s
	1	2	3	4	5		
(a) Results Using IS Template Set							
1	76	82	84	84	86	114	1976
2	80	82	82	86	86	139	2553
3	94	96	96	96	96	36	671
4	98	98	98	100	100	37	665
Average	87	89.5	90	91.5	92	81.5	1466
(b) Results Using IS \oplus NC Template Set							
1	82	88	88	88	88	111	2086
2	94	96	98	98	98	113	2308
3	94	98	98	98	98	10	203
4	94	94	94	96	96	40	675
Average	91	94	94.5	95	95	68.5	1318
(c) Results Using IS \oplus NC \oplus CO Template Set							
1	94	98	98	98	98	56	1011
2	92	94	94	94	94	70	1416
3	96	98	98	98	98	19	352
4	98	98	98	100	100	16	296
Average	95	97	97	97.5	97.5	40.3	769

time for the three-template-per-word set is about one-half that of the IS template set. Hence, the embedded templates yield considerably more accurate name classes than that obtained from the IS templates alone.

An analysis of the 10 name errors (in first candidate position) for the IS \oplus NC \oplus CO template set of Table VIc shows the following:

1. Four of the errors were due to errors in initials of people with the same last name. In all cases these errors were within letter class errors, i.e., JR confused with AR.

2. Four of the errors were due to a known flaw in the level-building algorithm²² in which the second best path to a given frame need not be the optimal second best path. Such cases could be potentially corrected at the expense of greatly increased computation in the LB algorithm.

3. Two of the errors were names that could not be matched by the individual letter patterns. Such cases were highly coarticulated letter sequences whose matches were extremely poor in the LB algorithm.

4.1 Recognition results—speaker-independent case

The same set of 200 names was used as a test of the connected letter directory listing retrieval system in a speaker-independent mode. For

Table VII—Percentage of individual recognition accuracies as a function of candidate position and search statistics for each talker for the speaker-independent case

Talker	Candidate Position					\bar{C}_s	\bar{N}_s
	1	2	3	4	5		
1	88	90	94	94	96	29	473
2	70	80	82	88	88	185	3137
3	84	90	90	92	92	110	2097
4	66	74	74	76	78	174	3011
Average	77	83.5	84	87	88	124.5	2179

this test the letter reference patterns were a set of 12 isolated templates per letter, the templates having been extracted from a clustering analysis of isolated occurrences of each letter by 100 talkers (50 male, 50 female).

The results of the recognition test are given in Table VII, which gives recognition accuracy as a function of candidate position for each of the four talkers (as well as the average), and the average search statistics. Overall, we can see that degraded performance results from the use of only isolated templates. An average name recognition accuracy of 77 percent is achieved, as opposed to the 95-percent accuracy in the speaker-dependent case. The inherent system difficulties are illustrated in the average search statistics, which show that it took about 124 class evaluations and 2179 name evaluations to find the best name—a factor of three to one greater than required for the speaker-trained case.

An analysis of the 46 name errors (out of the 200 names) shows:

1. Nine errors where only the initials were incorrect.
2. Twenty-two errors in which the last name was in error—i.e., a match to an incorrect last name was better than the match to the correct last name. In such cases the match to the initials was not able to correct the errors.
3. Fifteen errors in which the correct name could not be matched because of the LB flaw discussed earlier, or because the rate of articulation of the letters exceeded the rate at which a match could be achieved from isolated letter templates.

V. DISCUSSION

To get some perspective on the relevance of the results given in Section III, we must compare the current system performance against that achieved in earlier implementations subject to the experimental constraints of small sample populations (i.e., the use of only four test talkers). In the most relevant comparison, Myers and Rabiner¹⁸ studied a similar system in which a fixed set of 50 names was used as the

test by each of four talkers (different from those used here). Using isolated templates alone, recognition accuracies of 90.5 percent and 87.5 percent were achieved in the speaker-dependent and speaker-independent modes, respectively, for normally spoken names. Earlier work by Aldefeld et al. has shown that the 50 chosen names tended to give an overbound on true system performance as there was no adequate representation of the common problems in name spelling (e.g., multiple names with differing initials, names differing in a single letter, etc.).²¹ Hence the recognition accuracies of 87 percent and 77 percent for the case of isolated templates in the speaker-dependent and speaker-independent modes are comparable to those reported earlier.

The recognition performance using embedded training patterns in the speaker-dependent case indicates an improvement in recognition accuracy along with a significant reduction in search time to find the best name. Hence we conclude that, as in the connected digits recognition task, the use of embedded word training can and does enhance the recognition system performance.

At this point it is natural to ask "Where do we go from here to improve the performance of a connected word recognition task based on pattern matching techniques?" There are two obvious directions for making improvements.

First, the embedded training procedure should be able to provide more than a single embedded pattern when necessary. For example, it was clear that some letters are more influenced by context than others. In such cases the resulting robust embedded pattern was often a poor representative of the letter, and did not yield good matching scores in real names. Using two or more embedded tokens obtained via some clustering procedure would have aided greatly in such cases.

A second obvious direction for improvement is to make no decision on names in which two or more name candidates are within some reasonable distance of the best name score. In such cases (mostly involving initial errors) additional information should be requested from the talker to help resolve ambiguity. Such a strategy was used with great success by Aldefeld et al.²¹ in a practical implementation of this system with isolated letter input.

VI. SUMMARY

We have shown how a practical directory listing retrieval system could be implemented on the basis of connected letter name spelling. Our results indicate that improved recognition performance can be obtained when combining embedded letter patterns (suitably extracted from three-letter strings) with the standard isolated letter patterns to form an enhanced letter reference set. Using this combined set of

references, improvements in name accuracy of 8 percent and reductions in search time of a factor of two result, when the system is tested in a speaker-trained mode using dialed-up telephone line recordings.

VII. ACKNOWLEDGMENT

The authors thank Tom Gruenfelder and an anonymous *AT&T Bell Laboratories Technical Journal* reviewer for their comments and criticisms of this paper.

REFERENCES

1. F. Itakura, "Minimum Prediction Residual Principal Applied to Speech Recognition," *IEEE Trans. Acoustics, Speech, and Signal Processing, ASSP-23* (February 1975), pp. 67-72.
2. L. R. Rabiner and S. E. Levinson, "Isolated and Connected Word Recognition—Theory and Selected Applications," *IEEE Trans. Commun., COM-29*, No. 5 (May 1981), pp. 621-59.
3. W. A. Lea, ed., *Trends in Speech Recognition*, Englewood Cliffs, NJ: Prentice-Hall, 1980.
4. T. B. Martin, "Practical Applications of Voice Input to Machines," *Proc. IEEE*, 64 (April 1976), pp. 487-501.
5. G. R. Doddington and T. B. Schalk, "Speech Recognition: Turning Theory to Practice," *IEEE Spectrum*, 18, No. 9 (September 1981), pp. 26-32.
6. S. Moshier, "Talker Independent Speech Recognition in Commercial Environments," *Speech Commun. Papers 97th ASA Meeting*, (June 1979), pp. 551-3.
7. W. A. Lea, "Selecting the Best Speech Recognizer for the Job," *Speech Technology*, 1, No. 4 (January/February 1983), pp. 10-29.
8. H. Sakoe, "Two Level DP-Matching—A Dynamic Programming Based Pattern Matching Algorithm for Connected Word Recognition," *IEEE Trans. Acoustics, Speech, and Signal Processing, ASSP-27* (December 1979), pp. 588-95.
9. C. S. Myers and L. R. Rabiner, "Connected Digit Recognition Using a Level Building DTW Algorithm," *IEEE Trans. Acoustics, Speech, and Signal Processing, ASSP-29*, No. 3 (June 1981), pp. 351-63.
10. J. S. Bridle, M. D. Brown, and R. M. Chamberlain, "An Algorithm for Connected Word Recognition," *Automatic Speech Analysis and Recognition*, ed. J. P. Haton, Dordrecht, Holland; D. Rydell Publishing Co., 1982, pp. 191-204.
11. J. L. Gauvain and J. Mariani, "A Method for Connected Word Recognition and Word Spotting on a Microprocessor," *Proc. 1982 ICASSP* (May 1982), pp. 891-4.
12. M. H. Kuhn and H. H. Tomaschewski, "Improvements in Isolated Word Recognition," *IEEE Trans. Acoustics, Speech, and Signal Processing, ASSP-31*, No. 1 (February 1983), pp. 157-67.
13. L. R. Rabiner and J. G. Wilpon, "A Simplified Robust Training Procedure for Speaker Trained, Isolated Word Recognition Systems," *J. Acoust. Soc. Amer.*, 68, No. 5 (November 1980), pp. 1271-6.
14. L. R. Rabiner, A. Bergh, and J. G. Wilpon, "An Improved Training Procedure for Connected-Digit Recognition," *B.S.T.J.*, 61, No. 6 (July-August 1982), pp. 981-1001, pp. 157-67.
15. L. R. Rabiner, J. G. Wilpon, A. M. Quinn, and S. G. Terrace, "On the Application of Embedded Digit Training to Speaker Independent, Connected Digit Recognition," *IEEE Trans. on Acoustics, Speech, and Signal Processing, ASSP-32* (1984).
16. A. E. Rosenberg and C. E. Schmidt, "Automatic Recognition of Spoken Spelled Names for Obtaining Directory Listing," *B.S.T.J.*, 58, No. 8 (October 1979), pp. 1797-823.
17. A. E. Rosenberg, L. R. Rabiner, and J. G. Wilpon, "Recognition of Spoken Spelled Names for Directory Assistance Using Speaker-Independent Templates," *B.S.T.J.*, 59, No. 4 (April 1980), pp. 571-92.
18. C. S. Myers and L. R. Rabiner, "An Automated Directory Listing Retrieval System Based on Recognition of Connected Letter Strings," *J. Acoust. Soc. Am.*, 71, No. 3 (March 1982), pp. 716-27.

19. L. F. Lamel, L. R. Rabiner, A. E. Rosenberg, and J. G. Wilpon, "An Improved Endpoint Detector for Isolated Word Recognition," *IEEE Trans. Acoustics, Speech, and Signal Processing*, *ASSP-29*, No. 4 (August 1981), pp. 777-85.
20. B. Aldefeld, S. E. Levinson, and T. G. Szymanski, "A Minimum Distance Search Technique and Its Application to Automatic Directory Assistance," *B.S.T.J.*, 59 (October 1980), pp. 1343-56.
21. B. Aldefeld, L. R. Rabiner, A. E. Rosenberg, and J. G. Wilpon, "Automated Directory Listing Retrieval System Based on Isolated Word Recognition," *Proc. IEEE*, 68 (November 1980), pp. 1364-79.
22. C. S. Myers and L. R. Rabiner, "A Comparative Study of Several Dynamic Time-Warping Algorithms for Connected-Word Recognition," *B.S.T.J.*, 60, No. 7 (September 1981), pp. 1389-409.

AUTHORS

Lawrence R. Rabiner, S.B. and S.M., 1964, Ph.D., 1967 (Electrical Engineering), The Massachusetts Institute of Technology; Bell Laboratories, 1962—. Presently, Mr. Rabiner is engaged in research on speech communications and digital signal processing techniques. He is coauthor of *Theory and Application of Digital Signal Processing* (Prentice-Hall, 1975), *Digital Processing of Speech Signals* (Prentice-Hall, 1978), and *Multirate Digital Signal Processing* (Prentice-Hall, 1983). Member, National Academy of Engineering, Eta Kappa Nu, Sigma Xi, Tau Beta Pi. Fellow, Acoustical Society of America, IEEE.

Sandra G. Terrace, B.S. (summa cum laude, in Mathematics), 1975, Northeastern University, Boston, Massachusetts. Ms. Terrace works primarily from her home in Chelmsford, Massachusetts, where she and her husband own and operate a computer software consulting firm. She is a computer software consultant to the Acoustics Research Department of AT&T Bell Laboratories at Murray Hill, New Jersey. Since April 1980 she has been engaged in the development of speech-recognition and speech-processing algorithms with the CSPI MAP Array Processor. Programs have been developed using MAP Assembly languages and Data General FORTRAN to accomplish isolated and connected speech recognition, speech synthesis, and speech endpoint detection.

Jay G. Wilpon, B.S. and A.B. (cum laude) in Mathematics and Economics, respectively, 1977, Lafayette College, Easton, Pennsylvania; M.S. (Electrical Engineering/Computer Science), 1982, Stevens Institute of Technology, Hoboken, N.J.; AT&T Bell Laboratories, 1977—. Since June 1977 Mr. Wilpon has been with the Acoustics Research Department at AT&T Bell Laboratories, Murray Hill, N.J., where he is a Member of the Technical Staff. His interests include basic research in the field of speech recognition, training algorithms for speaker-dependent and speaker-independent recognizers, and speech endpoint detection.

An Improved Word-Detection Algorithm for Telephone-Quality Speech Incorporating Both Syntactic and Semantic Constraints

By J. G. WILPON,* L. R. RABINER,* and T. MARTIN*

(Manuscript received August 26, 1983)

Accurate location of the endpoints of spoken words and phrases is important for reliable and robust speech recognition. The endpoint detection problem is fairly straightforward for high-level speech signals in low-level stationary noise environments (e.g., signal-to-noise ratios greater than 30-dB rms). However, this problem becomes considerably more difficult when either the speech signals are too low in level (relative to the background noise), or when the background noise becomes highly nonstationary. Such conditions are often encountered in the switched telephone network when the limitation on using local dialed-up lines is removed. In such cases the background noise is often highly variable in both level and spectral content because of transmission line characteristics, transients and tones from the line and/or from signal generators, etc. Conventional speech endpoint detectors have been shown to perform very poorly (on the order of 50-percent word detection) under these conditions. In this paper we present an improved word-detection algorithm, which can incorporate both vocabulary (syntactic) and task (semantic) information, leading to word-detection accuracies close to 100 percent for isolated digit detection over a wide range of telephone transmission conditions.

I. INTRODUCTION

In an automatic speech recognition system, it is assumed that during a recording interval (which may be continuous) a user will speak a command, which he wants the recognizer to interpret and respond to

* AT&T Bell Laboratories.

Copyright © 1984 AT&T. Photo reproduction for noncommercial use is permitted without payment of royalty provided that each reproduction is done without alteration and that the Journal reference and copyright notice are included on the first page. The title and abstract, but no other portions, of this paper may be copied or distributed royalty free by computer-based and other information-service systems without further permission. Permission to reproduce or republish any other portion of this paper must be obtained from the Editor.

accordingly. The first task of a recognition system is to separate the input speech from the various types of nonspeech events that also occur during the recording. This task is referred to as endpoint detection.

Accurate detection of the spoken word has been shown to be crucial for reliable word recognition.^{1,2} Most research in the study of designing endpoint detectors has used speech databases, where the speech has been collected over clean transmission mediums [using close-talking, noise-canceling microphones, or telephone speech over local Private Branch Exchanges (PBXs)]. The signal-to-noise ratio (s/n) under these conditions is high (between 35 and 50-dB peak s/n). Also, the noise generated in such a system is usually stationary. This research has led to quite reliable endpoint detectors.

Endpoint detection becomes much more difficult when the transmission system is corrupted by the many noises one finds on a standard, dialed-up telephone line. Some of these problems include popping sounds, crackling noises, carrier frequency tones, background speech, and other nonstationary noises. The need for an accurate speech endpoint detector that works as well in these environments as in clean environments is a goal that has not been met. In an earlier study,¹ when telephone customers, speaking over randomly dialed telephone lines with various types of transmission distortion, were asked to speak their telephone number as a sequence of isolated digits, existing endpoint algorithms often failed.

To evaluate a new endpoint scheme, we must define the requirements on endpoint accuracy. An indirect measure of these requirements can be obtained directly from the recognizer as follows. Given a test set of many spoken words, use them as input to a word recognition system consisting of an endpoint detector and a recognizer. If, when substituting a new endpoint detection algorithm for an earlier one, we obtain higher word recognition accuracy, then we will say that the new endpoint detection algorithm is better than the earlier one.

One way of explicitly defining the requirements on endpoint accuracy is to perform the following experiment. Take a speech database of isolated words and manually detect the beginning and end of each word. Next, vary the beginnings and ends of each word over some specified range (e.g., ± 150 ms) and perform isolated word recognition. By examining sensitivity of the recognition scores to variability in endpoints, an explicit relationship can be found. Such an experiment was performed and will be described in this paper.

The purpose of this paper is to describe a new approach for determining the endpoints of spoken words, which incorporates both vocabulary (syntactic) and task (semantic) information, leading to word-detection accuracies close to 100 percent for isolated digit detection

over a wide range of telephone conditions. We call the new approach a top-down design. Simply put, we look for strong (vowel-like) peaks in the energy contour of a speech utterance and process the speech around the peaks to find potential beginning and ending points. Several rules involving duration, and onset and decay times are then used to refine the endpoint estimates.

This new algorithm is compared to an earlier endpoint algorithm by Lamel et al.,² which tries to find word endpoints based on the energy of the speech rising some fixed level above the background noise energy. We call this type of approach a bottom-up approach. In addition we will briefly identify several other algorithms that were investigated, none of which performed as well as the top-down approach.

The format of this paper will be as follows. In Section II we review the bottom-up approach to endpoint detection. We describe our new top-down word detector in Section III. In Section IV we describe the database used in all our tests, present results on the tests to explicitly measure requirements for word-detection accuracy, and give recognition results comparing the bottom-up approach to the new top-down method.

II. REVIEW OF BOTTOM-UP ENDPOINT DETECTOR

Figure 1 gives a block diagram of the bottom-up endpoint algorithm of Lamel et al.² First the input speech is bandpass filtered and sampled. Since we are working with a telephone bandwidth signal, we bandpass the speech signal from 100 to 3200 Hz and sample it at a 6.67-kHz rate. The digitized speech is then preemphasized using a simple first-order digital filter with a z transform:

$$H(z) = 1 - az^{-1}, \quad (1)$$

where $a = 0.95$. The digitized speech is then blocked into frames of N samples, with a shift between frames of L samples. Experimentation has found that N should be set to 300 samples and L should be set to 100 samples. This corresponds in time to 45-ms frames with a 15-ms shift between frames. Each frame of speech is then weighted by a Hamming window of the form

$$w(n) = 0.54 - 0.46 \cos\left(\frac{2\pi n}{N}\right), \quad 0 \leq n \leq N-1 \quad (2)$$

(where N is previously defined). Windowing reduces the truncation effects of the framing procedure. We denote the ℓ th frame of windowed speech as $s_\ell(n)$ defined for $0 \leq n \leq N-1$.

After this initial digital processing, the energy of the signal is

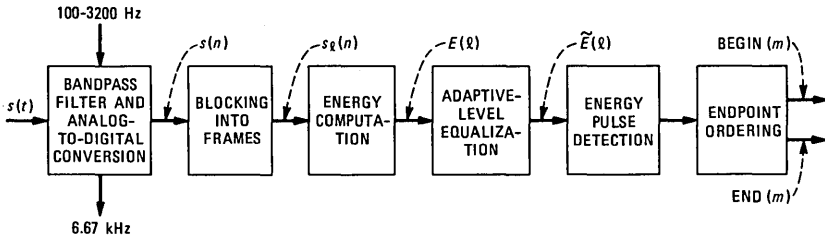


Fig. 1—Block diagram of bottom-up endpoint algorithm of Lamel et al.

computed. This computation can be made simply by summing the squares of the signal values during a frame of speech. However, since we are using a Linear Prediction Coding (LPC) recognizer,³⁻⁹ which requires that a p th-order autocorrelation analysis (in our case $p = 8$) be performed on the entire recording interval, the energy is extracted as a by-product of the analysis. That is,

$$E(\ell) = 10 \log_{10} R_\ell(0), \quad \ell = 1, 2, \dots, NF, \quad (3)$$

where NF is the total number of frames in the recording interval, $R_\ell(0)$ is the zeroth-order correlation coefficient,

$$R_\ell(0) = \sum_{n=0}^{N-1} [s_\ell(n)]^2, \quad (4)$$

and $E(\ell)$ is on a decibel scale.

The next step in the processing (called adaptive-level equalization in Fig. 1) is a normalization of the energy contour to compensate for the mean background noise level. First, E_{\min} is computed as

$$E_{\min} = \min_{1 \leq \ell \leq NF} (E(\ell)). \quad (5)$$

$\hat{E}(\ell)$ is then formed as the difference between $E(\ell)$ and E_{\min} ,

$$\hat{E}(\ell) = E(\ell) - E_{\min}, \quad \ell = 1, 2, \dots, NF. \quad (6)$$

Next, the background level estimate is refined even further by computing a histogram of the signal energies. The histogram is restricted to the lowest NP dB (typically $NP = 15$) of \hat{E} . We then apply a three-point median smoother to this histogram. Finally, we create the modified energy contour $\tilde{E}(\ell)$, $\ell = 1, 2, \dots, NF$,

$$\tilde{E}(\ell) = \hat{E}(\ell) - \text{Mode}, \quad (7)$$

where Mode is the mode of the smooth histogram generated above.

The remaining blocks of the bottom-up endpoint detector are the energy pulse detector and an endpoint ordering procedure. The energy pulse detector scans the modified energy contour and selects all

potential energy pulses within the recording interval. Pulse-combining rules are used to eliminate short pulses, and combine close pulses. Several parameters, along with their current settings, need to be defined in order to explain how these blocks operate. These parameters include:

1. K_1 , K_2 , and K_3 are energy thresholds used in determining the word boundaries (3, 10, 5 dB).
2. IT_1 and IT_2 are frame counter thresholds for determining the presence or absence of any breath noises at the boundary points of a detected utterance (5,5 frames).
3. IT_3 is the minimum length for a detected pulse (5 frames).
4. $NFMIN$ is the minimum length in frames for an utterance (10 frames).

Figure 2 shows a state representation of the operation of the energy pulse detector. The normalized energy (\tilde{E}) of the recording is scanned from left to right ($\ell = 1$ to $\ell = NF$). If $\tilde{E}(\ell)$ rises first above K_1 , then above K_2 (without falling below K_1), a beginning pulse marker is assigned to frame ℓ . Similarly, when the energy dips below K_3 an ending marker is assigned. The beginning IT_1 frames and ending IT_2 frames are checked for breath-type noises (i.e., low energy content throughout the IT_1 or IT_2 frames), and eliminated if necessary. All pulses must have a minimum length (IT_3). Pulses are then combined based on their proximity to other pulses. All final pulses are checked for duration and maximum energy content, and pulses that do not pass are eliminated. The final output of the endpoint detector is a set of ordered pairs of beginning and ending points of segments within the recording interval. It is assumed that each segment corresponds to a spoken word within the recording interval. The Lamel et al. bottom-up endpoint detector can be, and has been, implemented as a real-time endpoint detector.

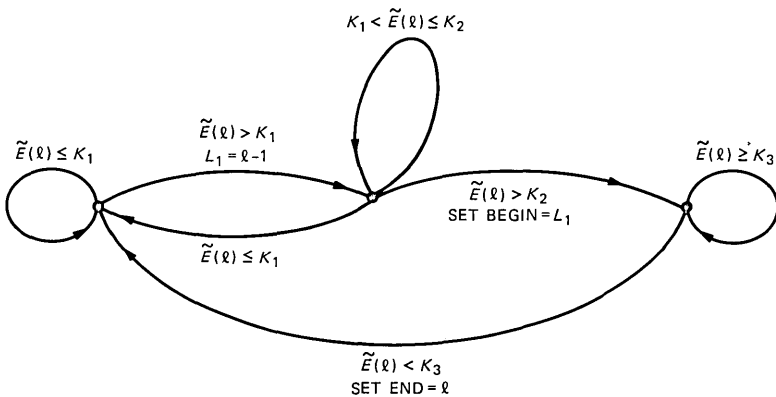


Fig. 2—State representation of energy pulse detector from Lamel et al. endpoint detector.

III. DESCRIPTION OF THE TOP-DOWN ENDPOINT DETECTOR

As discussed previously, the bottom-up endpoint detector works very well in stationary noise backgrounds with reasonably high signal-to-noise ratios. However, in highly variable noise background conditions it tends to fail at a very high rate. Hence, we now describe a top-down approach capable of finding words in highly nonstationary backgrounds.

The design of the top-down endpoint detector is similar to that of the bottom-up approach in that it computes a normalized energy array, finds pulses in the recording interval, and then combines them to get the final endpoint decisions. The differences lie in the energy pulse detection and endpoint processing procedures.

To understand the differences, we need to define some additional parameters along with their current settings, namely:

1. MXWD is the number of utterances within a recording interval (7 words).
 2. IGAP is the number of frames from which a pulse slope is computed (3 frames).
 3. ISLOPE is the pulse slope threshold (7 dB).
 4. NSEP, NSEP2 are pulse separation counters (2,7 frames).
- Figure 3 gives a flow diagram of the energy pulse detection procedure.

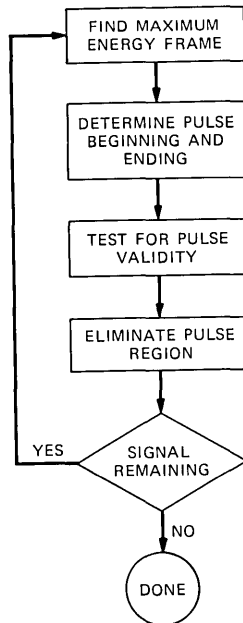


Fig. 3—Block diagram describing energy pulse detection procedure from top-down endpoint algorithm.

ture. The philosophy is to find the high energy frames in a local region and then try to define the energy pulse boundaries using the lower energy frames. In particular, the algorithm scans the entire recording interval (i.e., $\hat{E}(\ell)$, $\ell = 1, 2, \dots, NF$) until it finds the frame with the highest energy. The algorithm then analyzes the energy values of the surrounding frames. It looks at frames prior to the maximum energy frame until it finds a frame with energy less than the threshold $K1$, and it looks at frames beyond the maximum energy frame until it finds a second frame with energy less than the threshold $K3$. At this point the pulse detector has found a set of possible beginning and ending frames for an utterance—i.e., an energy pulse. Its next task is to try to eliminate any breath noises at the estimated boundaries of the energy pulse. This is performed by testing the first IT1 frames and last IT2 frames of the energy pulse for consistently low energy content. Next, the detected pulse (corresponding to the utterance) is checked to guarantee that its duration is greater than a minimum-length threshold and that its amplitude is above a minimum level. Pulses are eliminated if they do not pass these tests. This procedure is iterated throughout the recording interval. All previously detected pulses are eliminated from consideration in each new iteration. When this process is complete, a set of NPULSE pulses are found within the recording interval. Figure 4a shows a typical energy plot of a string of isolated digits indicating where pulses were detected. In this example, six energy pulses were detected; however, there are only four spoken digits in the recording interval.

The energy pulses are next sent to a pulse combiner algorithm, which attempts to combine two or more adjacent pulses to form longer pulses. This process works as follows. First, all pulses are sorted in order of decreasing peak energy. We then start with the pulse with the highest peak energy and try to add pulses to it based on the following rules.

For a prior pulse to be added to the beginning of the current energy pulse, first the Downward Slope (DS) (defined over the last IGAP frames of the pulse) of the pulse must be above a threshold. Such a sharp downward slope tends to occur during stop-gap-type pulses within a word. Second, the prior pulse must lie within NFW frames of the current pulse (where NFW is determined by DS). If these conditions occur, the prior pulse will be combined with the current pulse to give a single combined pulse. In a similar manner, a pulse can be added to the end of the current energy pulse. In addition to the slope constraint, there are other restrictions for combining pulses. The duration of the combined pulse must be below a maximum-length threshold. (Clearly, if the combining pulse duration is too long, it signifies that two distinct words were spoken close to each other, and

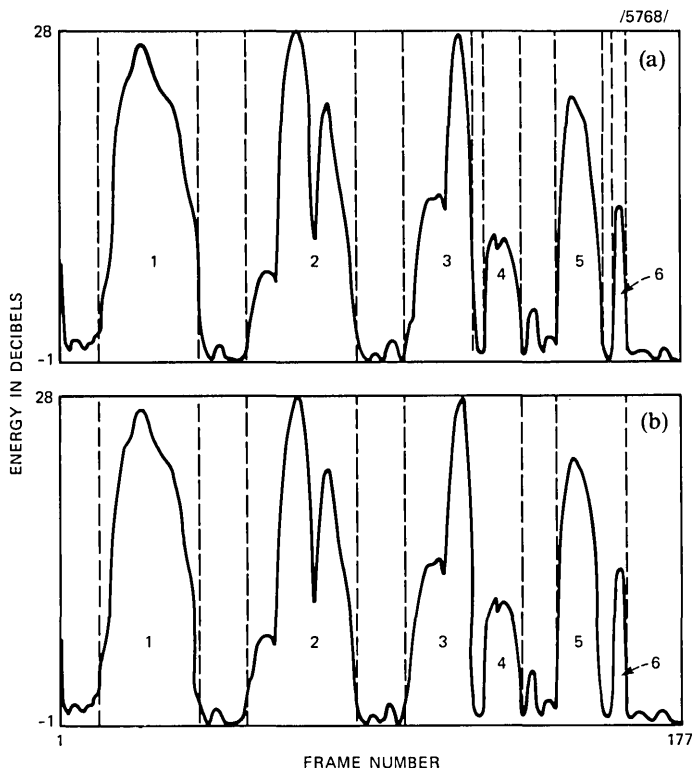


Fig. 4—Log energy contour from spoken string of isolated digits. Dashed lines indicate (a) where pulses were detected and (b) result of applying pulse combiner rules to pulses found in (a).

hence, should not be combined.) This restriction is not applied when the algorithm is detecting connected words as well as isolated word sequences. A second restriction is that the upward slope value (defined similarly to the downward slope value) between two combining pulses must also be above a threshold. This situation typically signifies a stop gap within a word. Figure 4b shows the result of applying the pulse combiner rules to the spoken sequence of Fig. 4a. Pulses 3 and 4 have been combined (this is the digit *six*), as have pulses 5 and 6 (this is the digit *eight*).

3.1 Syntactic constraints of digits

In the final decision block, the first task is to eliminate all endpoint utterances that are too short (i.e., less than the threshold NFMIN). The algorithm could terminate here, with the final output being a list of beginning and ending frame pointers for each detected utterance. However, we have incorporated several decision rules based on the

knowledge that we are detecting digit strings. For this special vocabulary, only two words (the digits *six* and *eight*) can possibly contain a stop gap. Thus, all other words in the vocabulary can be represented by a single energy pulse with no other pulses attached. Also, for the digits *six* and *eight*, the maximum energy pulse is always the first pulse when a secondary pulse is added. Given the rules for combining pulses, this implies that no pulse should be added to the beginning of a maximum energy pulse. Next, both the digits *six* and *eight* have at most only one stop gap present, implying that at most one pulse can be added to the end of a maximum energy pulse. By adding these additional rules to the endpoint detector, we can increase overall accuracy for this specialized vocabulary.

3.2 Semantic constraints from the digit recognition task

We further assume that the input speech is a sequence of MXWD isolated digits (e.g., MXWD equals seven for a telephone number). Thus, for this specialized case, we know the number of utterances within the recording interval. This information can also be incorporated into the algorithm. One way to implement this idea is to sort the final endpoint detector output in order of maximum peak energy level and to retain the top MXWD utterances. If the output of the pulse combiner indicates that fewer than MXWD words were found, we assume that some of the uttered words were spoken as connected sequences rather than as isolated words. This is because the pulse detector has its parameters set to find any spoken utterance with a peak energy of greater than 10 dB (note the average peak energy for utterances recorded previously is between 30 and 50 dB^{2,6}).

IV. EVALUATION OF THE TOP-DOWN APPROACH TO ENDPOINT DETECTION

To evaluate the top-down endpoint detector, a series of experiments were performed using telephone recordings from a subset of the data described in Ref. 1. This database consisted of 11,035 digits spoken by 3153 people in highly variable telephone transmission conditions. For evaluation purposes we used a subset of 820 digits spoken by 218 talkers. This particular subset of data was used because its statistics were similar to those of the entire 11,035-digit database. Also, the experiments we planned to perform were so computationally extensive we wanted to choose a small subset of the database.

For recognition purposes we used the 30-template-per-digit reference set used in Ref. 1. These templates were extracted from a subset of 3700 digit tokens using the Unsupervised Without Averaging (UWA) clustering algorithm.³

The first experiment concerned direct measurement of recognition

accuracy as a function of error (as measured with respect to hand-chosen endpoints) in endpoint location. The second set of experiments compared the bottom-up and top-down approaches on the 820-word test vocabulary.

4.1 Recognition as a function of endpoint location error

Based on the energy contour of the recording interval and on careful listening to the speech, we manually determined the endpoints for each of the 218 strings (to the nearest 15-ms interval). Figure 5 shows some typical speech utterances along with their manually determined endpoints. These examples show some of the typical problems associated with endpoint detection of this database. Figure 5a, which shows the energy contour for the string /391/, exhibits a nonstationary noise floor, where a person was talking in the background. Figure 5b, which shows the contour for the digit string /8292/, exhibits transients that were introduced by the transmission system (i.e., P_1, P_2, P_3, P_4 are the transients, while A_1, A_2, A_3, A_4 are the actual spoken digits). Note that the peak s/n is 31 dB, but the s/n's of most of the individual digits are

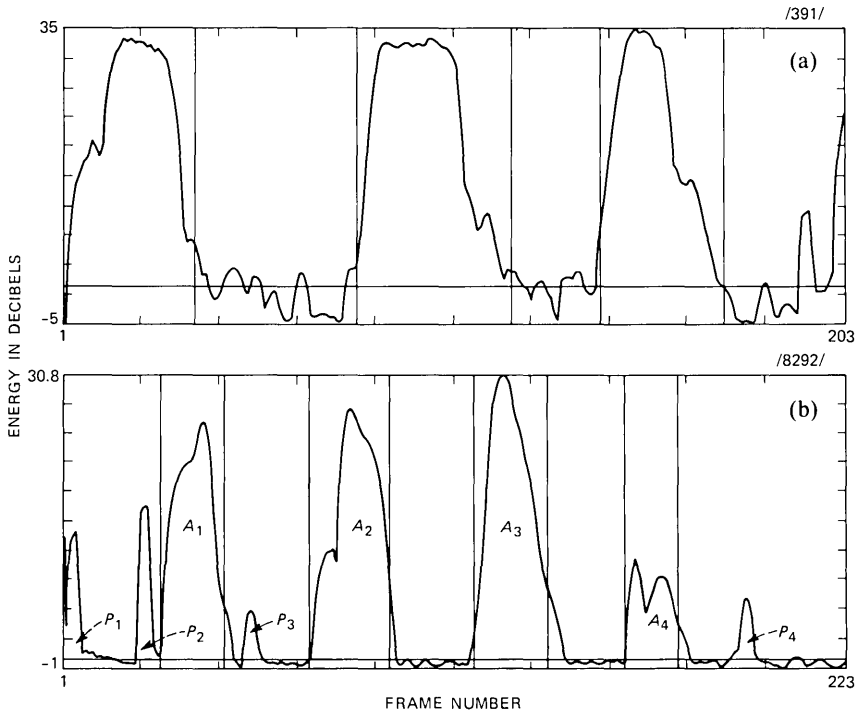


Fig. 5—Log-energy contour for the spoken strings (a) /391/ and (b) /8292/. Solid lines indicate manual placement of word endpoints.

lower (e.g., the second digit, *two*, has peak s/n of about 12 dB). After the endpoints were manually determined, recognition was performed on the isolated digit database. The recognizer used was the LPC-based recognizer,³⁻⁸ which has been used and studied extensively at AT&T Bell Laboratories. A simple K-nearest neighbor decision rule was used in all tests. The overall recognition accuracy obtained was 93.0 percent using the manual endpoints.

After recognition was performed, the manually detected beginning point and ending point of each word were automatically varied in 15-ms (single-frame) steps from 150 ms before the manually determined endpoint to 150 ms after the endpoint. Recognition was performed at each interval with the results tabulated in the form of a contour plot. Figure 6 shows a contour plot of overall recognition accuracy as a function of the change in the endpoint position in ms. Each ring represents a 1-percent change in recognition accuracy. The contour plot was obtained by averaging over all digits in the test database. Figure 6 shows, as anticipated, that the best recognition score, 93.0 percent, was obtained when the exact manually determined endpoints were used.

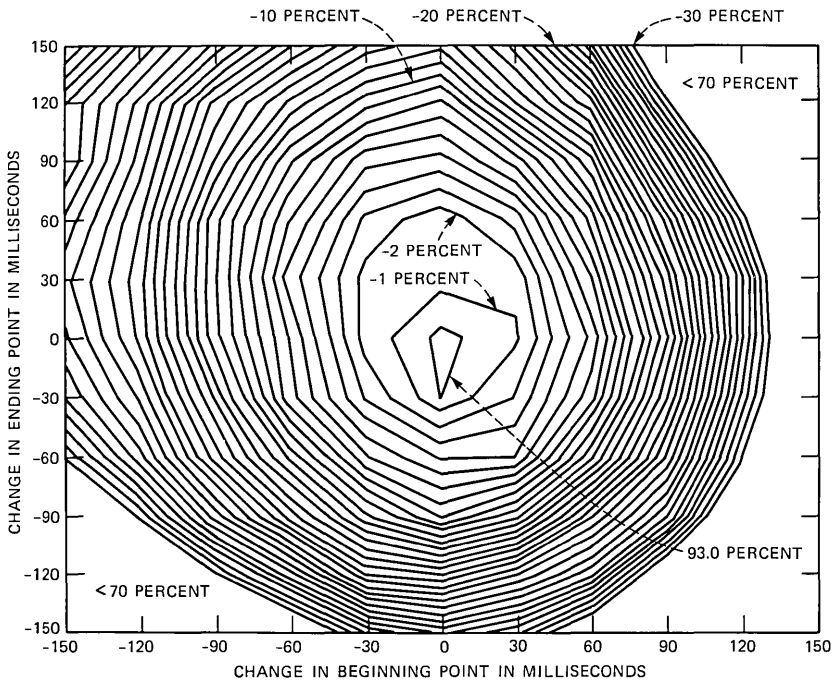


Fig. 6—Contour plot showing results of recognition experiment where manually placed endpoints were varied by ± 150 ms. Results are averaged over all digits. Each ring represents a 1-percent change in recognition accuracy.

The contour plot of Fig. 6 also implies that if the endpoints were varied only slightly from the hand-placed endpoints, the recognition accuracy would drop. For example, a 3-percent reduction in accuracy occurred if both the endpoints were in error by ± 60 ms. We see that the rings of the contour plots are fairly concentric, implying a uniform decrease in recognition accuracy as the endpoints are placed further away from manually chosen ones.

If we look at contour plots of the individual digits, we see that their rings are definitely not concentric, and that the best recognition accuracy from most of the digits was not obtained using the manually determined endpoints. Table I gives the best recognition scores on a per-digit basis, along with the changes that were made to the endpoints in order to obtain those results. Figures 7 through 9 show contour plots for some of the digits. We can make several observations from these curves. Figure 7 shows the contour plot for the word *zero*. The best accuracy for this word (averaged over all occurrences of the word) was obtained if the manually determined beginning points were moved in (i.e., closer to the ending point) by 30 ms. It can be seen that the digit *zero* is more sensitive to variations in the ending point than the beginning point. For the digit *one* (see Fig. 8), we see the best results (96.1 percent) were obtained if the ending point was moved out by 90 ms (six frames). This is quite a large amount, and may be justified by the fact that the nasal sound at the end of the word *one* is of such low energy that, using the energy contour and human listening, accurate placement of the ending point cannot be made. This plot also shows that the beginning point of the digit *one* is much more sensitive than the ending point. If the beginning points are varied by -60 ms (from the optimal point), the recognition accuracy drops by 28 percent, but if the ending point is varied by -60 ms, the recognition accuracy drops only 1.5 percent. Figure 9 shows the contour plot for the word *six*. We

Table I—Recognition results from test run with modified endpoints

Digit	Percent Correct	Change in Beginning Point (ms)	Change in Ending Point (ms)
0	90.4	30	0
1	96.1	0	90
2	94.9	0	-60
3	95.6	0	0
4	93.8	0	-30
5	96.7	0	0
6	95.7	0	-90
7	97.2	-30	30
8	97.1	0	-30
9	88.9	0	30
Total over all digits	93.0	0	0

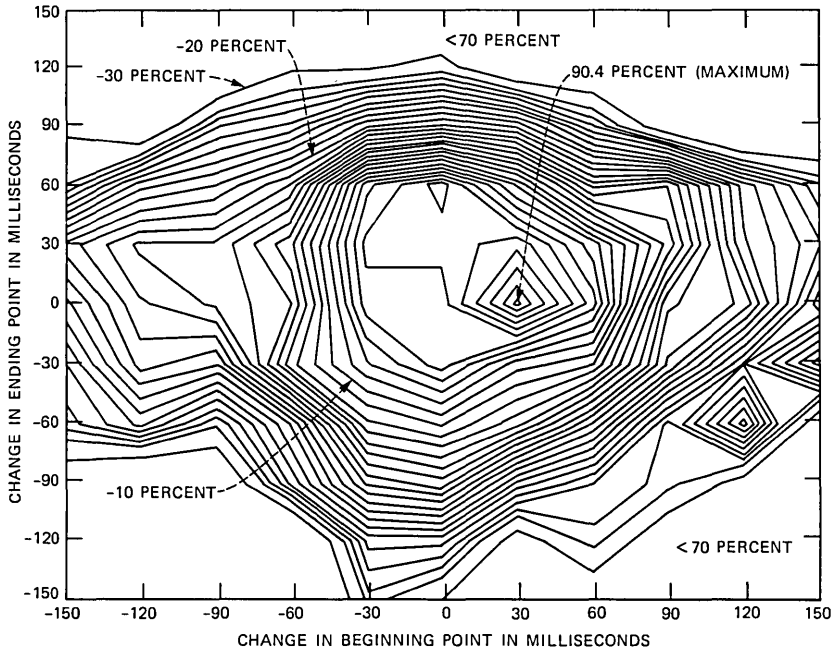


Fig. 7—Contour plot showing results of recognition experiment where manually placed endpoints were varied by ± 150 ms. Results are only for the digit zero. Each ring represents a 1-percent change in recognition accuracy.

see that the rings are highly nonuniform, with several local maxima present throughout the plot. The best recognition accuracy for *six* was obtained when the ending points were cut back by 90 ms (95.7 percent). However, a cutback in the ending points of only 30 ms coupled with a 30-ms increase in the beginning points also yielded the same results (95.7 percent). Similar observations can be made for the rest of the digits.

The main point to emphasize is that extremely accurate determination of the speech endpoints must be made, in order to obtain the highest system accuracy using our LPC-based recognition system.

4.2 Accuracy of automatically determined endpoints

Endpoints were automatically determined for the 820-digit database using both the bottom-up and top-down approaches. Figure 10 shows a histogram of the error in frame location of the top-down endpoints compared to the manually determined endpoints for the 820 digits. Figure 10a shows results for the beginning frame; Fig. 10b shows results for the ending frame. The automatically determined endpoints agree with the manual endpoints within ± 1 frame 68.2 percent of the

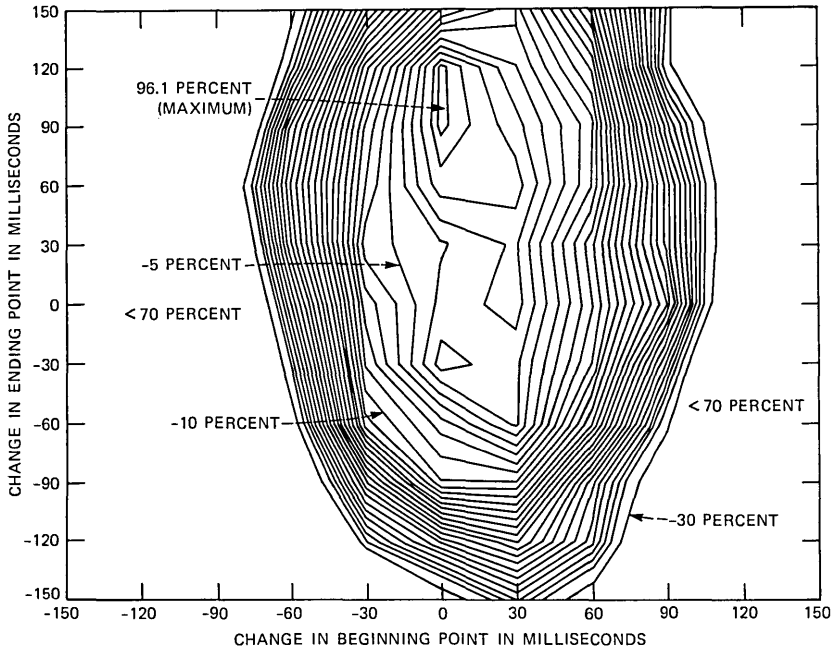


Fig. 8—Contour plot showing results of recognition experiment where manually placed endpoints were varied by ± 150 ms. Results are only for the digit *one*. Each ring represents a 1-percent change in recognition accuracy.

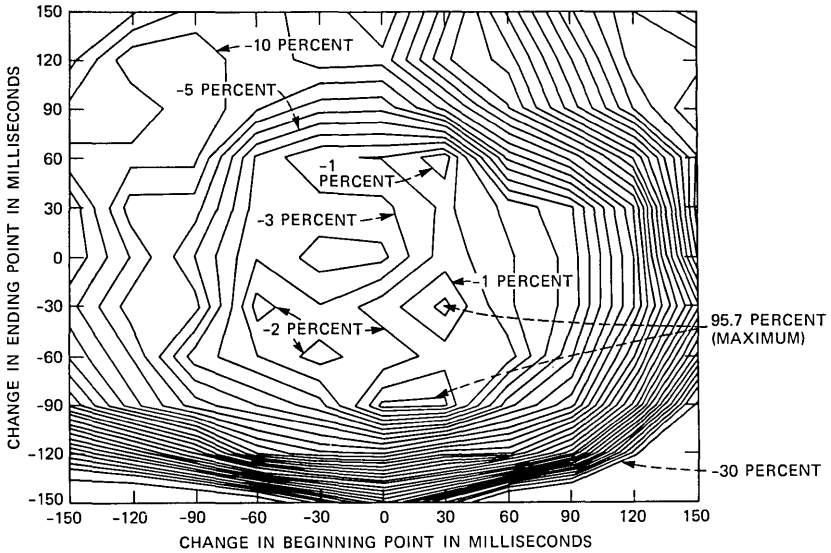


Fig. 9—Contour plot showing results of recognition experiment where manually placed endpoints were varied by ± 150 ms. Results are only for the digit *six*. Each ring represents a 1-percent change in recognition accuracy.

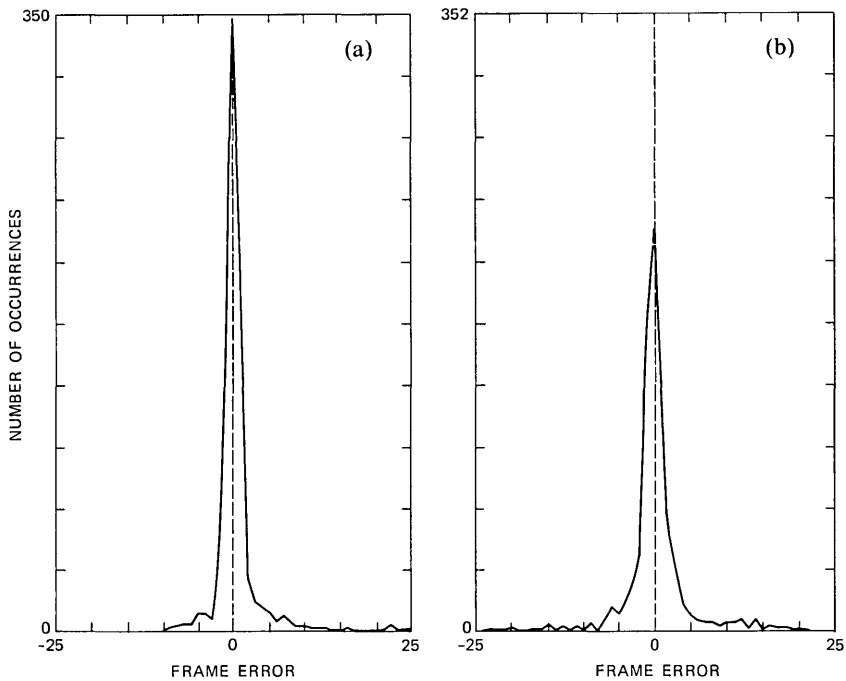


Fig. 10—Histogram of error in frame location of top-down endpoints compared to manually determined endpoints for (a) beginning frame, and (b) ending frame.

time, within ± 2 frames 78.5 percent, and within ± 5 frames 90.0 percent for the combined beginning and ending points.

Figure 11 shows some examples of how the new automatic endpoint detector worked on several representative strings of digits. Shown are log-energy contours with dashed lines indicating where the algorithm determined the digit endpoint locations to have been. The string in Fig. 11a, /2226242/, is an example of speech spoken in the presence of highly variable background noise. The peak s/n for this example is 21.7 dB; however, the s/n's for most of the digits in the string are well below that figure. Under laboratory conditions (speech over a local PBX) the peak s/n is usually between 35 and 50 dB. The string in Fig. 11b, /6854566/, is an example of how the endpoint detector is sometimes able to split connected words (the 68 and 4566 are connected). The string in Fig. 11c, /4736354/, shows a fully connected string of digits. The first three digits /473/ were determined to be one utterance, and the next four digits, /6354/, were split into separate utterances. Finally, the string in Fig. 11d, /2294761/, shows that the new endpoint detector can work very well even on very bad background conditions. Note the extremely variable background noise level (peak s/n of only 17 dB).

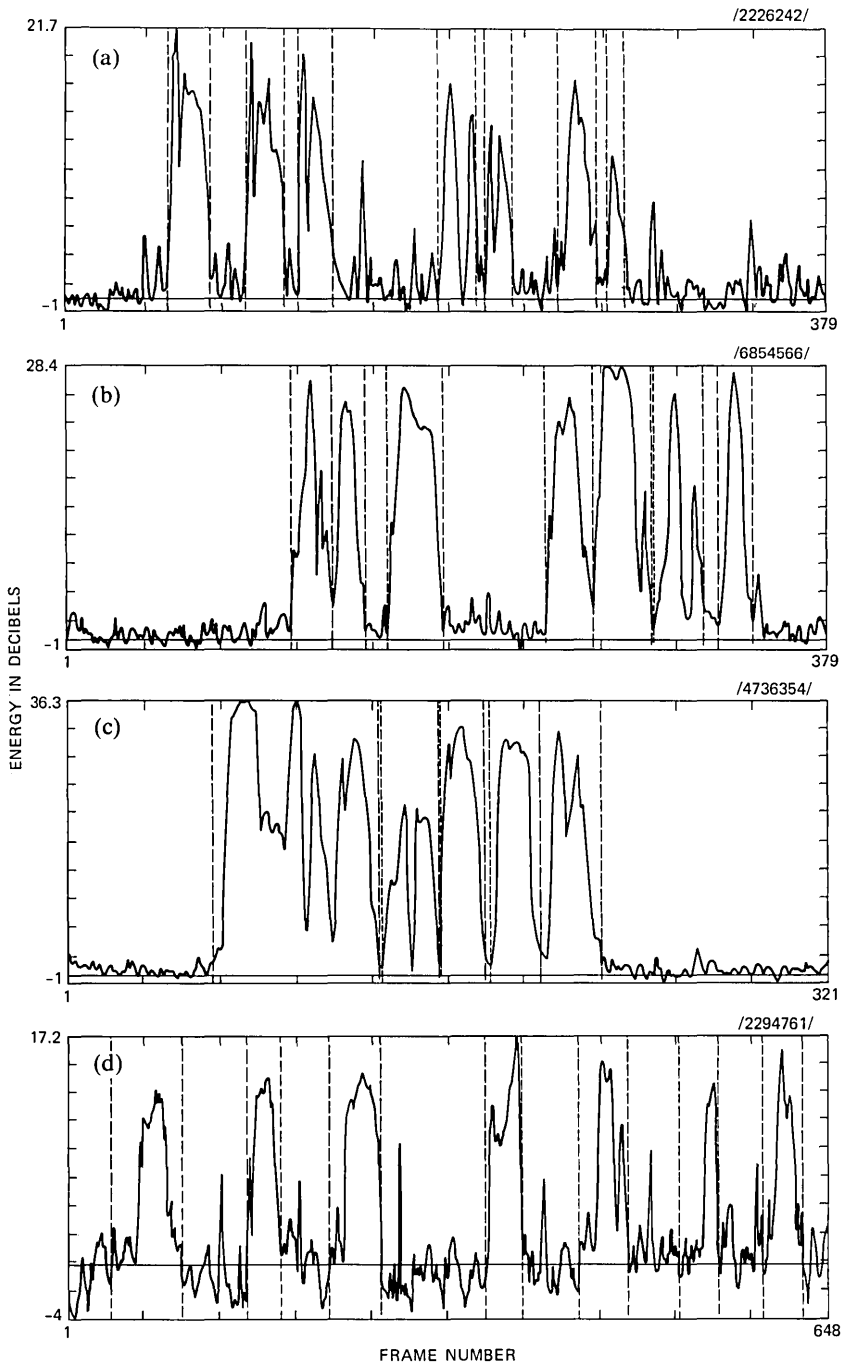


Fig. 11—Log-energy contours from several representative digit strings showing how top-down endpoint detector performed. Dashed lines indicate where algorithm placed beginning and ending word markers. (a) String /2226242/ shows speech spoken over highly variable background noise. (b) String /6854566/ shows how endpoint detector can split connected words. (c) String /4736354/ shows a fully connected string of digits. (d) String /2294761/ shows speech carried over very noisy telephone lines.

4.3 Recognition results using the bottom-up approach

Recognition was run on the 820 digits database using the bottom-up endpoint detector. For this algorithm, only 68.5 percent of the 820 digits were detected. Of the detected words, 85.2 percent were correctly recognized.

4.4 Recognition results using the top-down approach

The top-down endpoint detector was substituted for the bottom-up approach and the entire recognition process was repeated. The new endpoint detector found 800 of the 820 digits (97.6 percent). In looking further we found that 10 double words (connected) were found by the endpoint detector and 5 false alarms were also made. Therefore, the new endpoint detector actually found 805 of the 820 digits in the database (98.2 percent). The recognition accuracy on this test set was 90.0 percent, with 711 of the 790 utterances correctly recognized. Since we are using an isolated word recognition system, the recognition errors produced by the 10 double utterances were removed. The 79 errors in the isolated word recognition system were attributed to the following causes:

1. For 10 words, the beginning point included too much of the background noise.
2. For 8 words, the ending point included too much of the background noise.
3. For 4 words, both endpoints were greatly in error.
4. The endpoint detector failed to find the entire word in 12 cases. These all occurred for the digit *six*, where the /IX/ was left out.
5. For the remaining 40 errors, the endpoint detector found the correct endpoints; however, the recognizer was unable to recognize the words.

These errors can be thought of in two ways. Either they were attributable to the endpoint detector, or they were recognizer errors. Types 1, 2, and 3 above are clearly endpoint detector errors. Type 5 is clearly a recognizer error. Type 4 can also be considered a recognizer error, as the template set has tokens for the word *six* without the final /IX/.

If we were to compute a recognition error rate due entirely to the endpoint detector, the errors we would include would be types 1, 2, and 3 above, plus the 5 false alarms and the 15 words missed entirely by the endpoint detector. We are not including the 10 double words found because they clearly were connected words, which could possibly be recognized by a connected word recognition system. Therefore, a total of 42 errors out of a total of 805 utterances (790 utterances plus 15 utterances not found) were due to the endpoint algorithm. This yields an endpoint detector hit rate of 94.8 percent. The corresponding

recognizer accuracy, if we eliminate the endpoint error rate, would be 93.3 percent (711 utterances correct out of a possible 763 words). Hence, our recognition results are comparable to those obtained from manual endpoints; however, we suffer a 5-percent error rate in digit detection.

4.5 Alternatives to top-down approach

Several other methods of endpoint detection were examined during our study. Initially, we tried to improve the bottom-up algorithm by first filtering the speech into four bands. Endpoint detection was implemented in each of the four bands and then combined based on a set of rules. The filter bank that we implemented used filters from 100 to 500 Hz, 500 to 1000 Hz, 1000 to 2000 Hz, and 2000 to 3200 Hz, with a small amount of overlapping. This approach yielded results significantly worse than the top-down approach described here. We then included the filter bank approach in the top-down endpoint detector. This also degraded the overall system accuracy. Another technique that was examined, though computationally expensive, was the level-building speech recognition algorithm of Myers and Rabiner.⁹ This allowed for an open-ended dynamic time-warp space, and, therefore, the recognizer itself could possibly find the correct endpoints. This approach neither increased nor decreased the accuracy of the endpoint detector.

V. DISCUSSION

Table II shows the results of the recognition experiments run on the different endpoint detection algorithms. The first point to make is that while the new endpoint detector accurately detected 94.8 percent of all words, the old approach only found 68.5 percent. This translates into an recognition error rate component due entirely to nondetection of speech of 5.2 percent and 31.5 percent for the top-down and bottom-up algorithms, respectively.

We also see that the bottom-up algorithm correctly recognized 85.2 percent of the words it detected, while the top-down approach recog-

Table II—Comparison of bottom-up endpoint detector with new top-down endpoint detector

Endpoint Algorithm	Words Detected (Percent)	Recognition	Overall
		Accuracy on Words Detected (Percent)	Recognition Accuracy (Percent)
Bottom-up	68.5	85.2	59.1
Top-down	98.2	90.0	89.4

nized 90.0 percent of the words it detected. If we take into account all errors (endpoints and recognizer) made in processing the 820-word database, the bottom-up endpoint approach led to a total recognition accuracy of 59.1 percent, while the top-down approach had an overall digit recognition accuracy of 89.4 percent. Clearly the top-down endpointing algorithm is superior to the bottom-up approach.

VI. SUMMARY

We have described a new approach to word endpoint detection. We call it a top-down design. Experimental results have been presented indicating that this new approach is able to detect words in highly variable noise environments, as are observed in the telephone network, with much higher accuracy than an earlier implementation of the endpoint detector. The performance of this new technique approaches that of manual endpoint detection—i.e., their recognition accuracies were comparable.

REFERENCES

1. J. G. Wilpon and L. R. Rabiner, "On the Recognition of Isolated Digits From a Large Telephone Customer Population," *B.S.T.J.*, 62, No. 7, Part 1 (September 1983), pp. 1977-2000.
2. L. F. Lamel, L. R. Rabiner, A. E. Rosenberg, and J. G. Wilpon, "An Improved Endpoint Detector for Isolated Word Recognition," *IEEE Trans. Acoustics, Speech, and Signal Processing, ASSP-29*, No. 4 (August 1981), pp. 777-85.
3. L. R. Rabiner and J. G. Wilpon, "Considerations in Applying Clustering Techniques to Speaker Independent Word Recognition," *J. Acoust. Soc. Amer.*, 66, No. 3 (September 1979), pp. 663-73.
4. L. R. Rabiner and S. E. Levinson, "Isolated and Connected Recognition—Theory and Selected Applications," *IEEE Trans. Commun.*, 29, No. 5 (May 1981), pp. 621-59.
5. F. Itakura, "Minimum Prediction Residual Principle Applied to Speech Recognition," *IEEE Trans. Acoustics, Speech, and Signal Processing, ASSP-23*, No. 1 (February 1975), pp. 67-72.
6. L. R. Rabiner, S. E. Levinson, A. E. Rosenberg, and J. G. Wilpon, "Speaker Independent Recognition of Isolated Words Using Clustering Techniques," *IEEE Trans. Acoustics, Speech, and Signal Processing, ASSP-27*, No. 4 (August 1979), pp. 336-49.
7. L. R. Rabiner and J. G. Wilpon, "Speaker Independent, Isolated Word Recognition for a Moderate Size (54 word) Vocabulary," *IEEE Trans. Acoustics, Speech, and Signal Processing, ASSP-27*, No. 6 (December 1979), pp. 583-7.
8. J. G. Wilpon, L. R. Rabiner, and A. F. Bergh, "Speaker Independent Isolated Word Recognition Using a 129 Word Airline Vocabulary," *J. Acoust. Soc. Amer.*, 72, No. 2 (August 1982), pp. 390-6.
9. C. S. Myers and L. R. Rabiner, "A Level Building Dynamic Time Warping Algorithm for Connected Word Recognition," *IEEE Trans. Acoustics, Speech, and Signal Processing, ASSP-29*, No. 2 (April 1981), pp. 284-297.

AUTHORS

Lawrence R. Rabiner, S.B. and S.M., 1964, Ph.D., 1967 (Electrical Engineering), The Massachusetts Institute of Technology; AT&T Bell Laboratories, 1962—. Presently, Mr. Rabiner is engaged in research on speech communications and digital signal processing techniques. He is coauthor of *Theory*

and Application of Digital Signal Processing (Prentice-Hall, 1975), *Digital Processing of Speech Signals* (Prentice-Hall, 1978), and *Multirate Digital Signal Processing* (Prentice-Hall, 1983). Member, National Academy of Engineering, Eta Kappa Nu, Sigma Xi, Tau Beta Pi. Fellow, Acoustical Society of America, IEEE.

Jay G. Wilpon, B.S., A.B. (cum laude) in Mathematics and Economics, respectively, 1977, Lafayette College, Easton, PA; M.S., 1982 (Electrical Engineering/Computer Science), Stevens Institute of Technology, Hoboken, NJ; AT&T Bell Laboratories, 1977—. Since June 1977 Mr. Wilpon has been with the Acoustics Research Department at AT&T Bell Laboratories, where he is a Member of Technical Staff. His interests include basic research in the field of speech recognition, training algorithms for speaker-dependent and speaker-independent recognizers, and speech endpoint detection.

Performance of Cross-Polarized M-ary QAM Signals Over Nondispersive Fading Channels

By M. KAVEHRAD*

(Manuscript received June 1, 1983)

This paper presents performance analysis of dual-polarized M-ary Quadrature Amplitude Modulated (QAM) signals over nondispersive radio channels. In particular, dual-polarized, 16-QAM signals are examined. A simple method for adaptive cancellation of static and fade-induced cross-polarization interference is introduced. The cancellation is performed at baseband. For this canceler, two adaptation methods are studied. The results indicate that dual-polarized M-ary QAM is not feasible over fading channels unless means of adaptive cancellation of the cross-polarization interference are provided. The results also indicate that the adaptive algorithm employed in cross-polarization interference cancellation should take into account noise power reduction.

I. INTRODUCTION

Consider transmission of two orthogonally polarized Quadrature Amplitude Modulated (QAM) carriers over a single communication route. As an example, envision a dual-polarization radio communication system where the available bandwidth is "reused" in order to double the route capacity by transmitting two independent M-ary QAM signals over the same Radio Frequency (RF) channel, using orthogonally polarized waves. Because of channel impairments, such as fades or antenna imperfections, however, the orthogonally polarized waves are received depolarized at the receiver. Consequently, there

* AT&T Bell Laboratories.

Copyright © 1984 AT&T. Photo reproduction for noncommercial use is permitted without payment of royalty provided that each reproduction is done without alteration and that the Journal reference and copyright notice are included on the first page. The title and abstract, but no other portions, of this paper may be copied or distributed royalty free by computer-based and other information-service systems without further permission. Permission to reproduce or republish any other portion of this paper must be obtained from the Editor.

will be some interference imposed on each signal, causing errors in the detection process. We refer to this effect as cross-polarization (x-pol) distortion. For such a case, the x-pol parameters have randomly time-variant characteristics unknown to the receiver in advance.

Several methods for canceling the x-pol distortion (XPD) in dual-polarized systems have been proposed by investigators.¹⁻⁵ The first two references assume access to some beacon signals for cancellation of the x-pol distortion. For instance, Chu² considers the use of two pilot tones, one for each polarization, to estimate the scattering matrix of the radio channel, and applies a differential phase and attenuation in the receive antenna feed to eliminate the x-pol interference and restore the orthogonality. Steinberger³ proposes a recursive equalization structure that operates at RF and experimentally shows that the device can cancel the x-pol distortion induced by fades over a terrestrial radio link when dual-polarized eight-phase shift keying signals are employed. RF/IF x-pol cancellation schemes are suitable when the dual-polarized signals have to be transmitted over several nonregenerative hops, with cancellation occurring on each hop. Such might be the case in many terrestrial radio communication applications where, by avoiding baseband x-pol cancellation, the operation is more cost-effective in terms of a reduced number of required modems. However, for digitally modulated carriers, especially if used over a regenerative transmission hop, the x-pol distortion can be eliminated directly at baseband as a part of the information detection process. Attempts in the area of baseband x-pol cancellation have been made by Culmone,⁴ and Nichols et al.⁵

In this study we suggest a very simple adaptive baseband canceler to eliminate the x-pol distortion in dual-polarized M-ary QAM systems. Two methods of canceler taps adaptation are evaluated. We analyze the performance of such systems by deriving an average probability of error as a function of signal-to-noise ratio (s/n), x-pol distortion, and nondispersive fade level with or without the baseband canceler. The results indicate that over a typical fading radio channel with static x-pol of about -25 dB, dual polarization of M-ary QAM signals is possible only if some x-pol distortion cancellation method is employed. In Section II, we explain the mathematical modeling of the dual channel. The adaptive baseband canceler is described in Section III. Section IV presents the performance analysis of dual-polarized, M-ary QAM systems with or without x-pol distortion cancellation. Section V gives the numerical performance results for 16-QAM systems. It should be noted that even though the analysis is a baseband analysis, the results are also applicable to RF or Intermediate Frequency (IF) cancellation systems employing similar adaptation algorithms.

II. DUAL-POLARIZATION CHANNEL MODEL

We consider transmission of two independent, orthogonally M-ary QAM carriers with the same bandwidth and center frequency. The bandpass signal on either of the two orthogonal channels can be represented by

$$S_i(t) = R_e\{\tilde{s}_i(t)\exp(j\omega_c t)\}, \quad i = 1, 2, \quad (1)$$

where $R_e\{\cdot\}$ denotes the real part, $\tilde{s}_i(t)$ is the low-pass complex envelope, and ω_c is the nominal carrier frequency. The complex envelope can be expressed as

$$\tilde{s}_i(t) = \sum_{m=0}^{\infty} \tilde{\alpha}_i(m)\tilde{h}(t - mT), \quad i = 1, 2, \quad (2)$$

where $\tilde{\alpha}_i(m)$ denotes the complex-valued information symbol stream, and $\tilde{h}(t)$ is the complex low-pass equivalent of the overall system impulse response. The complex-valued symbols are denoted by

$$\tilde{\alpha}_i(m) = \delta_i(m) + j\beta_i(m), \quad i = 1, 2,$$

where $\delta_i(m)$ and $\beta_i(m)$ take on elements of the set $\{\pm c, \pm 3c, \dots, \pm(L-1)c\}$, with $L = \sqrt{M}$, and M the number of levels of the M-ary signal. The parameter, L , is chosen to be even. The constant, c , denotes the distance of each point in the signal constellation from its nearest decision region boundary. The random variables, $\delta_i(m)$ and $\beta_i(m)$, are identically distributed and take on the specified values with equal probability. Note that in eq. (1) it is assumed that the data sequences are synchronized and carrier signals are coherent. These assumptions, however, may not be necessary in practice.

The channel is assumed to be of the slowly time-variant nondispersive type that takes two independent streams of data and distorts the transmission by introducing a fraction of one stream into the other. A practical model of such a channel might be a satellite channel with rain-induced attenuation and depolarization, which is usually nondispersive across the channel bandwidth; hence, depolarization of the dual-polarized signals over such a channel resembles the described scenario.

It is known that deep multipath fading of the main polarization signals on microwave radio routes, in general, is dispersive. However, because of the lack of empirical data concerning the dispersiveness of the cross-polarized parameters, we confine this analysis to those radio channels where all the signals are subjected to nondispersive fading (for example, satellite channels).

The dual channel matrix is characterized by

$$\mathbf{A} = \begin{bmatrix} a_{11} & a_{12} \\ a_{21} & a_{22} \end{bmatrix}, \quad (3)$$

in which the a_{jk} 's, $j = 1, 2, k = 1, 2$, are complex-valued quantities used to represent the channel attenuation and phase shift. These quantities are randomly time variant; however, the time variations are assumed to be slow in comparison to the symbol rate of the signals. Such slow variations can be tracked and canceled adaptively. The received low-pass equivalent signals can be expressed as

$$\begin{cases} r_1(t) = a_{11}\hat{s}_1(t) + a_{12}\hat{s}_2(t) + \eta_1(t) \\ r_2(t) = a_{21}\hat{s}_1(t) + a_{22}\hat{s}_2(t) + \eta_2(t), \end{cases} \quad (4)$$

where $\eta_1(t)$ and $\eta_2(t)$ are independent, zero-mean, white Gaussian processes. The received signals are filtered by receive filters matched to the transmit signals and sampled at every symbol period. The sampled signals are denoted by $x_i(k)$, $i = 1, 2$, and are expressed as

$$\begin{cases} x_1(k) = a_{11}\tilde{\alpha}_1(k) + a_{12}\tilde{\alpha}_2(k) + n_1(k) \\ x_2(k) = a_{21}\tilde{\alpha}_1(k) + a_{22}\tilde{\alpha}_2(k) + n_2(k). \end{cases} \quad (5)$$

The colored noise sequences, $\{n_1(k)\}$ and $\{n_2(k)\}$, are independent samples of zero-mean, complex-valued Gaussian processes with equal variances

$$E\{|n_i(k)|^2\} = \sigma_n^2, \quad i = 1, 2,$$

where $E\{\cdot\}$ denotes the statistical average. The factors a_{11} and a_{22} represent the in-line attenuation and phase shift; the factors a_{12} and a_{21} represent the x-pol coupling on the two channels.

Data calculated by Chu⁶ show that for linearly polarized waves, the behavior of the cross-polarized signal amplitude can be described by

$$\overline{\text{XPL}} = \frac{|a_{ij}|^2}{|a_{ii}|^2}, \quad i = 1, 2, \quad j = 1, 2, \quad i \neq j, \quad (6)$$

where $\overline{\text{XPL}}$ is defined as cross-polarization factor of linearly polarized waves⁶ and

$$\overline{\text{XPL}} = \frac{1}{2} \left(\frac{C}{D} e^{-4\sigma_\Theta^2} \right) [1 - \cos(4\tau e^{-8\sigma_m^2})] \delta, \quad (7)$$

where σ_m is the standard deviation of time-varying, mean-canting angle Θ_m over various rainstorms, σ_Θ is the standard deviation of anisotropy angle Θ , τ is the orientation angle of the quasi-vertical

polarization, δ is proportional to in-line attenuation factor, and C/D is proportional to differential propagation constants. Measured data from COMSTAR II follow these calculations closely.⁶ The comparison is shown in Fig. 1 of Ref. 6. We will use these results to introduce an average probability of error as a function of in-line attenuation level.

In the next section we describe a simple structure that can reduce the x-pol distortion in such systems.

III. ADAPTIVE BASEBAND CANCELER MODEL

The adaptive canceler that attempts to remove the x-pol distortion is characterized by

$$\mathbf{W} = \begin{bmatrix} w_{11} & w_{12} \\ w_{21} & w_{22} \end{bmatrix},$$

where w_{ij} 's, $i = 1, 2, j = 1, 2$ are the canceler coefficients. This adaptive device, which is a part of the M-ary QAM detector circuit, is studied under two adaptation methods. The first method employs a Least Mean-Square (LMS) error algorithm and the second applies channel matrix diagonalization. Figure 1 shows the LMS canceler structure. The samples at the matched filter output of each receiver are inputs to a bank of adaptive filters formed by a set of multiplier accumulators (MACs). To update the coefficients of the canceler, each MAC contains storage elements for storing the result of the multiplication of the signal-sample detection error and the complex conjugate of the corresponding received signal sample at the matched filter output. The calculated coefficients are multiplied by the signal samples at the matched filter output and used to cancel the x-pol distortion. The detectors shown in Fig. 1 are part of the M-ary QAM demodulators.

The canceler structure consists of a simple adaptive filter, which minimizes the least mean-square error in symbol estimation. The theory of this type of filter is well known⁷ and is solely based on the statistical orthogonality principle. According to this theory, mean-square error is minimum when the error in symbol estimation is statistically orthogonal to the variable being observed. In the case at hand, we show the signal-sample estimation error by

$$\epsilon_i(k) = \hat{\alpha}_i(k) - \tilde{\alpha}_i(k), \quad i = 1, 2, \quad (8)$$

where $\hat{\alpha}_i(k)$ is the detector input, as shown in Fig. 1. We now select those canceler coefficients for which the mean-square error is minimum, i.e., the results of solving $\min E\{|\epsilon_1(k)|^2 + |\epsilon_2(k)|^2\}$. After proceeding with the minimization process, the following set of equations will lead to the optimum determination of the coefficients w_{ij}^0 , $i = 1, 2, j = 1, 2$:

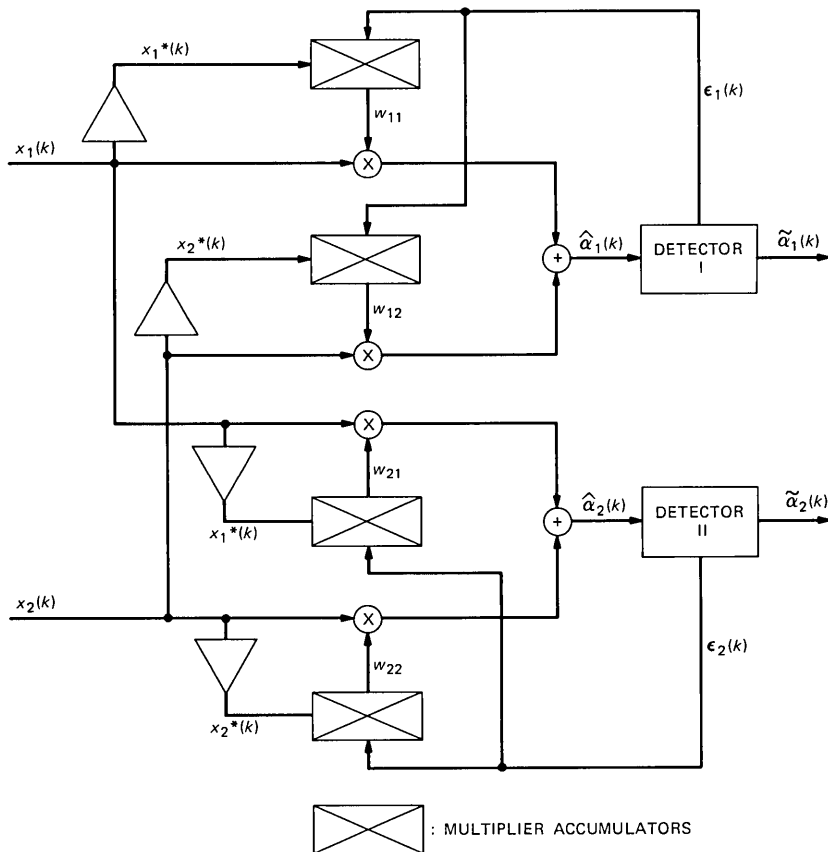


Fig. 1—Block diagram of adaptive LMS baseband canceler.

$$\begin{aligned}
 [|a_{11}|^2 + |a_{12}|^2 + \sigma_n^2]w_{11}^0 + [a_{21}a_{11}^* + a_{12}^*a_{22}]w_{12}^0 &= a_{11}^* \\
 [a_{21}^*a_{11} + a_{12}a_{22}^*]w_{11}^0 + [|a_{21}|^2 + |a_{22}|^2 + \sigma_n^2]w_{12}^0 &= a_{21}^* \\
 [|a_{11}|^2 + |a_{12}|^2 + \sigma_n^2]w_{21}^0 + [a_{21}a_{11}^* + a_{12}^*a_{22}]w_{22}^0 &= a_{12}^* \\
 [a_{21}^*a_{11} + a_{12}a_{22}^*]w_{21}^0 + [|a_{21}|^2 + |a_{22}|^2 + \sigma_n^2]w_{22}^0 &= a_{22}^*. \quad (9)
 \end{aligned}$$

As Fig. 1 shows, the signal samples at the canceler output for each channel can be expressed as

$$\begin{cases} \hat{\alpha}_1(k) = w_{11}x_1(k) + w_{12}x_2(k) \\ \hat{\alpha}_2(k) = w_{21}x_1(k) + w_{22}x_2(k), \end{cases} \quad (10)$$

where $\hat{\alpha}_1$ and $\hat{\alpha}_2$ are complex quantities. In eq. (10), by substituting $x_m(k)$'s, $m = 1, 2$ of eq. (5) and the coefficients w_{ij}^0 , $i = 1, 2, j = 1, 2$ of

eq. (9), one can form a decision variable for each channel for the derivation of probability of error.

An alternate solution to this type of optimization problem, which uses the steepest descent algorithm and is simple to implement, was suggested by Widrow.⁸ The solution is recursive and states that

$$w_{ij}^{(k+1)} = w_{ij}^{(k)} + \epsilon_i(k)x_j^*(k), \quad i = 1, 2, \quad j = 1, 2, \quad (11)$$

where * denotes the complex conjugate and k represents the sampling instant. In eq. (11) the noisy estimates of the cross-correlation of the observed signal and error signal are used as unbiased estimates to update the canceler coefficients at every baud interval. Such algorithms are well known in adaptive filtering and equalization. The realization of eq. (11) is shown in Fig. 1. The MACs in the figure update eq. (11) by storing the result of multiplication of signal samples and detection error samples.

As an alternative adaptation method, we consider a case where the canceler coefficients are determined by forcing the x-pol interference on each channel to zero.⁹ This is equivalent to diagonalizing the overall channel matrix; i.e., substituting $x_m(k)$'s of eq. (5) into eq. (10) and forcing the coefficient of the undesired signal to zero on each channel, i.e., by

$$\begin{cases} w_{11}a_{12} + w_{12}a_{22} = 0 \\ w_{21}a_{11} + w_{22}a_{21} = 0. \end{cases} \quad (12)$$

In this case we refer to the canceler as a diagonalizer. Amitay describes the realization of an IF diagonalizer.⁹ In analogy to intersymbol-interference removal by zero-forcing equalization, this method can also be referred to as zero-forcing cancellation. Figure 2 shows a block diagram of the diagonalizer. Note that in canceling the interference, the diagonalizer neglects the thermal noise completely.

In the following section we will evaluate the canceler for both cases described.

IV. SYSTEM PERFORMANCE ANALYSIS

In this section we derive an upper bound on the average probability of error for dual-polarized M-ary QAM signals with and without the x-pol distortion canceler. Throughout this section it is assumed the data sequences on the two polarized channels are independent, equally likely, M-ary QAM signals. The channel is characterized by the matrix introduced earlier. To simplify the derivation, with no loss of generality, we can assume the phase angles of a_{11} and a_{22} are zero and use the normalized notations

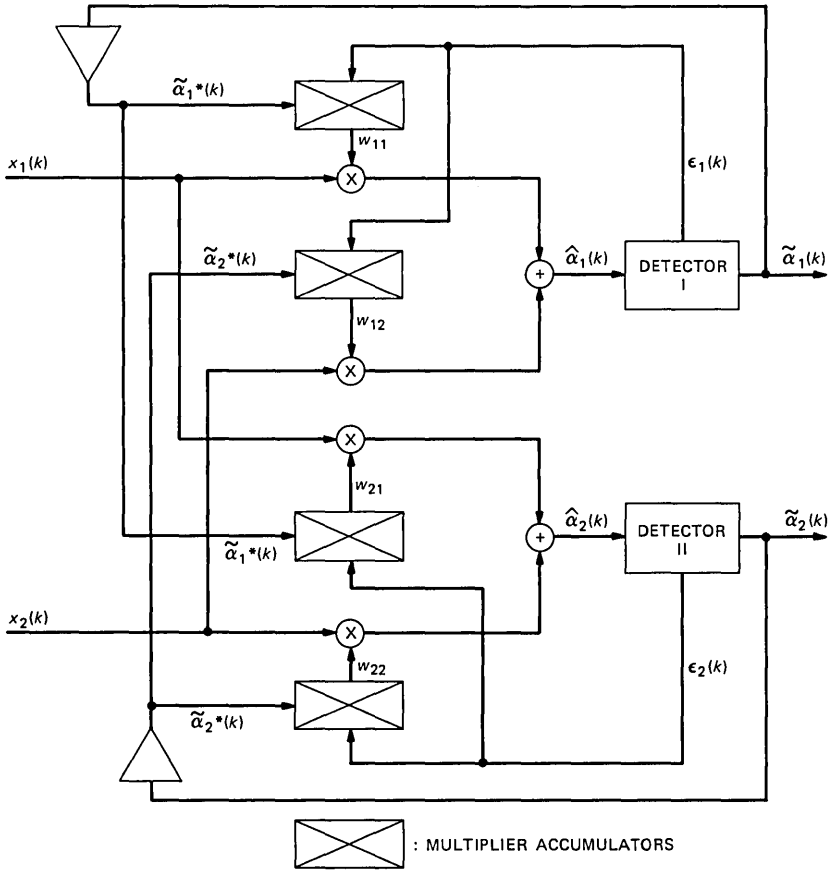


Fig. 2—Block diagram of adaptive diagonalizer.

$$\frac{a_{12}}{a_{11}} = \xi_1 \exp(j\phi_1),$$

$$\frac{a_{21}}{a_{22}} = \xi_2 \exp(j\phi_2),$$

and

$$\left| \frac{a_{11}}{a_{22}} \right| = \xi_0. \quad (13)$$

All the variables introduced in eq. (13) are time variant, but the time variations are slow relative to symbol rate so the receiver can obtain perfect estimates of the channel matrix components. The phase parameters ϕ_1 and ϕ_2 in eq. (13) are uniformly distributed over $[-\pi, \pi]$.

Also, to further simplify the presentation of the results, we assume $\xi_1 = \xi_2 = \xi$, and $\xi_0 = 1$. This model was shown by Chu to be a valid model for depolarization of dual-polarized waves due to heavy rainfall.¹⁰ Furthermore, this simplified model of a x-pol channel still provides means of evaluating the canceler performance, and the error probability bounds derived should be useful in preliminary system planning.

4.1 Performance in the presence of the canceler

In this section we first derive an average probability of error applying the diagonalizer. Then we proceed with deriving an average error probability for the LMS canceler.

To calculate a simple upper bound on the probability of error performance when the diagonalizer is present, we use the complex valued estimates of the data symbols at the canceler output given in eq. (10), along with the constraints in eq. (12) and matched filter outputs of eq. (5), to define the following simplified decision variables for the two channels:

$$\begin{cases} \hat{a}_1(k) = a_{11}[1 - \xi^2 e^{j(\phi_1 + \phi_2)}] \tilde{\alpha}_1(k) + n_1(k) - n_2(k) \xi e^{j\phi_1} \\ \hat{a}_2(k) = a_{22}[1 - \xi^2 e^{j(\phi_1 + \phi_2)}] \tilde{\alpha}_2(k) + n_2(k) - n_1(k) \xi e^{j\phi_2}. \end{cases} \quad (14)$$

As this equation shows, the decision variable for channel i depends on the parameters of channel j , $i \neq j$, $i = 1, 2$, $j = 1, 2$, namely, ϕ_j and n_j . Now consider the in-phase and quadrature-phase components of each channel. The decision variable for channel 1 in eq. (14) can be expressed in terms of its real and imaginary parts as

$$\begin{aligned} z_R(k) &= -\delta(k) \xi^2 \cos(\phi_1 + \phi_2) + \beta(k) \xi^2 \sin(\phi_1 + \phi_2) \\ &\quad + \frac{1}{a_{11}} n_{1R}(k) + \frac{1}{a_{11}} n_{2I}(k) \xi \sin(\phi_1) \\ &\quad - \frac{1}{a_{11}} n_{2R}(k) \xi \cos(\phi_1) \\ z_I(k) &= -\beta(k) \xi^2 \cos(\phi_1 + \phi_2) - \delta(k) \xi^2 \sin(\phi_1 + \phi_2) \\ &\quad + \frac{1}{a_{11}} n_{1I}(k) - \frac{1}{a_{11}} n_{2I}(k) \xi \cos(\phi_2) \\ &\quad - \frac{1}{a_{11}} n_{2R}(k) \xi \sin(\phi_2), \end{aligned} \quad (15)$$

where $n_{iR}(k)$ and $n_{iI}(k)$, $i = 1, 2$, are the real and imaginary parts of Gaussian noise samples at sampling instant k , which are identically distributed random variables with the same variance, σ_n^2 . Now, an

error is made on channel 1 if $|z_R| > c$ or $|z_I| > c$, where c , as stated earlier, is the signal distance from its nearest decision region boundary in the signal constellation. Therefore, the probability of error on channel 1 can be expressed as

$$P_e = \frac{L-1}{2L} \{P_r(|z_R| > c) + P_r(|z_I| > c)\}. \quad (16)$$

To derive the error probability, we apply the well-known¹¹ Chernoff bound, which states

$$P_r\{z > c\} \leq \exp(-\lambda c) E\{\exp(\lambda z)\}, \quad \lambda \geq 0, \quad (17)$$

where $E\{\cdot\}$ denotes the statistical average of the random variable z . This is valid for any $\lambda \geq 0$. Using the positive λ that minimizes the right-hand side of eq. (17) establishes the least upper bound. Hence, we apply eq. (17) to eqs. (15) and (16) combined. The actual derivation of the upper bound is in Appendix A.

The resulting probability of error bound is

$$P_e \leq \frac{L-1}{L} \exp \left[-\frac{3}{2(L^2-1)} \frac{\gamma |a_{ii}|^2}{1 + \gamma \xi^4 |a_{ii}|^2 + \xi^2} \right], \quad i = 1, 2, \quad (18)$$

where

$$\gamma = \frac{L^2-1}{3} \frac{c^2}{\sigma_n^2} = \text{the unfaded s/n}$$

$$|a_{ii}| = \text{the in-line voltage on channel } i, \quad i = 1, 2.$$

We define

$$\text{XPD} = 20 \log_{10} \xi, \text{ dB} \quad (19)$$

as a measure of x-pol distortion to represent the cross-coupling between the two channels, and

$$v = 20 \log_{10} |a_{ii}|, \text{ dB} \quad i = 1, 2 \quad (20)$$

as a measure of flat-fade level. When there is no fade, $v = 0$ dB and the only contribution to x-pol distortion is due to the static effects, such as antenna imperfections, in which case XPD is denoted by XPD_0 . The fade-induced part of the x-pol distortion is put into effect when $|a_{ii}| < 1$, $i = 1, 2$. Now, eq. (7) can be applied to relate the average probability of error to in-line attenuation and to remove the x-pol factor in eq. (18). That is,

$$P_e(|a_{ii}|^2) \leq \frac{L-1}{L} \exp \left[-\frac{3}{2(L^2-1)} \cdot \frac{\gamma |a_{ii}|^2}{1 + \gamma \overline{\text{XPL}}^2 |a_{ii}|^2 + \overline{\text{XPL}}} \right], \quad i = 1, 2. \quad (21)$$

We now proceed with reevaluating the probability of error when the LMS canceler is employed. As we stated in Section III, the LMS canceler adaptively calculates its coefficients so that the mean-square error is minimized. By using the optimum set of coefficients of eq. (9) in eq. (10), we can define a new decision variable for each channel; that is,

$$\left\{ \begin{array}{l} \hat{a}_1 = (w_{11}^0 a_{11} + w_{12}^0 a_{21}) \tilde{\alpha}_1 + (w_{11}^0 a_{12} + w_{12}^0 a_{22}) \tilde{\alpha}_2 \\ \quad + w_{11}^0 n_1 + w_{12}^0 n_2 \\ \hat{a}_2 = (w_{21}^0 a_{11} + w_{22}^0 a_{21}) \tilde{\alpha}_1 + (w_{21}^0 a_{12} + w_{22}^0 a_{22}) \tilde{\alpha}_2 \\ \quad + w_{21}^0 n_1 + w_{22}^0 n_2, \end{array} \right. \quad (22)$$

where w_{ij}^0 's are the optimum coefficients. As we see again, the decision variable for channel i depends on the parameters of channel j , $i \neq j$, $i = 1, 2, j = 1, 2$. In a manner similar to what was explained for the diagonalizer, we can calculate the probability of error for the LMS canceler. The actual derivation of the bound is in Appendix B. The resulting probability of error is

$$P_e \leq \frac{L-1}{L\pi} \int_0^{2\pi} \left(1 - \frac{\phi}{2\pi} \right) \exp \left\{ -\frac{3}{2(L^2-1)} \cdot \frac{\gamma \nabla(\phi)}{\gamma \Theta(\phi) + \Delta(\phi)} \right\} d\phi, \quad (23)$$

where

$$\gamma = \frac{L^2 - 1}{3} \frac{c^2}{\sigma_n^2},$$

and $\nabla(\phi)$, $\Theta(\phi)$, and $\Delta(\phi)$ are defined in eq. (34) of Appendix B. An attempt to solve eq. (23) in a closed form turned out to be inconclusive, so it was calculated on a computer numerically. To express eq. (23) only in terms of fade level, again we can use eq. (7) to remove ξ .

To make a comparison, we remove the canceler and repeat the derivation of the probability of error for a baseline, dual-polarized, M-ary QAM system.

4.2 Performance of baseline, dual-polarized, M-ary QAM system

In this case the error-bound derivation is simplified because for channel i the decision variables are independent of the other channel's

parameters, namely, ϕ_j and n_j , $j \neq i$, $i = 1, 2$, $j = 1, 2$. Therefore, eq. (15) is reduced to

$$\begin{cases} z_R(k) = \xi\delta_2(k)\cos(\phi_1) - \xi\beta_2(k)\sin(\phi_1) + \frac{1}{a_{11}} n_{1R}(k) \\ z_I(k) = \xi\beta_2(k)\cos(\phi_1) + \xi\delta_2(k)\sin(\phi_1) + \frac{1}{a_{11}} n_{1I}(k). \end{cases} \quad (24)$$

Using a similar approach, as for the previous cases, we derive an upper bound on the error probability. This derivation is given in Appendix C. The result is

$$P_e \leq \frac{L-1}{L} \exp \left\{ -\frac{3}{2(L^2-1)} \frac{\gamma |a_{ii}|^2}{1 + \gamma \xi^2 |a_{ii}|^2} \right\}, \quad i = 1, 2. \quad (25)$$

This is a simple bound to calculate, and in terms of fade level, it can be expressed as

$$P_e(|a_{ii}|^2) \leq \frac{L-1}{L} \exp \left[-\frac{3}{2(L^2-1)} \cdot \frac{\gamma |a_{ii}|^2}{1 + \gamma |a_{ii}|^2 \cdot \overline{\text{XPL}}} \right], \quad i = 1, 2. \quad (26)$$

The numerical results in the following section illustrate the performance.

V. NUMERICAL PERFORMANCE FOR 16 QAM

In this section we evaluate the bounds derived in the previous section for dual-polarized 16-QAM signals.

First, we consider 16 QAM with no cancellation. The upper bound of eq. (25) is shown in Fig. 3 for three different static x-pol distortion (XPD_0) values. These curves represent the average error probability bound for 16-QAM signals as a function of static x-pol distortion and s/n when no cancellation is adopted and no fading exists. Figure 3 also shows the theoretical performance of the 16 QAM and the theoretical calculated upper bound, i.e., for the case when there is no fade and no x-pol distortion. As we see, the upper bound curve is very close to the actual theoretical curve. These results indicate that improving the static x-pol can improve the overall performance substantially. Figure 4 demonstrates the bound in eq. (26) for 5-dB flat fade, using Fig. 1 of Reference 6, which predicts an $\overline{\text{XPL}}$ of 28 dB for a 5-dB flat fade. As we see, the sensitivity of the error probability to the fade level is quite high.

Next, we apply the canceler and the diagonalizer described earlier

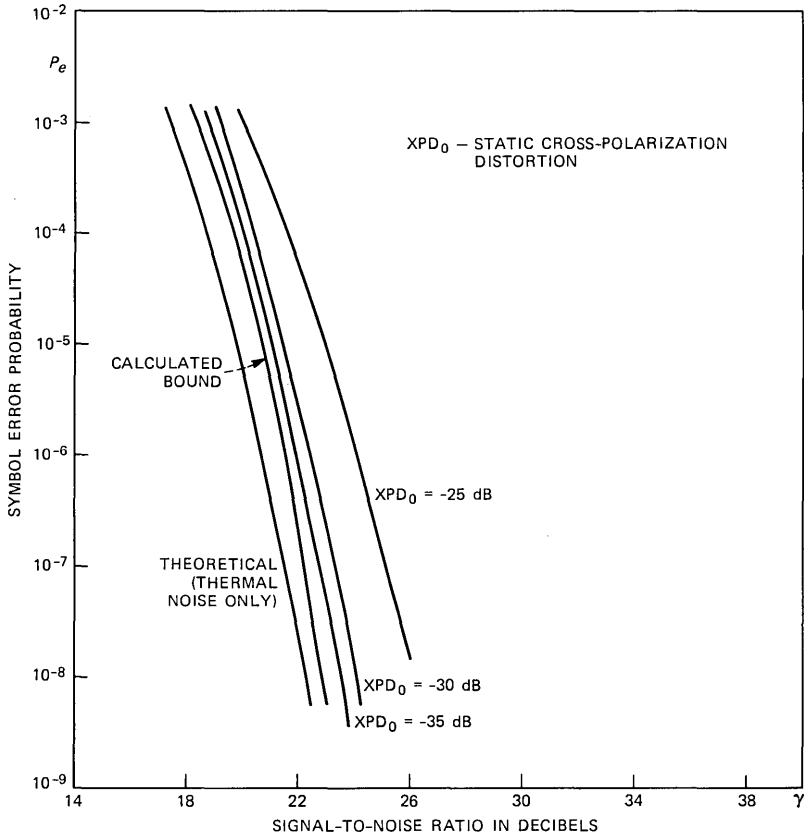


Fig. 3—Probability of error vs. s/n for dual 16 QAM without canceler; no fading exists.

and show the bounds in eqs. (18) and (23) in Fig. 5 for different XPD_0 s. High values of XPD_0 s could occur in poorly aligned antenna systems. As Fig. 5 illustrated, the LMS canceler and the diagonalizer behave quite differently. The LMS canceler improves the performance significantly even at rather poor XPDs, e.g., $XPD_0 = -5$ dB, while the diagonalizer is almost useless for such a case. As the XPD_0 value is improved, e.g., for a $XPD_0 = -25$ dB, the performance of the two cancelers becomes the same. This is because as XPD increases, the diagonalizer coefficients grow in a direction to cancel XPD, while neglecting the thermal noise completely; consequently, the noise power in each channel is increased strongly. The LMS canceler, however, by minimizing the combined noise and XPD power, produces an acceptable performance. On the other hand, as XPD is improved, the diagonalizer becomes as attractive as the LMS canceler since there is

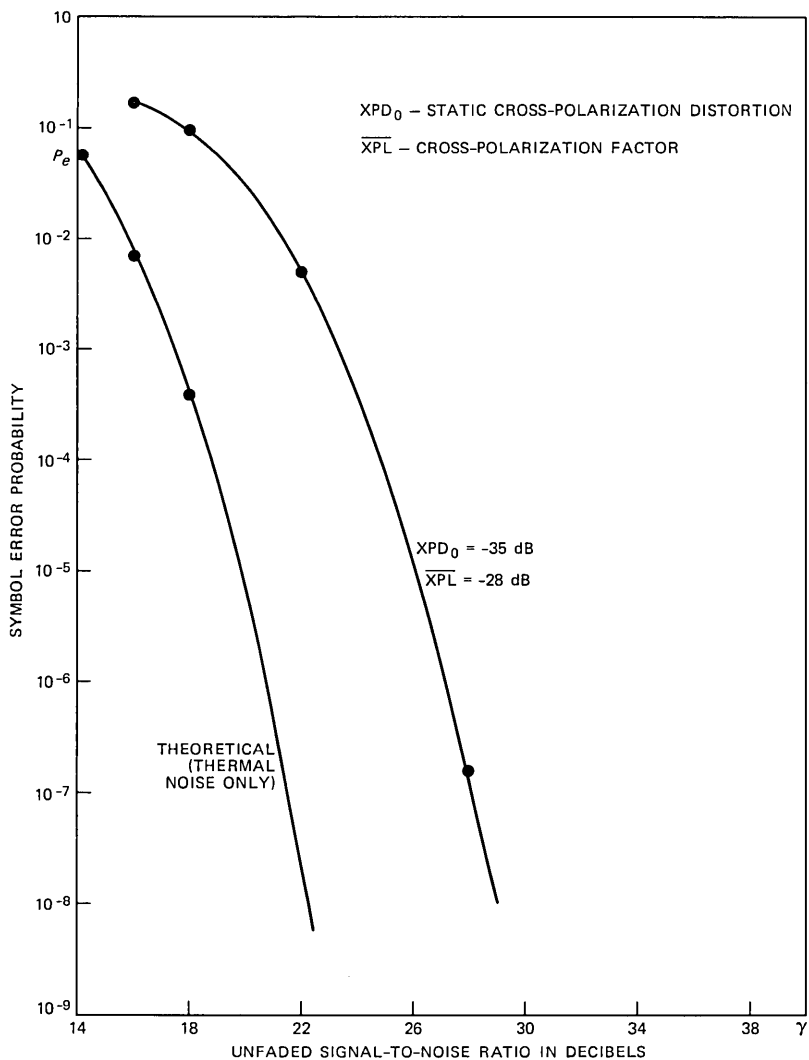


Fig. 4—Probability of error vs. s/n for dual 16 QAM without canceler; 5-dB flat fade applied.

not much XPD to cancel; consequently, there is not much noise enhancement. However, over fading channels where XPD, dB can even be positive, use of the LMS canceler will ensure a more reliable system.

We then apply 5-dB flat fade and draw the average error rate bounds for both cancelers as a function of fade level in Fig. 6. As we see, the XPD is removed for a practically reasonable static XPD. The horizon-

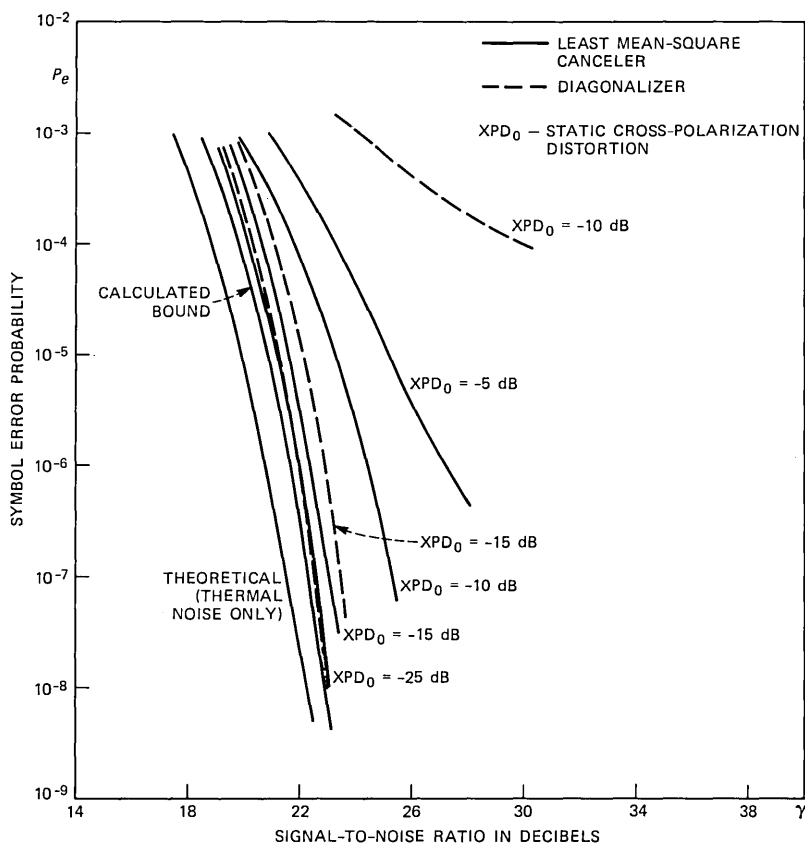


Fig. 5—Probability of error vs. s/n for dual 16 QAM with canceler; no fading exists.

tal translation of the curves reflects the 5-dB signal power loss due to fade since we have employed unfaded s/n in sketching these figures.

Note that rain fading increases the system noise temperature as follows. If we assume the noise temperature of the receiver and the following stages to be T_0 , and in the presence of rain, T_p , the increased system noise temperature in rain is

$$T_p = T_0 + (1 - \nu)T_{\text{rain}},$$

where

$$\nu = |a_{ii}| = \text{in-line fade level}$$

$$T_{\text{rain}} = \text{effective temperature of the rain.}$$

For example, for a flat fade of 5 dB and rain temperature of 280K, the

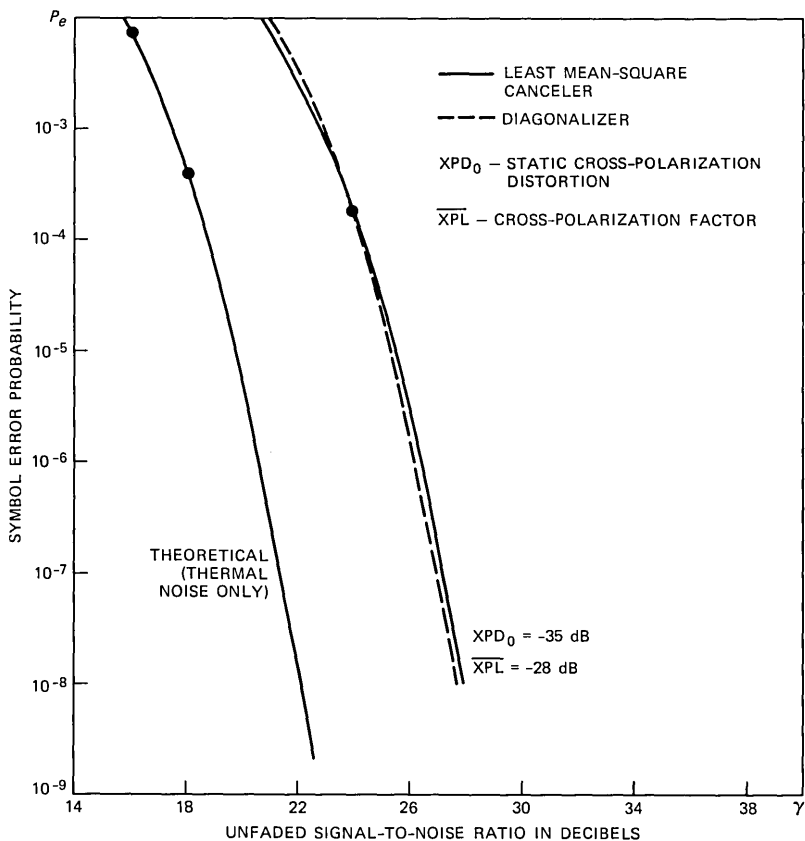


Fig. 6—Probability of error vs. s/n for dual 16 QAM with canceler; 5-dB flat fade applied.

system noise temperature increases by 122.5K. The additional increase in noise temperature will further translate the curves in Fig. 6 to the right, horizontally. In practice the noise power increase has to be factored in system power budget.

VI. CONCLUSIONS

In this paper we studied the performance of dual-polarized, M-ary QAM signals in terms of average probability of error as a function of s/n, x-pol distortion, and fade level. An x-pol cancellation method operating at baseband was suggested. Two different adaptation methods were considered in calculating the canceler coefficients. In particular, the performance was evaluated with and without the XPD cancellation for 16-QAM signals in dual polarization with or without fade. The results indicate that without applying some kind of x-pol

cancellation, dual polarization of M-ary QAM signals is not feasible. The results also indicate that the adaptive algorithm employed in cross-polarization interference cancellation should take into account noise power reduction.

REFERENCES

1. T. S. Chu, "Restoring the Orthogonality of Two Polarization in Radio Communication Systems, I," *B.S.T.J.*, 50, No. 9 (November 1971), pp. 3063-9.
2. T. S. Chu, "Restoring the Orthogonality of Two Polarization in Radio Communication Systems, II," *B.S.T.J.*, 52, No. 3 (March 1973), pp. 319-29.
3. M. L. Steinberger, "Design of a Terrestrial Cross Pol Canceler," *IEEE ICC*, Philadelphia, June 1982, pp. 2B.6.1-5.
4. A. F. Culmone, "Polarization Diversity with Adaptive Channel Decoupling," *IEEE NTC*, New Orleans, December 1975, pp. 25-22 to 25-27.
5. E. Nichols and J. Proakis, "Maximum Likelihood Detection of Digital Signals in the Presence of Interchannel-Interference," *Int. Symp. on Inf. Theory*, Sweden, January 1976.
6. T. S. Chu, "Microwave Depolarization of an Earth-Space Path," *B.S.T.J.*, 59, No. 6 (July 1980), pp. 987-1007.
7. A. Papoulis, *Probability, Random Variables, and Stochastic Processes*, New York: McGraw-Hill, 1965, Chapter 11.
8. B. Widrow, "Adaptive Filters," *Aspects of Network and System Theory*, New York: Holt, Rinehart & Winston, 1971, pp. 563-87.
9. N. Amitay, "Signal-to-Noise Ratio Statistics for Nondispersive Fading in Radio Channels with Cross-Polarization Interference Cancellation," *IEEE Trans. Commun.*, COM-27, No. 2 (February 1979), pp. 498-502.
10. T. S. Chu, "Rain-Induced Cross-Polarization at Centimeter and Millimeter Wavelengths," *B.S.T.J.*, 53, No. 8 (October 1974), p. 1557.
11. J. M. Wozencraft and I. M. Jacobs, *Principles of Communication Engineering*, New York: Wiley, 1965, pp. 47-106.

APPENDIX A

Derivation of Error Bound for the Diagonalizer

Consider one of the dual-polarized channels, e.g., channel 1. Using the Chernoff bound for the in-phase rail of the M-ary QAM signal and eq. (15) in Section 4.1,

$$P_{e1} = P_r\{|z_R| > c\} \leq \exp(-\lambda c) \left(E \left\{ \exp \left[-\lambda \delta \xi^2 \cos(\phi) + \lambda \beta \xi^2 \cdot \sin(\phi) + \frac{\lambda}{\bar{a}_{11}} n_{1R} - \frac{\lambda \xi}{\bar{a}_{11}} \left(n_{2R} \cos(\phi_1) - n_{2I} \sin(\phi_1) \right) \right] \right\} \right), \quad (27)$$

where

$$\phi = \phi_1 + \phi_2.$$

Since the terms in the argument of the inner exponential are inde-

pendent of each other, given that ϕ and ϕ_1 are known, we can average over independent variables first and then take the average of the result with respect to phase variables. So,

$$P_{e_1} \leq \exp(-\lambda c) E_{\phi, \phi_1} \left\{ E_{\delta} [\exp(-\lambda \delta \xi^2 \cos \phi)] \cdot E_{\beta} [\exp(\lambda \beta \xi^2 \sin \phi)] \right. \\ \cdot E_{n_{1R}} \left[\exp \left(\frac{\lambda}{a_{11}} n_{1R} \right) \right] \cdot E_{n_{2R}} \left[\exp \left(-\frac{\lambda \xi}{a_{11}} n_{2R} \cos(\phi_1) \right) \right] \\ \left. \cdot E_{n_{2I}} \left[\exp \left(\frac{\lambda \xi}{a_{11}} n_{2I} \sin(\phi_1) \right) \right] \right\}, \quad (28)$$

where δ and β are the real and imaginary parts of a uniformly distributed, complex-valued random variable. We now calculate the statistical averages in eq. (28):

$$\Gamma_1 = E_{n_{1R}} \left[\exp \left(\frac{\lambda}{a_{11}} n_{1R} \right) \right] = \exp \left[\frac{\lambda^2}{2a_{11}^2} \sigma_n^2 \right] \\ \Gamma_2 = E_{\delta} \{ \exp(-\lambda \delta \xi^2 \cos \phi) \} = \frac{2}{L} \sum_{i=1}^{L/2} \cosh \{ \lambda \xi^2 c (2i - 1) \cos(\phi) \}.$$

And, since

$$\frac{2}{L} \sum_{i=1}^{L/2} \cosh \{ (2i - 1)x \} \leq \exp \left[\frac{L^2 - 1}{3} \frac{x^2}{2} \right],$$

then,

$$\Gamma_2 \leq \exp \left[\frac{\lambda^2 \xi^4 c^2}{2} \frac{L^2 - 1}{3} \cos^2(\phi) \right].$$

Similarly,

$$\Gamma_3 = E_{\beta} \{ \exp(\lambda \beta \xi^2 \sin(\phi)) \} \leq \exp \left[\frac{L^2 - 1}{3} \frac{\lambda^2 \xi^4 c^2}{2} \sin^2(\phi) \right] \\ \Gamma_4 = E_{n_{2R}} \left\{ \exp \left(-\frac{\lambda \xi}{a_{11}} n_{2R} \cos(\phi_1) \right) \right\} = \exp \left[\frac{\lambda^2 \xi^2 \sigma_n^2}{2a_{11}^2} \cos^2(\phi_1) \right] \\ \Gamma_5 \leq E_{n_{2I}} \left\{ \exp \left(\frac{\lambda \xi}{a_{11}} n_{2I} \sin(\phi_1) \right) \right\} \leq \exp \left[\frac{\lambda^2 \xi^2 \sigma_n^2}{2a_{11}^2} \sin^2(\phi_1) \right].$$

Therefore,

$$E_{\phi, \phi_1\{\cdot\}} = \exp \left[\frac{L^2 - 1}{3} \frac{\lambda^2 \xi^4 c^2}{2} + \frac{\lambda^2 \sigma_n^2}{2a_{11}^2} + \frac{\lambda^2 \xi^2 \sigma_n^2}{2a_{11}^2} \right]$$

and

$$P_{e_1} \leq \exp \left[-\lambda c + \lambda^2 \sigma_n^2 \left(\frac{1}{2a_{11}^2} + \frac{L^2 - 1}{3} \frac{\xi^4 c^2}{2\sigma_n^2} + \frac{\xi^2}{2a_{11}^2} \right) \right]. \quad (29)$$

If we repeat the derivation for $P_{e_2} = P_r\{|z_I| > c\}$, because of the symmetry, we will find out that the result is the same as for P_{e_1} ; i.e.,

$$P_e = \frac{L - 1}{2L} (P_{e_1} + P_{e_2}).$$

We now calculate the least upper bound on P_{e_1} by minimizing the argument of the exponential in eq. (29) with respect to λ . The result for

$$\lambda_{\min} = \frac{c}{\sigma_n^2 \left[\frac{1}{a_{11}^2} + \frac{L^2 - 1}{3} \frac{\xi^4 c^2}{\sigma_n^2} + \frac{\xi^2}{a_{11}^2} \right]}$$

is

$$P_e \leq \frac{(L - 1)}{L} \exp \left\{ -\frac{3}{2(L^2 - 1)} \frac{\gamma |a_{11}|^2}{1 + \gamma \xi^4 |a_{11}|^{2+\xi^2}} \right\}. \quad (30)$$

For channel 2 we find a similar result using $|a_{22}|^2$ in eq. (30) instead of $|a_{11}|^2$.

APPENDIX B

Derivation of Error Bound for the LMS Canceler

The derivation of error bound is somewhat tedious in this case. We employ the decision variables of eq. (22) of Section 4.1 and after some mathematical manipulations, find their real and imaginary parts. For example, for channel 1, by introducing

$$\nu = |a_{11}| \quad \text{and} \quad \phi = \phi_1 + \phi_2 \quad (31)$$

$$\hat{z}_{1R} = \text{Re}\{\hat{\alpha}_1 - \tilde{\alpha}_1\} = \frac{1}{H} [A \cdot \delta_1 + B \cdot \delta_2 - C \cdot \beta_2 + D \cdot n_{1R} \\ - E \cdot n_{1I} + F \cdot n_{2R} - G \cdot n_{2I}]$$

$$\hat{z}_{1I} = \text{Im}\{\hat{\alpha}_1 - \tilde{\alpha}_1\} = \frac{1}{H} [A \cdot \beta_1 + B \cdot \beta_2 + C \cdot \delta_2 + D \cdot n_{1I} \\ + E \cdot n_{1R} + F \cdot n_{2I} + G \cdot n_{2R}],$$

where

$$\begin{aligned}
 A &= -(\nu^2 \sigma_n^2 + \nu^2 \xi^2 \sigma_n^2 + \sigma_n^4) \\
 B &= \xi \nu^2 \sigma_n^2 [\cos \phi_1 + \cos \phi_2] \\
 C &= \xi \nu^2 \sigma_n^2 [\sin \phi_1 - \sin \phi_2] \\
 D &= \nu^3 + \nu \sigma_n^2 - \nu^3 \xi^2 \cos \phi \\
 E &= \nu^3 \xi^2 \sin \phi \\
 F &= -\nu^3 \xi \cos \phi_1 + [\nu^3 \xi^3 + \nu \xi \sigma_n^2] \cos \phi_2 \\
 G &= -\nu^3 \xi \sin \phi_1 - [\nu^3 \xi^3 + \nu \xi \sigma_n^2] \sin \phi_2 \\
 H &= [\nu^2 \xi^2 + \nu^2 + \sigma_n^2]^2 - 2\nu^4 \xi^2 [1 + \cos \phi]. \tag{32}
 \end{aligned}$$

In a similar manner as in Appendix A, we find an upper bound on $P_{e_1} = P_r\{|\hat{z}_{1R}| > c\}$ using the Chernoff bound.

Following the method used in Appendix A, we define

$$\begin{aligned}
 \Gamma_0 &= E_{\delta_1} \left\{ \exp \left(\lambda \left(\frac{A}{H} \right) \delta_1 \right) \right\} = \frac{2}{L} \sum_{i=1}^{L/2} \cosh \left\{ \lambda \left(\frac{A}{H} \right) (2i-1)c \right\} \\
 &\leq \exp \left[\frac{\lambda^2 c^2}{2} \frac{L^2 - 1}{3} \left(\frac{A}{H} \right)^2 \right].
 \end{aligned}$$

Similarly,

$$\Gamma_1 \leq \exp \left[\frac{\lambda^2 c^2}{2} \frac{L^2 - 1}{3} \left(\frac{B}{H} \right)^2 \right]$$

and

$$\Gamma_2 \leq \exp \left[\frac{\lambda^2 c^2}{2} \frac{L^2 - 1}{3} \left(\frac{C}{H} \right)^2 \right].$$

Also,

$$\Gamma_3 = E_{n_{1R}} \left\{ \exp \left(\lambda \left(\frac{D}{H} \right) n_{1R} \right) \right\} = \exp \left[\frac{\lambda^2}{2} \sigma_n^2 \left(\frac{D}{H} \right)^2 \right].$$

Similarly,

$$\Gamma_4 = \exp \left[\frac{\lambda^2}{2} \sigma_n^2 \left(\frac{E}{H} \right)^2 \right],$$

so

$$\Gamma_5 = \exp \left[\frac{\lambda^2}{2} \sigma_n^2 \left(\frac{F}{H} \right)^2 \right]$$

and

$$\Gamma_6 = \exp \left[\frac{\lambda^2}{2} \sigma_n^2 \left(\frac{G}{H} \right)^2 \right].$$

Therefore, using the Chernoff bound,

$$P_{e_1} \leq E_{\Phi} \left\{ \exp \left[-\lambda c + \frac{\lambda^2 c^2}{2} \frac{L^2 - 1}{3} \frac{A^2 + B^2 + C^2}{H^2} + \frac{\lambda^2}{2} \sigma_n^2 \frac{D^2 + E^2 + F^2 + G^2}{H^2} \right] \right\},$$

where $E_{\Phi}\{\cdot\}$ is the expectation with respect to ϕ . We can minimize the argument of the $\exp\{\cdot\}$ with respect to λ . The least upper bound corresponds to

$$P_{e_1} \leq E_{\Phi} \left\{ \exp \left[-\frac{3}{2(L^2 - 1)} \cdot \frac{\gamma \nabla(\phi)}{\gamma \Theta(\phi) + \Delta(\phi)} \right] \right\}. \quad (33)$$

This bound is conditioned on ϕ_1 and ϕ_2 , so by taking the average over ϕ_1 and ϕ_2 , the actual bound can be obtained. In eq. (33)

$$\begin{aligned} \Theta(\phi) &= A^2 + B^2 + C^2 \\ \Delta(\phi) &= D^2 + E^2 + F^2 + G^2 \\ \nabla(\phi) &= H^2. \end{aligned}$$

Hence,

$$\left\{ \begin{aligned} \Theta(\phi) &= (\nu^2 \sigma_n^2 + \nu^2 \xi^2 \sigma_n^2 + \sigma_n^4)^2 + 2\xi^2 \nu^4 \sigma_n^4 (1 + \cos \phi) \\ \Delta(\phi) &= \nu^2 (\nu^4 + \sigma_n^4 + 2\nu^2 \sigma_n^2 + \nu^4 \xi^4 + \nu^4 \xi^2 + \nu^4 \xi^6 \\ &\quad + 2\nu^2 \xi^4 \sigma_n^2 + \xi^2 \sigma_n^4) - 2\nu^4 \xi^2 [\nu^2 \xi^2 + 2\sigma_n^2 + \nu^2] \cos \phi \\ \nabla(\phi) &= \{(\nu^2 + \nu^2 \xi^2 + \sigma_n^2)^2 - 2\nu^4 \xi^2 (1 + \cos \phi)\}^2. \end{aligned} \right. \quad (34)$$

Since ϕ_1 and ϕ_2 are two independent random variables that are uniformly distributed over $(-\pi, \pi)$ and $\phi = \phi_1 + \phi_2$, the probability density function of ϕ is

$$f_{\Phi}(\phi) = \frac{1}{2\pi} \left(1 - \frac{1}{2\pi} |\phi| \right), \quad 0 \leq |\phi| \leq 2\pi. \quad (35)$$

By using $f_{\Phi}(\phi)$, we can calculate the statistical average of the right-hand side of the bound in eq. (33) and find the least upper bound on P_{e_1} . Again, by symmetry

$$P_{e_2} = P_r\{|\hat{z}_{1T}| > c\} = P_{e_1},$$

so

$$P_e = \frac{L-1}{2L} \{P_{e_1} + P_{e_2}\} = \frac{L-1}{L} P_{e_1}$$

and

$$P_e \leq \frac{L-1}{L} \int_0^{2\pi} \frac{1}{\pi} \left(1 - \frac{\phi}{2\pi}\right) \cdot \exp \left\{ -\frac{3}{2(L^2-1)} \cdot \frac{\gamma \nabla(\phi)}{\gamma \Theta(\phi) + \Delta(\phi)} \right\} d\phi, \quad (36)$$

in which $\gamma = \frac{L^2-1}{3} \frac{c^2}{\sigma_n^2}$ and $\nabla(\phi)$, $\Theta(\phi)$, and $\Delta(\phi)$ are defined in eq. (34).

APPENDIX C

Derivation of Error Bound for the Baseline System

If we use a similar approach,

$$P_e \leq \frac{L-1}{L} \exp(-\lambda c) \cdot E \left\{ \exp \left[\lambda \xi \delta_2 \cos(\phi_1) - \lambda \xi \beta_2 \sin(\phi_1) + \frac{\lambda}{|a_{11}|} n_{1R} \right] \right\}. \quad (37)$$

Following what was done in Appendices A and B,

$$\begin{aligned} \Gamma_1 &= E_{n_{1R}} \left[\exp \left\{ \frac{\lambda n_{1R}}{|a_{11}|} \right\} \right] = \exp \left\{ \frac{\lambda^2 \sigma_n^2}{2|a_{11}|^2} \right\} \\ \Gamma_2 &= E_{\delta_2} \left[\exp \left\{ \lambda \xi \delta_2 \cos(\phi_1) \right\} \right] \\ &= \frac{2}{L} \sum_{j=1}^{L/2} \cosh[(2j-1)c\lambda\xi \cos(\phi_1)] \\ &\leq \exp \left[\frac{\lambda^2 \xi^2 c^2}{2} \frac{L^2-1}{3} \cos^2(\phi_1) \right] \\ \Gamma_3 &= E_{\beta_2} \left[\exp \left\{ -\lambda \xi \beta_2 \sin(\phi_1) \right\} \right] \\ &= \frac{2}{L} \sum_{j=1}^{L/2} \cosh[(2j-1)c\lambda\xi \sin(\phi_1)] \\ &\leq \exp \left[\frac{\lambda^2 \xi^2 c^2}{2} \frac{L^2-1}{3} \sin^2(\phi_1) \right]. \end{aligned} \quad (38)$$

Therefore,

$$P_e \leq \frac{(L-1)}{L} \exp(-\lambda c) \cdot E_{\phi_1} \{ \Gamma_1 \cdot \Gamma_2 \cdot \Gamma_3 \}$$

or

$$P_e \leq \frac{(L-1)}{L} \exp \left[-\lambda c + \frac{1}{2} \frac{\lambda^2}{|a_{11}|^2} \sigma_n^2 + \frac{1}{2} \frac{L^2-1}{3} \lambda^2 c^2 \xi^2 \right]. \quad (39)$$

By minimizing the argument of $\exp[\cdot]$ with respect to λ and substituting λ_{\min} in eq. (37), the corresponding least upper bound is

$$P_e \leq \frac{(L-1)}{L} \exp \left[-\frac{3}{2(L^2-1)} \frac{\gamma |a_{11}|^2}{1 + \gamma \xi^2 |a_{11}|^2} \right], \quad (40)$$

where

$$\gamma = \frac{L^2-1}{3} \frac{c^2}{\sigma_n^2},$$

and, similarly, the probability of error for channel 2 can be obtained by substituting $|a_{22}|^2$ instead of $|a_{11}|^2$ in eq. (40).

AUTHOR

Mohsen Kavehrad, B.S. (Electrical Engineering), 1973, Tehran Polytechnic Institute; M.S. (Electrical Engineering), 1975, Worcester Polytechnic Institute; Ph.D. (Electrical Engineering), 1977, Polytechnic Institute of New York; Fairchild Industries, 1977–1978; GTE, 1978–1981; AT&T Bell Laboratories, 1981—. At Fairchild Mr. Kavehrad worked on NASA space communications analysis projects. At GTE he worked in satellite communications and computer communication networks areas. At AT&T Bell Laboratories he is a member of the Radio Transmission Laboratory, where his current work involves exploratory studies in microwave radio subsystems. He teaches Communication Theory courses at the Northeastern University Continuing Education Program. He is a Technical Associate Editor for the IEEE Communications Magazine. Member, IEEE, Sigma Xi.

PAPERS BY AT&T BELL LABORATORIES AUTHORS

COMPUTING/MATHEMATICS

- Ackerman A. F., Buckley F. J., **Software Standards Take Shape.** *Datamation* 29(10):259+, 1983.
- Bertz S. H., **On the Complexity of Graphs and Molecules.** *B Math Biol* 45(5):849-855, 1983.
- Dalal S. R., Hall W. J., **Approximating Priors by Mixtures of Natural Conjugate Priors.** *J Roy Sta B* 45(2):278-286, 1983.
- Fishburn P. C., **Dimensions of Election Procedures—Analyses and Comparisons (Review).** *Theor Decis* 15(4):371-397, 1983.
- Garzia M. R., Loparo K. A., Martin C. F., **Riccati Group Invariants of Linear Hamiltonian Systems.** *Int J Contr* 38(5):897-911, 1983.
- Hawkins D. T., **Online Information-Retrieval Bibliography Sixth Update (Review).** *Online Rev* 7(2):127-187, 1983.
- Storer, J. A., **On the Complexity of Chess.** *J Comput Sy* 27(1):77-100, 1983.

ENGINEERING

- Aspnes D. E., **Recombination at Semiconductor Surfaces and Interfaces.** *Surf Sci* 132(1-3): 406-421, 1983.
- Bates R. J. S., Spalink J. D., Butterfield S. J., Lipson J., Burrus C. A., Lee T. P., Logan R. A., **1.3 μm /1.5 μm Bidirectional WDM Optical-Fibre Transmission System Experiment at 144 Mbit/s.** *Electr Lett* 19(13):458-459, 1983.
- Burr D. J., **Designing a Handwriting Reader (Letter).** *IEEE Patt A* 5(5):554-559, 1983.
- Campbell J. C., Dentai A. G., Holden W. S., Kasper B. L., **High-Performance Avalanche Photo-Diode With Separate Absorption Grading and Multiplication Regions.** *Electr Lett* 19(20):818-820, 1983.
- Capasso F., **New Device Applications of Bandedge Discontinuities in Multilayer Heterojunction Structures.** *Surf Sci* 132(1-3):527-539, 1983.
- Dragone C., **First-Order Correction of Aberrations in Cassegrainian and Gregorian Antennas.** *IEEE Antenn* 31(5):764-775, 1983.
- Drukarev A., Costello D. J., **Hybrid ARQ Error Control Using Sequential Decoding.** *IEEE Info T* 29(4):521-535, 1983.
- Dudderar T. D., Gilbert J. A., **Fiber Optic Pulsed Laser Holography.** *Appl Phys L* 43(8):730-732, 1983.
- Feit M. D., Fleck J. A., McCaughan L., **Comparison of Calculated and Measured Performance of Diffused Channel-Waveguide Couplers.** *J Opt Soc* 73(10):1296-1304, 1983.
- Feldman, L. C. **Application of Channeling to Surface Science.** *Phys Scr* 28(3):303-307, 1983.
- Feuer M. D., Hendel R. H., Kiehl R. A., Hwang J. C. M., Keramidas V. G. Allyn C. L., Dingle R., **High-Speed Low-Voltage Ring Oscillators Based on Selectively Doped Heterojunction Transistors.** *IEEE Elec D* 4(9):306-307, 1983.
- Hagelbarger D. W., Thompson R. A., **Human-Factors Engineering—Experiments in Teleterminal Design.** *IEEE Spectr* 20(10):40-45, 1983.
- Hwang F. K., **Control Algorithms for Rearrangeable Clos Networks.** *IEEE Commun* 31(8):952-954, 1983.
- Iannuzzi M., **Reliability and Failure Mechanisms of Nonhermetic Aluminum SICs: Literature Review and Bias Humidity Performance.** *IEEE Compon* 6(2):181-190, 1983.
- Judd F. F., **Large Capacity Magnetic-Bubble Memories for Government Applications.** *IEEE Aer El* 19(4):561-567, 1983.
- Kaminow I. P., Stulz L. W., Ko J. S., Miller B. I., Feldman R. D., Dewinter J. C.,

- Pollack M. A., **Low Threshold Ridge Waveguide Laser at 1.55 μm** . *Electr Lett* 19(21):877-879, 1983.
- Kastalsky A., Luryi S., **Novel Real-Space Hot-Electron Transfer Devices**. *IEEE Elec D* 4(9):334-336, 1983.
- Kiehl R. A., Feuer M. D., Hendel R. H., Hwang J. C. M., Keramidas V. G., Allyn C. L., Dingle R., **Selectively Doped Heterostructure Frequency Dividers (Letter)**. *IEEE Elec D* 4(10):377-379, 1983.
- La Porte D., **Bell Laboratories—The Beginnings of Scientific Research in an Industrial Setting**. *Ann NY Acad* 412(OCT):85-100, 1983.
- Lee W. C. Y., **Estimating Unbiased Average Power of Digital Signal in the Presence of High-Level Impulses**. *IEEE Instr* 32(3):403-409, 1983.
- Lin C. L., Tomita A., **Chirped Picosecond Injection-Laser Pulse Transmission in Single-Mode Fibers in the Minimum Chromatic Dispersion Region**. *Electr Lett* 19(20):837-838, 1983.
- Logan R. A., Van Der Ziel J. P., Temkin H., **InGaAsP Buried Crescent Lasers With Separate Optical Confinement**. *P Soc Photo* 380:181-185, 1983.
- Malik R. J., Hayes J. R., Capasso F., Alavi K., Cho A. Y., **High-Gain $\text{Al}_{0.48}\text{In}_{0.52}\text{As}/\text{Ga}_{0.53}\text{As}$ Vertical N-P-N Heterojunction Bipolar-Transistors Grown by Molecular-Beam Epitaxy (Letter)**. *IEEE Elec D* 4(10):383-385, 1983.
- Olsson N.A., Tsang W.T., **Wideband Frequency-Shift Keying With a Spectrally Bistable Cleaved-Coupled-Cavity Semiconductor Laser**. *Electr Lett* 19(20):808-809, 1983.
- Osinski J. S., **Characterization of Fast-Cure Resins for Reaction Injection Molding**. *Polym Eng S* 23(13):756-762, 1983.
- Pleibel W. et al., **Polarization-Preserving Coupler With Self-Aligning Birefringent Fibers**. *Electr Lett* 19(20):825-826, 1983.
- Ross I., **The Myths of High Technology**. *Electronics* 56(20):24, 1983.
- Sandberg I. W., **Expansions for Discrete-Time Nonlinear Systems**. *Circ Syst S* 2(2):179-192, 1983.
- Sandberg I. W., **Series Expansions for Nonlinear Systems**. *Circ Syst S* 2(1):77-87, 1983.
- Schiavone L. M., Craighead H. G., Howard R. E., Shay J. L., **Studies of Fabrication Parameters of Textured Storage Media**. *P Soc Photo* 390:144-148, 1983.
- Schmidt R. L., Haskell B. G., **Transmission of Two NTSC Color-Television Signals Over a Single Satellite Transponder Via Time-Frequency Multiplexing (Letter)**. *IEEE Commun* 31(11):1257-1266, 1983.
- Shieh C. L., Wagner S., Jackel L. D., Howard R. E., Hu E. L., **A Silicon Phototransistor With a MIS Tunnel Junction Emitter**. *IEEE Elec D* 4(8):291-293, 1983.
- Sinden F. W., **Inventing the Low-Energy House (Editorial)**. *B Atom Sci* 39(9):56-58, 1983.
- Sondhi M. M., **Acoustic Imaging by Backpropagation of the Pressure Field**. *P Soc Photo* 413:150-152, 1983.
- Tam S., Hsu F. C., Ko P. K., Hu C., Muller R. S., **Spatially Resolved Observation of Visible-Light Emission From Si MOSFETs (Letter)**. *IEEE Elec D* 4(10):386-388, 1983.
- Temkin H., Van Der Ziel J. P., Linke R. A., Logan R. A., **Single-Mode Operation of 1.5- μm Cleaved-Coupled-Cavity InGaAsP Lasers**. *Appl Phys L* 43(8):723-725, 1983.
- Walker S. S., Connelly J. A., **A New Negative-Resistance Oscillator Model**. *Circ Syst S* 2(2):213-238, 1983.
- Weste N., Burr D. J., Ackland B. D., **Dynamic Time Warp Pattern-Matching Using an Integrated Multiprocessing Array**. *IEEE Comput* 32(8):731-744, 1983.

MANAGEMENT/ECONOMICS

- Chen S. N., Brown S. J., **Estimation Risk and Simple Rules for Optimal Portfolio Selection**. *J Finance* 38(4):1087-1093, 1983.

PHYSICAL SCIENCES

- Abrahams S. C., Marsh P., Ravez J., **Reinvestigation of the Structure of Tetracadmium Sodium Orthovanadate, $Cd_4Na(VO_4)_3$.** Act Cryst C 39(JUN):680-683, 1983.
- Agrawal G. P., **Effect of Index Antiguinding on the Far-Field Distribution of Stripe-Geometry Lasers.** Opt Commun 47(4):283-287, 1983.
- Agrawal G. P., **Saturation Effects in Degenerate Four-Wave Mixing on Homogeneously Broadened Coupled Transitions.** Phys Rev A 28(4):2286-2295, 1983.
- Ahlers F. J., Lohse F., Spaeth J. M., Mollenaur L. F., **ODMR Study of Tl^0 Centers in KCl.** Radiat Eff 73(1-4):19-24, 1983.
- Aronovitz J. A., Banavar J. R., Marcus M. A., Phillips J. C., **Structural Models and Vibrational-Spectra of Tetrahedral Chalcogenide Crystals and Glasses.** Phys Rev B 28(8):4454-4460, 1983.
- Auston D. H., **Subpicosecond Electrooptic Shock Waves.** Appl Phys L 43(8):713-715, 1983.
- Banavar J. R., Cieplak M., **Renormalization-Group Analysis on Fractals—Ising Spin-Glass and the Schrodinger Equation.** Phys Rev B 28(7):3813-3817, 1983.
- Banavar J. R., Phillips J. C., **Cluster-Models of the Neutron and Infrared Vibrational-Spectra of Vitreous Silica.** Phys Rev B 28(8):4716-4723, 1983.
- Brand H. R., Cladis P. E., Finn P. L., **The First Bilayer Ferroelectric Liquid-Crystal.** J Phys Lett 44(18):L771-L776, 1983.
- Buck T. M., Wheatley G. H., Marchut L., **Order-Disorder and Segregation Behavior at the $Cu_3Au(001)$ Surface.** Phys Rev L 51(1):43-46, 1983.
- Celler G. K., Robinson M., Trimble L. E., Lischner D. J., **Spatial Melt Instabilities in Radiatively Melted Crystalline Silicon.** Appl Phys L 43(9):868-870, 1983.
- Chabal Y. J., Higashi G. S., Christman S. B., **Hydrogen Chemisorption on $Si(111)-(7 \times 7)$ and $Si(111)-(1 \times 1)$ Surfaces—A Comparative Infrared Study.** Phys Rev B 28(8):4472-4479, 1983.
- Cohen U., Koch F. B., Sard R., **Electroplating of Cyclic Multilayered Alloy (CMA) Coatings.** J Elchem So 130(10):1987-1995, 1983.
- Cross M. C., **Flow Dissipation in the He^3 Superfluids.** AIP Conf PR1983(103):325-355, 1983.
- Fleming J. W., Wood D. L., **Refractive-Index Dispersion and Related Properties in Fluorine Doped Silica.** Appl Optics 22(19):3102-3104, 1983.
- Frankenthal R. P., Siconolfi D. J., Sinclair W. R., Bacon D. D., **Thermal-Oxidation of Niobium Nitride Films at Temperatures From 20 Degrees C to 400 Degrees C. 1. The Surface Reaction.** J Elchem So 130(10):2056-2060, 1983.
- Gallagher P. K., Sinclair W. R., Bacon D. D., Kammlott G. W., **Oxidation of Sputtered Niobium Nitride Films.** J Elchem So 130(10):2054-2056, 1983.
- Gibson J. M., Phillips J. M., **Analysis of Epitaxial Fluoride-Semiconductor Interfaces.** Appl Phys L 43(9):828-830, 1983.
- Gordon J. P., **Interaction Forces Among Solitons in Optical Fibers.** Optics Lett 8(11):596-598, 1983.
- Graebner J. E., Allen L. C., **Tunneling Systems in Amorphous Germanium.** Phys Rev L 51(17):1566-1569, 1983.
- Griffiths J. E., Espinosa G. P., Phillips J. C., Remeika J. P., **Raman-Spectra and Athermal Laser Annealing of $Ge(S_xSe_{1-x})_2$ Glasses.** Phys Rev B 28(8):4444-4453, 1983.
- Gyorgy E. M., Walker L. R., Wernick J. H., **Torque and Rotational Hysteresis in a Metallic Spin Glass.** Phys Rev L 51(18):1684-1687, 1983.
- Hasegawa A., Wakatani M., **Finite-Larmor-Radius Magnetohydrodynamic Equations for Microturbulence (Letter).** Phys Fluids 26(10):2770-2772, 1983.
- Hutton R. S., Roth H. D., Bertz S. H., **Nuclear-Spin Polarization Effects in Systems With Large Hyperfine Couplings—Limitations of Kapteins Rules.** J Am Chem S 105(21):6371-6377, 1983.
- Ibbotson D. E., Flamm D. L., Donnelly V. M., **Crystallographic Etching of GaAs With Bromine and Chlorine Plasmas.** J Appl Phys 54(10):5974-5981, 1983.
- Jayaraman A., Batlogg B., Van Uitert L. G., **High-Pressure Raman Study of**

- Alkaline-Earth Tungstates and a New Pressure-Induced Phase Transition in BaWO₄.** Phys Rev B 28(8):4774-4777, 1983.
- Johnson L. F., Guggenheim H. J., Bahnck D., Johnson A. M., **Phonon-Terminated Laser Emission From Ni²⁺ Ions in KMgF₃.** Optics Lett 8(7):371-373, 1983.
- Johnson R. E., Brown W. L., Lanzerotti L. J., **Energetic Charged-Particle Erosion of Ices in the Solar System.** J Phys Chem 87(21):4218-4220, 1983.
- Jopson R. M., Freeman R. R., Cooke W. E., Bokor J., **Electron Shake-Up in Two-Photon Excitation of Core Electrons to Rydberg Auto-Ionizing States.** Phys Rev L 51(18):1640-1643, 1983.
- Kinzel W., **Current Oscillations of Charge-Density Waves Pinned by Impurities.** Phys Rev L 51(19):1787-1790, 1983.
- Krimigis S. M., et al., **General Characteristics of Hot Plasma and Energetic Particles in the Saturnian Magnetosphere—Results From the Voyager Spacecraft.** J Geo R-S P 88(NA11):8871+, 1983.
- Lanzerotti L. J., et al., **Impulsive Particle-Precipitation and Concurrent Magnetic-Field Changes Observed in Conjugate Areas Near L = 4.** J Geo R-S P 88(NA11):9115-9124, 1983.
- Lanzerotti L. J., MacLennan C. G., Brown W. L., Johnson R. E., Barton L. A., Reimann C. T., Garrett J. W., Boring J. W., **Implications of Voyager Data for Energetic Ion Erosion of the Icy Satellites of Saturn.** J Geo R-S P 88(NA11):8765-8770, 1983.
- Larson R. G., **Analysis of Isothermal Fiber Spinning With the Doi-Edwards Constitutive Equation.** J Rheol 27(5):475-496, 1983.
- Levin R. M., **The Influence of Back End Processing on the Fixed Charges Density in the Si-SiO₂ Interface.** J Elchem So 130(10):2060-2064, 1983.
- Lewerenz H. J., et al., **Surface Modification of Polycrystalline P-CuInS₂ and P-CuInSe₂ Electrodes for Improved Solar-Cell Performance.** Sol Energy M 9(2):159-166, 1983.
- Linke R. A., Guelin M., Langer W. D., **Detection of H¹⁵NN⁺ and HN¹⁵N⁺ in Interstellar Clouds.** Astrophys J 271(2):L85-L88, 1983.
- Lourenco J. A., **Delineation of P-N Junction in Thin InGaAsP Layers Using Chemical Etching.** J Elchem So 130(10):2097-2099, 1983.
- Lovinger A. J., et al., **Crystallographic Changes Characterizing the Curie Transition in Three Ferroelectric Co-Polymers of Vinylidene Fluoride and Trifluoroethylene. 1. As Crystallized Samples.** Polymer 24(10):1225-1232, 1983.
- Lovinger A. J., et al., **Crystallographic Changes Characterizing the Curie Transition in Three Ferroelectric Co-Polymers of Vinylidene Fluoride and Trifluoroethylene. 2. Oriented or Poled Samples.** Polymer 24(10):1233-1239, 1983.
- MacLenna C. G., Lanzerotti L. J., Krimigis S. M., Lepping R. P., **Low-Energy Particles at the Bow Shock, Magnetopause, and Outer Magnetosphere of Saturn.** J Geo R-S P 88(NA11):8817+, 1983.
- Mattheiss L. F., Hamann D. R., **Electronic Structure of BaPb_{1-x}Bi_xO₃.** Phys Rev B 28(8):4227-4241, 1983.
- Meaudre M., Meaudre R., Hauser J. J., **High-Field Variable Range Hopping of Holelike Polarons in RF Sputtered SiO₂-Films (Letter).** J Non-Cryst 58(1):145-150, 1983.
- Mollenaur L. F., Vieira N., Szeto L., **Optical-Properties of the Ti⁰(1) Center in KCl.** Radiat Eff 73(1-4):13-18, 1983.
- Munier G. B., Psota-Kelty L. A., Sinclair J. D., **Chloride Accumulation on Indoor Zinc and Aluminum Surfaces.** J Elchem So 130(10):1983-1987, 1983.
- Ormejohnson N. R., et al., **Oxidation-State Dependence of Proton-Exchange Near the Iron-Sulfur Centers in Ferredoxins and High-Potential Iron-Sulfur Proteins.** Bioc Biop A 748(1):68-72, 1983.
- Ota Y., **Growth of High-Quality Ge MBE Film.** J Cryst Gr 61(3):431-438, 1983.
- Paalanen M. A., et al., **Critical Scaling of the Conductance in a Disordered Insulator.** Phys Rev L 51(20):1896-1899, 1983.
- Patel D. J., Kozlowski S. A., Bhatt R., **Sequence Dependence of Base-Pair Stacking in Right-Handed DNA in Solution—Proton Nuclear Overhauser Effect NMR Measurements.** P Nas Biol 80(13):3908-3912, 1983.

- Penzias A. A., **Isotopic Fractionation and Mass Motion in Giant Molecular Clouds.** *Astrophys J* 273(1):195-201, 1983.
- Rossetti R., Beck S. M., Brus L. E., **Resonance Raman Investigation of the π^* Antibonding Distribution in Excited Triplet Aqueous *p*-Benzoquinone.** *J Phys Chem* 87(16):3058-3061, 1983.
- Sham L. J., Schluter M., **Density-Functional Theory of the Energy-Gap.** *Phys Rev L* 51(20):1888-1891, 1983.
- Silfvast W. T., Macklin J. J., Wood O. R., **High-Gain Inner-Shell Photo-Ionization Laser in Cd Vapor Pumped by Soft X-Ray Radiation From a Laser-Produced Plasma Source.** *Optics Lett* 8(11):551-553, 1983.
- Smith H. I., Thompson C. V., Geis M. W., Lemons R. A., Bosch M. A., **The Mechanism of Orientation in Si Graphoepitaxy by Laser or Strip Heater Recrystallization.** *J Elchem So* 130(10):2050-2053, 1983.
- Stillinger F. H., Schweitzer K. S., **Ice Under Pressure—Transition to Symmetrical Hydrogen-Bonds.** *J Phys Chem* 87(21):4281-4288, 1983.
- Stillinger F. H., Weber T. A., **Dynamics of Structural Transitions in Liquids.** *Phys Rev A* 28(4):2408-2416, 1983.
- Stormer H. L., **Electron Mobilities in Modulation-Doped GaAs-(AlGa)As Heterostructures.** *Surf Sci* 132(1-3):519-526, 1983.
- Sulewski P. E., Bishop D. J., **Acoustical Contrast of a Dislocation Line in an Isotropic Medium.** *J Appl Phys* 54(10):5715-5717, 1983.
- Sulewski P. E., Dynes R. C., Mahajan S., Bishop D. J., **Study of Defects in Optoelectronic Materials Using a Scanning Acoustic Microscope.** *J Appl Phys* 54(10):5711-5714, 1983.
- Teo B. K., Antonio M. R., Coucouvanis D., Simhon E. D., Stremple P. P., Mo, W, and Fe EXAFS of the $[\text{Cl}_2\text{FeS}_2\text{MS}_2\text{FeCl}_2]^{2-}$ ($M = \text{Mo}, \text{W}$) Dianions—A Comparison With the Mo EXAFS of Nitrogenase. *J Am Chem S* 105(18):5767-5770, 1983.
- Tersoff J., Kevan S. D., **Nonlifetime Effects in Photoemission Linewidths.** *Phys Rev B* 28(8):4267-4270, 1983.
- Tu C. W., Sheng T. T., Read M. H., Schlier A. R., Johnson J. G., Johnson W. D., Bonner W. A., **Growth of Single-Crystalline Epitaxial Group 2 Fluoride Films on InP(001) by Molecular-Beam Epitaxy.** *J Elchem So* 130(10):2081-2087, 1983.
- Viner J. M., Lamey D., Huang C. C., Pindak R., Goodby J. W., **Heat Capacity Near the Smectic-A Hexatic-B and Hexatic-B-E Transitions of Normal Hexyl-4' Normal Pentylxybiphenyl-4-Carboxylate (65OBC).** *Phys Rev A* 28(4):2433-2441, 1983.
- Weber, T. A., Stillinger F. H., **Molecular-Dynamics Study of Ice Crystallite Melting.** *J Phys Chem* 87(21):4277-4281, 1983.
- Wiesenfeld J. M., Greene B. I., **Femtosecond Relaxation Dynamics of Molecular Rydberg States Using Time-Resolved Multiphoton Ionization.** *Phys Rev L* 51(19):1745-1748, 1983.
- Wudl F., et al., **Electron-Density Distribution in the Organic Superconductor (TMTSF)₂AsF₆.** *Science* 222(4622):415-417, 1983.
- Yan M. F., Rhodes W. W., **Low-Temperature Sintering of TiO₂.** *Mater Sci E* 61(1):59-66, 1983.
- Yuen M. F., Lauks I., Dautremont-Smith W. C., **pH Dependent Voltammetry of Iridium Oxide-Films.** *Sol St Ion* 11(1):19-29, 1983.

SOCIAL AND LIFE SCIENCES

- Chang F. R., **Perspectives on Cognitive Science—Norman, D. A. (BOOK REVIEW).** *Cont Psycho* 28(7):536-537, 1983.
- Jepson C., Krantz D. A., Nisbett R. E., **Inductive Reasoning—Competence or Skill.** *Behav Brain* 6(3):494-501, 1983.
- Leyenberger L. A., Paul L. M., **A Variable-Interval Timer.** *Behav Res M* 15(4):429-432, 1983.
- Nisbett R. E., Krantz D. H., Jepson C., Kunda Z., **The Use of Statistical Heuristics in Everyday Inductive Reasoning.** *Psychol Rev* 90(4):339-363, 1983.

Olson R. K., Kliegl R., Davidson B. J., **Dyslexic and Normal Readers Eye Movements.** *J Exp Psy P* 9(5):816-825, 1983.

SPEECH AND ACOUSTICS

Dautrich B. A., Rabiner L. R., Martin T. B., **On the Effects of Varying Filter Bank Parameters on Isolated Word Recognition.** *IEEE Acoust* 31(4):793-807, 1983.

Hohne H. D., Coker C., Levinson S. E., Rabiner L. R., **On Temporal Alignment of Sentences of Natural and Synthetic Speech.** *IEEE Acoust* 31(4):807-813, 1983.

Levinson S. E., Schmidt C. E., **Adaptive Computation of Articulatory Parameters From the Speech Signal.** *J Acoust So* 74(4):1145-1154, 1983.

CONTENTS, APRIL 1984

An Experimental Investigation of Wide-Angle Sidelobe Suppression
in a Pyramidal Horn-Reflector Antenna

C. A. Siller

BER Degradations Caused by Switching in Digital Mobile Radio
Systems Using Base Station Diversity

B. Glance

Processing Channel-Bank Spectrometer Data

H. E. Rowe

Weighting Strategies for Companded PCM Transmitted Over Ray-
leigh Fading and Gaussian Channels

C.-E. Sundberg, W. C. Wong, and R. Steele

On the Use of Hidden Markov Models for Speaker-Independent Rec-
ognition of Isolated Words From a Medium-Size Vocabulary

L. R. Rabiner, S. E. Levinson, and M. M. Sondhi

Probabilistic Analysis of Interframe Tie Requirements for Cross-
Connect Systems

C. L. Monma and D. R. Smith

A Nonlinear, Zero-One, Combinatorial, Goal-Programming Model and
Constructive Algorithm for Solving Multiobjective Assignment
Problems

K. R. Lipske and J. H. Fletcher

AT&T BELL LABORATORIES TECHNICAL JOURNAL is abstracted or indexed by *Abstract Journal in Earthquake Engineering*, *Applied Mechanics Review*, *Applied Science & Technology Index*, *Chemical Abstracts*, *Computer Abstracts*, *Current Contents/Engineering, Technology & Applied Sciences*, *Current Index to Statistics*, *Current Papers in Electrical & Electronic Engineering*, *Current Papers on Computers & Control*, *Electronics & Communications Abstracts Journal*, *The Engineering Index*, *International Aerospace Abstracts*, *Journal of Current Laser Abstracts*, *Language and Language Behavior Abstracts*, *Mathematical Reviews*, *Science Abstracts (Series A, Physics Abstracts; Series B, Electrical and Electronic Abstracts; and Series C, Computer & Control Abstracts)*, *Science Citation Index*, *Sociological Abstracts*, *Social Welfare, Social Planning and Social Development*, and *Solid State Abstracts Journal*. Reproductions of the Journal by years are available in microform from University Microfilms, 300 N. Zeeb Road, Ann Arbor, Michigan 48106.



AT&T
Bell Laboratories